Supporting information

A Marvel of Chiral Squaraine Aggregates: Chiroptical Spectra beyond the Exciton Model

Davide Giavazzi, Marvin F. Schumacher, Luca Grisanti, Mattia Anzola, Francesco Di Maiolo, Jennifer Zablocki, Arne Lützen, Manuela Schiek, Anna Painelli

April 25, 2023

Note: citation numbers refer to the specific bibliography of this document

Contents

1 Additional UV/Vis absorbance and ellipticity spectra

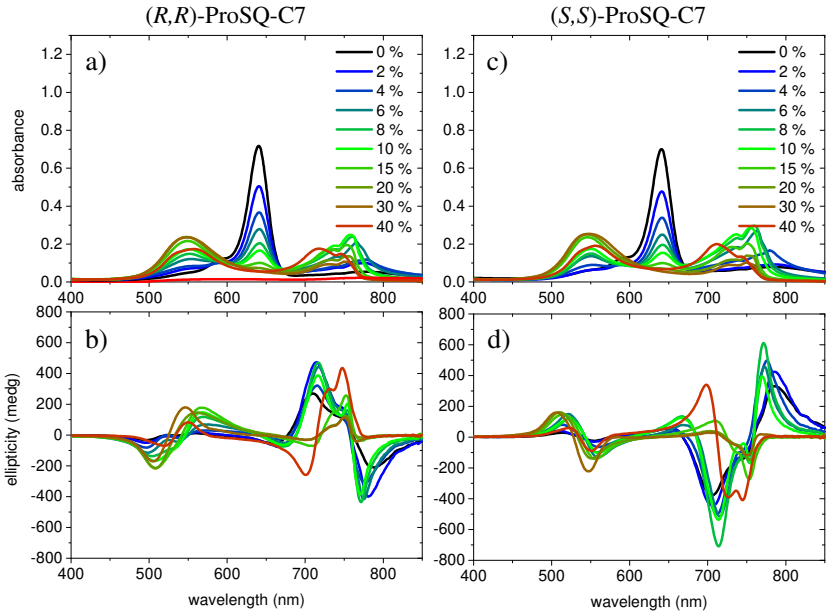

Figure S1: Experimental UV/Vis absorbance spectra a), c), and corresponding ellipticity spectra b), d) for the (*R,R*)-ProSQ-C7 (a) and b)) and (*S,S*)-ProSQC7 compounds (b) and c)). The legend indicates the volume-percentage of water in the methanol-water mixture and applies for all plots.

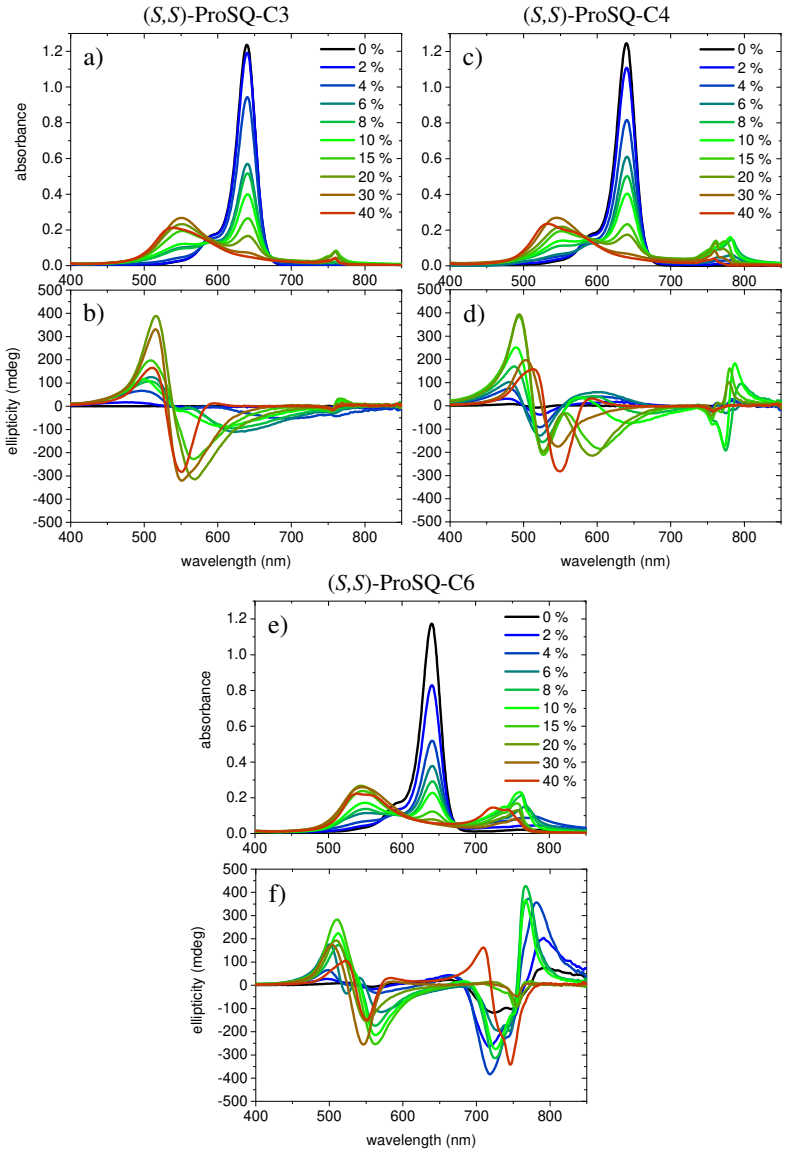

Figure S2: Experimental UV/Vis absorbance spectra a), c), e), and ellipticity spectra b), d), f) for the(*S,S*)-ProSQ compounds with varying alkyl chains: C3 in a) and b), C4 in c) and d), and C6 in e) and f). The legend indicates the volume-percentage of water in the methanol-water mixture and applies for all plots.

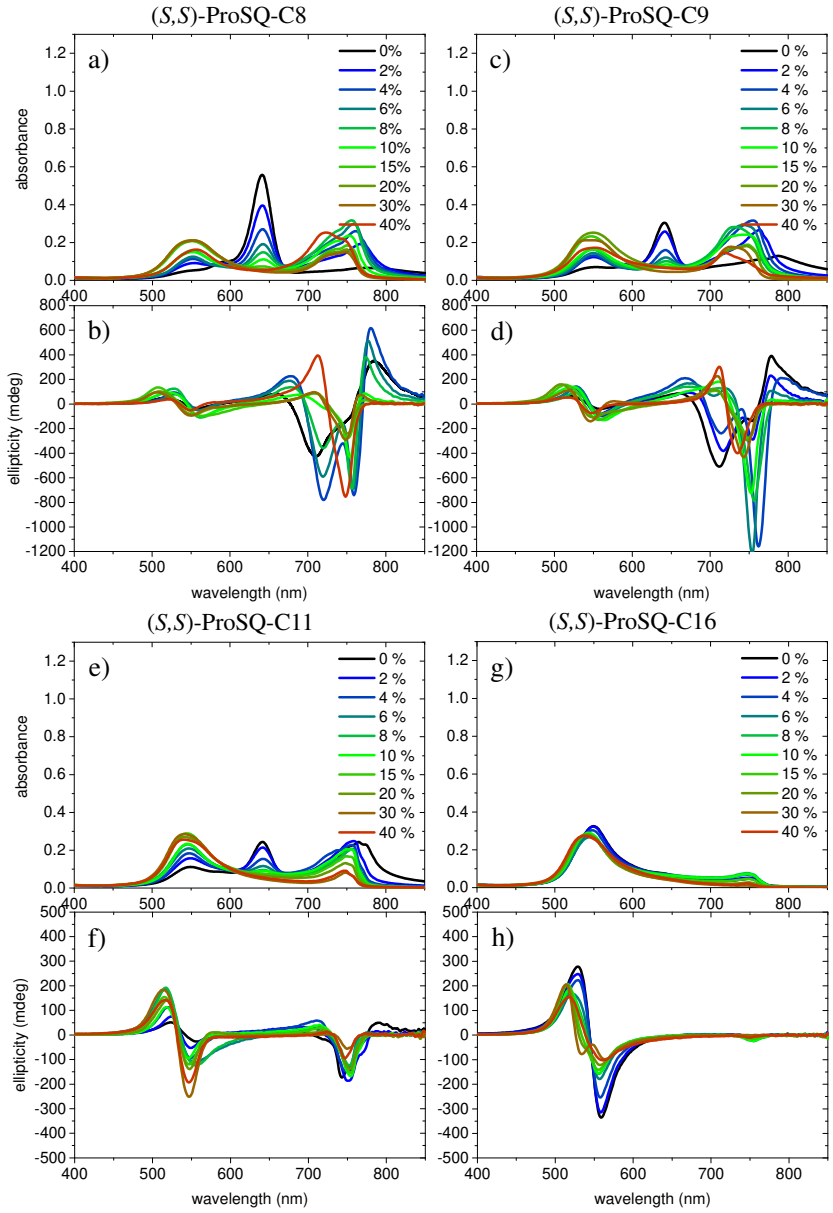

Figure S3: Experimental UV/Vis absorbance spectra a), c), e), g) and corresponding ellipticity spectra b), d), f), h) for the(*S,S*)-ProSQ compounds with varying alkyl chain lengths: C8 in a) and b), C9 in c) and d), C11 in e) and f), and C16 in g) and h). The legend indicates the volume-percentage of water in the methanol-water mixture and applies for all plots. For both enantiomers of the C16 compound titration experiments with acetonitrile as poor solvent can be found in reference [1].

2 Aggregate models: further details

2.1 The Exciton Model

The simplest model to account for electrostatic intermolecular interactions in molecular aggregates is the celebrated exciton model.[2, 3, 4] In this very simple model, a single transition is considered on each molecule with frequency ω_c (the correction of the excitation energy of the monomer due to the inclusion of the molecule in the aggregate is often neglected or phenomenologically introduced as a correction to ω_c). In the hypothesis that intermolecular interactions are small if compared with the excitation energies, only degenerate states are mixed up. Specifically, if interested to linear spectral properties, it is enough to diagonalize the Hamiltonian written on the basis of the states bearing a single excited molecule (single exciton subspace). Accordingly, for an aggregate of N molecules the relevant basis is comprised of the states where the i molecule (i runs from 0 to N) is in the excited state, while all other molecules are in the ground state state. Electrostatic intermolecular interactions are typically introduced in the dipolar approximation so that the interaction between the two states where either molecule i or j is in the excited state reads:

$$J_{ij} = \frac{\mu_c^2}{4\pi\epsilon_0\eta^2 d_{ij}^3}\mu_c^2 G_{ij} \tag{1}$$

where μ_c is the transition dipole moment (as experimentally estimated for the isolated dye), ϵ_0 is the vacuum dielectric constant, η is the medium refractive index and G_{ij} is a purely geometric factor that only depends on the distance and relative orientation of the transition dipole moments on the two molecules:

$$G_{ij} = \vec{e}_i \cdot \vec{e}_j - 3(\vec{e}_i \cdot \vec{e}_{ij})(\vec{e}_j \cdot \vec{e}_{ij}) \tag{2}$$

where $\vec{e}_i$ is the unit vector parallel to the dipole moment on molecule i and $\vec{e}_{ij}$ is the unit vector associated with the $i-j$ direction. The diagonalization of the $N \times N$ exciton Hamiltonian gives the excitonic eigenstates ϕ_k, with energies ϵ_k as linear combitations of the basis states.

To address absorption spectra, transition dipole moments must be calculated from the ground state (the state where all molecules are not excited) and the ϕ_k

eigenstates. To do so, the total dipole moment operator is defined as the vectorial sum of the molecular dipole moment operators, so that the transition dipole moment and the rotational strength for the k-th exciton transition are easily expressed on the basis of the transition dipole moments on each dye and their relative orientation and positions.[5] Since in the exciton model the dimension of the relevant subspace is equal to N, the number of dyes in the aggregates, very large aggregates, easily up to thousands of dyes, can be addressed.

2.2 Rotational strength in ESM-CT

The magnetic dipole is proportional to the total angular momentum:

$$\hat{\vec{M}} \propto -\hat{\vec{L}} = -\sum_k \hat{\vec{l}}_k \tag{3}$$

where k runs on all electrons and the angular momentum of k electron is related to its linear momentum $\hat{\vec{p}}_k$ by

$$\hat{\vec{l}}_k = \vec{r}_k \wedge \hat{\vec{p}}_k \tag{4}$$

Finally the linear momentum can be obtained as

$$\hat{\vec{p}}_k = -\frac{i}{\hbar}[\hat{\vec{\mu}}_k, H] \tag{5}$$

The problem is that in a real-space description we cannot address the properties of a single electron.

To overcome the problem we start evaluating the total linear momentum. For the sake of clarity, we address only its x component:

$$\hat{P}_x = -\frac{i}{\hbar}[\hat{D}_x, H] \tag{6}$$

where $\hat{D}_x$ is the x component of the total dipole moment, defined in Eq. 11. The dipole moment operator commutes with all terms in the Hamiltonian in Eq. 9 but the intra- and inter-molecular hopping terms. Accordingly:

$$\begin{aligned} \hat{P}_x &= \frac{i}{\hbar} t \sum_{i=1}^{N} [(x_{i2} - x_{i1})\hat{v}_{i1,i2} + (x_{i3} - x_{i2})\hat{v}_{i2,i3}] \\ &+ \frac{i}{\hbar}\beta \sum_{i=1}^{N-1} \left[(x_{(i+1)1} - x_{i2})\hat{v}_{i2,(i+1)1} + (x_{(i+1)2} - x_{i3})\hat{v}_{i3,(i+1)2}\right] \end{aligned} \tag{7}$$

where the bond velocity is the antiHermitian operator

$$\hat{v}_{ip,jq} = \hat{b}_{ip,jq} - \hat{b}^{\dagger}_{ip,jq} = \hat{b}_{ip,jq} - \hat{b}_{jq,ip} \tag{8}$$

The vectorial product $\hat{\vec{D}} \wedge \hat{\vec{P}}$ is not the total angular momentum in Eq. 3. Indeed $\hat{\vec{L}}$ and hence the magnetic dipole operator is a one-electron operator, while $\hat{\vec{R}} \wedge \hat{\vec{P}}$ does contain both one-electron and two-electron terms. We then define for our purposes $\hat{\vec{L}}$ selecting out of the $\hat{\vec{D}} \wedge \hat{\vec{P}}$ operator only the one-electron terms. Accordingly:

$$\begin{aligned}
\hat{L}_x \;=\; & -\frac{i}{\hbar} t \sum_{i=1}^{N} \Big[(z_{i2} - z_{i1})(y_{i1}\hat{b}_{i1,i2} - y_{12}\hat{b}_{i2,i1}) + (z_{i3} - z_{i2})(y_{i2}\hat{b}_{i23} - y_3\hat{b}_{32}) \Big] \\
& -\frac{i}{\hbar}\beta \sum_{i=1}^{N-1} \Big[(z_{(i+1)1} - z_{i,2})(y_{i,2}\hat{b}_{i2,(i+1)1} - y_{(i+1)1}\hat{b}_{(i+1)1,i2}) \\
& +(z_{(i+1)2} - z_{i3})(y_{i3}\hat{b}_{i3,(i+1)2} - y_{(i+1)2}\hat{b}_{(i+1)2,i3}) \Big] \\
& +\frac{i}{\hbar} t \sum_{i=1}^{N} \Big[(y_{i2} - y_{i1})(z_{i1}\hat{b}_{i1,i2} - z_{12}\hat{b}_{i2,i1}) + (y_{i3} - y_{i2})(z_{i2}\hat{b}_{i23} - z_3\hat{b}_{32}) \Big] \\
& +\frac{i}{\hbar}\beta \sum_{i=1}^{N-1} \Big[(y_{(i+1)1} - y_{i,2})(z_{i,2}\hat{b}_{i2,(i+1)1} - z_{(i+1)1}\hat{b}_{(i+1)1,i2}) \\
& +(y_{(i+1)2} - y_{i3})(z_{i3}\hat{b}_{i3,(i+1)2} - z_{(i+1)2}\hat{b}_{(i+1)2,i3}) \Big]
\end{aligned} \tag{9}$$

Analogous expressions for $\hat{L}_y$ and $\hat{L}_z$ can be obtained upon cyclic permutation of x, y, z indices. Remembering that $-\hat{\vec{L}} \propto \hat{\vec{M}}$ we are now in the position to calculate rotational strengths using Eq. 7.

2.3 The real space basis for the ESM-CT model

The definition of the basis relevant to the Hamiltonian in Eq. 9 describing delocalized electrons in the aggregate is a delicate issue. The basis selected by Spano and coworkers[6] that comprises only 15 states for a dimer is not complete. Specifically, only the charge distribution is accounted for, neglecting spin degrees of freedom, or, in more technical terms, electrons are approximated as spinless fermions. If electronic spin is accounted for the smallest basis is the valence-bond basis, that limit attentions to subspaces with the total spin quantum number S is conserved. Just as an example, fig. S4 shows how a single diagram in the

spinless fermion representation, corresponding to a specific charge distribution, actually corresponds to two valence bond-diagrams in the singlet states $S = 0$.

The valence bond basis is very convenient in terms of reduced dimension of the subspaces, but it has the main disadvantage of being non-orthonormal, leading to a somewhat cumbersome calculation of the matrix elements. We therefore adopt the much simpler real-space basis where electrons are located in the site orbitals and only states with the total projection of the spin operator equal to zero are considered, S_z=0. This leads to a much larger basis set than in valence bond, since it also includes S_z=0 components from triplet and higher spin states, but with the advantage of working with an orthonormal basis. Specifically, fig. S4 shows that the spinless Fermion state in panel (a) corresponds to 6 real space states in panel (c).

We use a bit representation for the real space basis, assigning 2 bits to each site, the first bit refers to the α spin, the second bit to β spin. An, of course 0/1 means that the specific spin state is void/occupied. Considering a single squaraine, just as an example, the $|N\rangle$ state is represented as 110011, while $|Z1\rangle$ is a singlet state, represented as a linear combination of 100111 and 011011. For the SQ dimer the real space basis is composed of 53 diagrams, listed in Fig 2. The diagonalization of the Hamiltonian matrix written on the real space basis gives relevant eigenstates $\psi_i\rangle$ and energies E_i.

2.4 Calculation of absorption and CD spectra

Irrespective of the specific model adopted for the calculation, spectra are calculated from the eigenstates, $|\psi_i\rangle$, where $|\psi_0\rangle$ is the ground states (the lowest energy states). Specifically absorption spectra are calculated as:

$$Abs(\omega) = \frac{1}{N}\hbar\omega \sum_i e^{-\frac{\hbar\omega-\hbar\omega_i}{2\sigma^2}} |\langle\psi_i|\hat{\vec{D}}|\psi_0\rangle|^2 \tag{10}$$

where N is the number of molecules in the aggregate, $\hbar\omega_i$ is the energy of the $|\psi_0\rangle \rightarrow |\psi_0\rangle$ transition and $\hat{\vec{D}}$ is the aggregate dipole moment as defined in the main text according to the specific model. A Gaussian bandshape with standard deviation σ is assigned to each absorption transition.

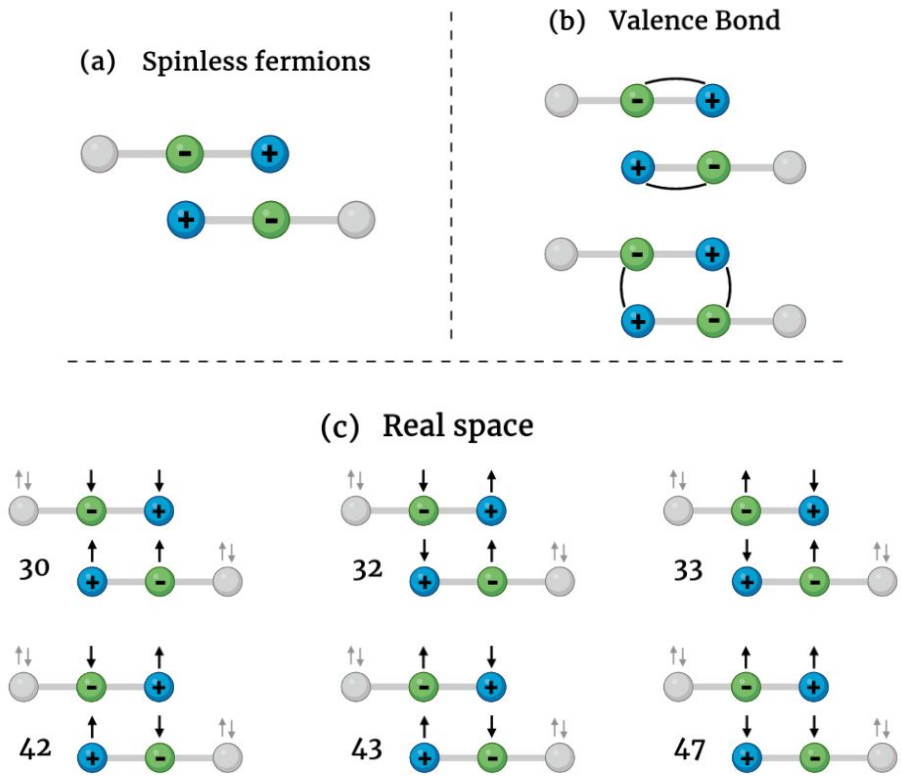

Figure S4: (a) Specific charge distribution for a dimer, corresponding to a single basis state in the spinless fermion approximation adopted in ref. [6]. (b) The two valence bond states corresponding to the same charge distribution as in (a) where the black lines mark two electrons paired in a singlet state, in the standard representation by Pauling. (c) The six real space diagrams corresponding to the charge distribution in (a), the numbers assigned to each diagram correspond to the labels in Fig. S5

1	1275	110111 110010	28	3318	011011 110011
2	1467	110111 011010	29	3321	100111 110011
3	1515	110101 111010	30	3435	110101 101011
4	1530	010111 111010	31	3450	010111 101011
5	1659	110111 100110	32	3483	110110 011011
6	1719	111011 010110	33	3495	111001 011011
7	1755	110110 110110	34	3507	110011 011011
8	1767	111001 110110	35	3510	011011 011011
9	1779	110011 110110	36	3513	100111 011011
10	1782	011011 110110	37	3546	010110 111011
11	1785	100111 110110	38	3555	110001 111011
12	2295	111011 110001	39	3558	011001 111011
13	2427	110111 101001	40	3561	100101 111011
14	2487	111011 011001	41	3570	010011 111011
15	2523	110110 111001	42	3675	110110 100111
16	2535	111001 111001	43	3687	111001 100111
17	2547	110011 111001	44	3699	110011 100111
18	2550	011011 111001	45	3702	011011 100111
19	2553	100111 111001	46	3705	100111 100111
20	2679	111011 100101	47	3735	111010 010111
21	2775	111010 110101	48	3765	101011 010111
22	2805	101011 110101	49	3795	110010 110111
23	3195	110111 100011	50	3798	011010 110111
24	3255	111011 010011	51	3801	100110 110111
25	3291	110110 110011	52	3813	101001 110111
26	3303	111001 110011	53	3825	100011 110111
27	3315	110011 110011			

Figure S5: The 53 diagrams composing the real state basis of a dimer. The first column numbers the diagrams, the second column is the integer number representative of each state, the third column is the corresponding bit representation

Similarly, CD spectra are calculated as:

$$CD(\omega) = \frac{1}{N} \sum_i e^{-\frac{\hbar\omega - \hbar\omega_i}{2\sigma^2}} R_i \tag{11}$$

where for a system with localized electrons the rotational strenghts R_i are calculated following eq. 8 in the main text, while for a system with delocalized electrons the more general equation 7 (main text) is used, where $\vec{\tilde{M}}$ is evaluated according to equations S4 and S10.

3 Calculated spectra: additional results

In the following we report additional calculated spectra (absorption in the top panels and CD in the bottom panels) obtained in different approximations and varying the parameters entering the calculation (the number of molecules N, the angle α, the refractive index η and the amount of intermolecular charge transfer β; parameter values are specified in the figures).

3.1 Standard exciton model

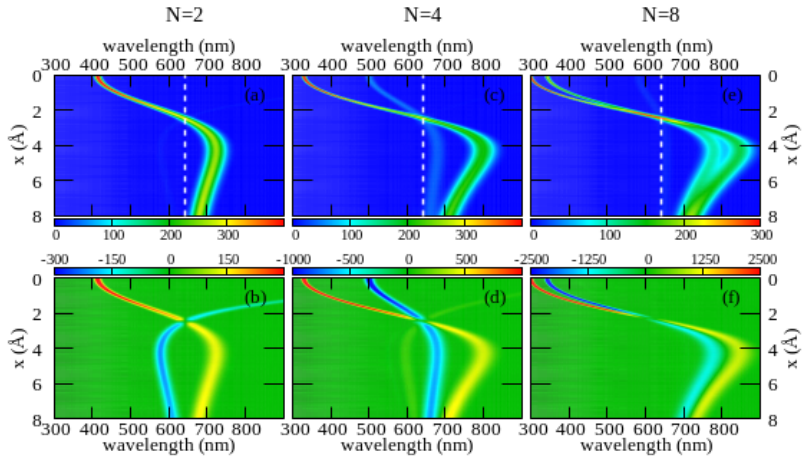

Figure S6: Results for aggregates of 2, 4 and 8 molecules obtained in the standard exciton model for the same geometries as in Fig. 4 (main text) and setting the molecular parameters entering the model as ω_c=1.93 eV, μ_c=12.5 D (values from ref. 41 in main text). Same quantities as in main text fig. 4. All intensities, in arbitrary units, are normalized to the number of molecules.

3.2 ESM-ES model

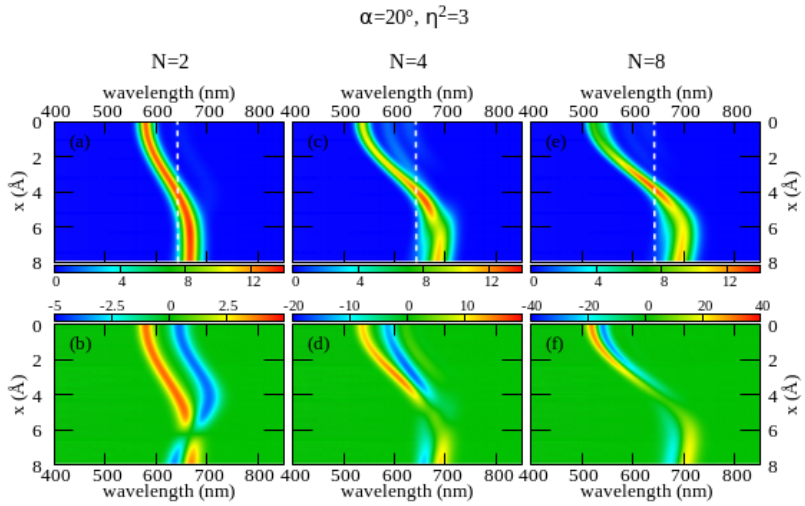

Figure S7: Results for aggregates of 2, 4 and 8 molecules with the same molecular parameters as in Fig. 4 (main text) and r=3.5 Å, α=20° and $\eta^2 = 3$.

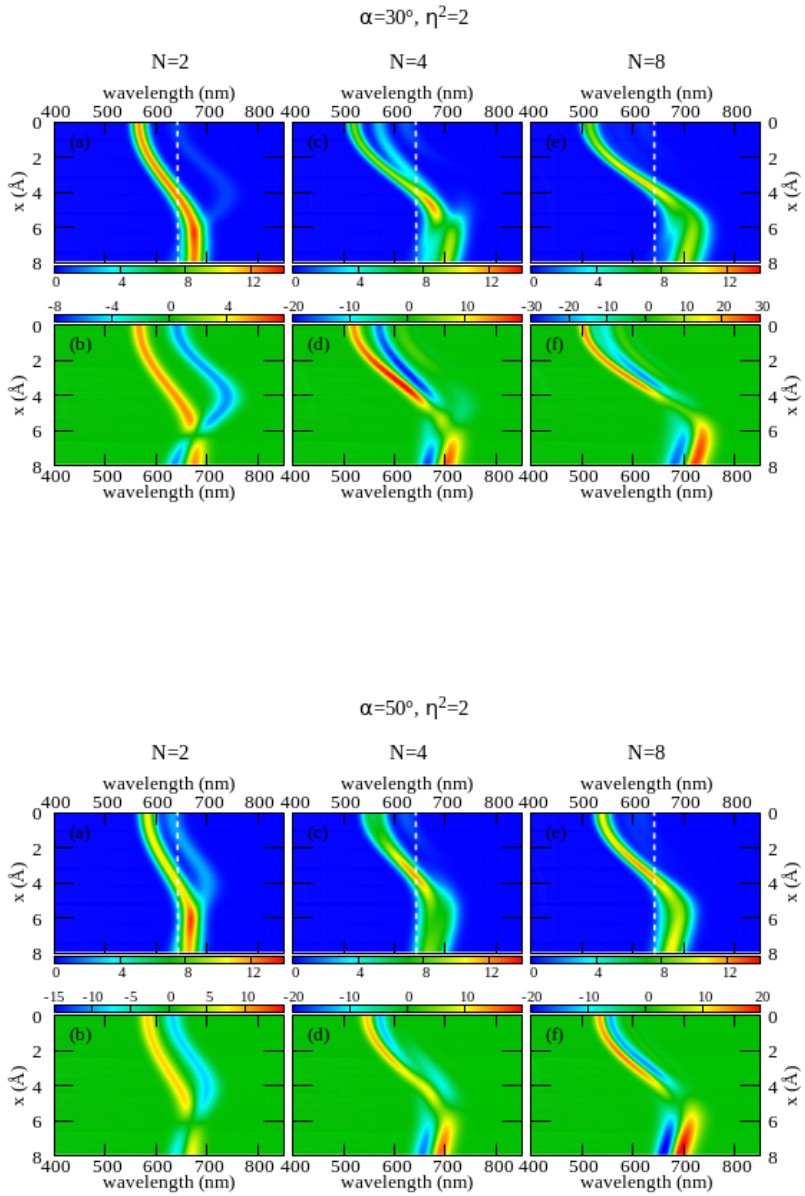

Figure S8: Results for aggregates of 2, 4 and 8 molecules with with the same molecular parameters as in Fig. 4 (main text) and r=3.5 Å, $\eta^2 = 2$, α=30° (topmost panels) and α=50° (bottom panels).

3.3 ESM-CT model

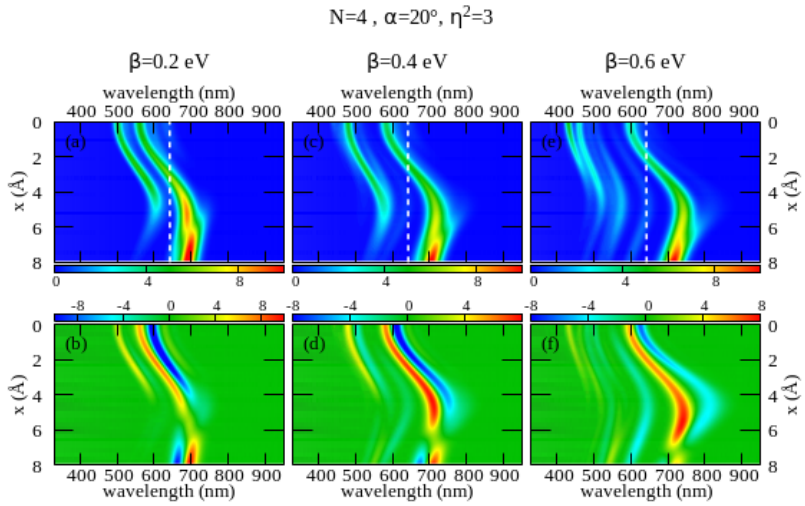

Figure S9: Results for aggregates of 4 molecules with the same molecular parameters as in Fig. 4 (main text) and for β =0.2, 0.4 and 0.6 eV with r=3.5 Å, α=20° and $\eta^2 = 3$.

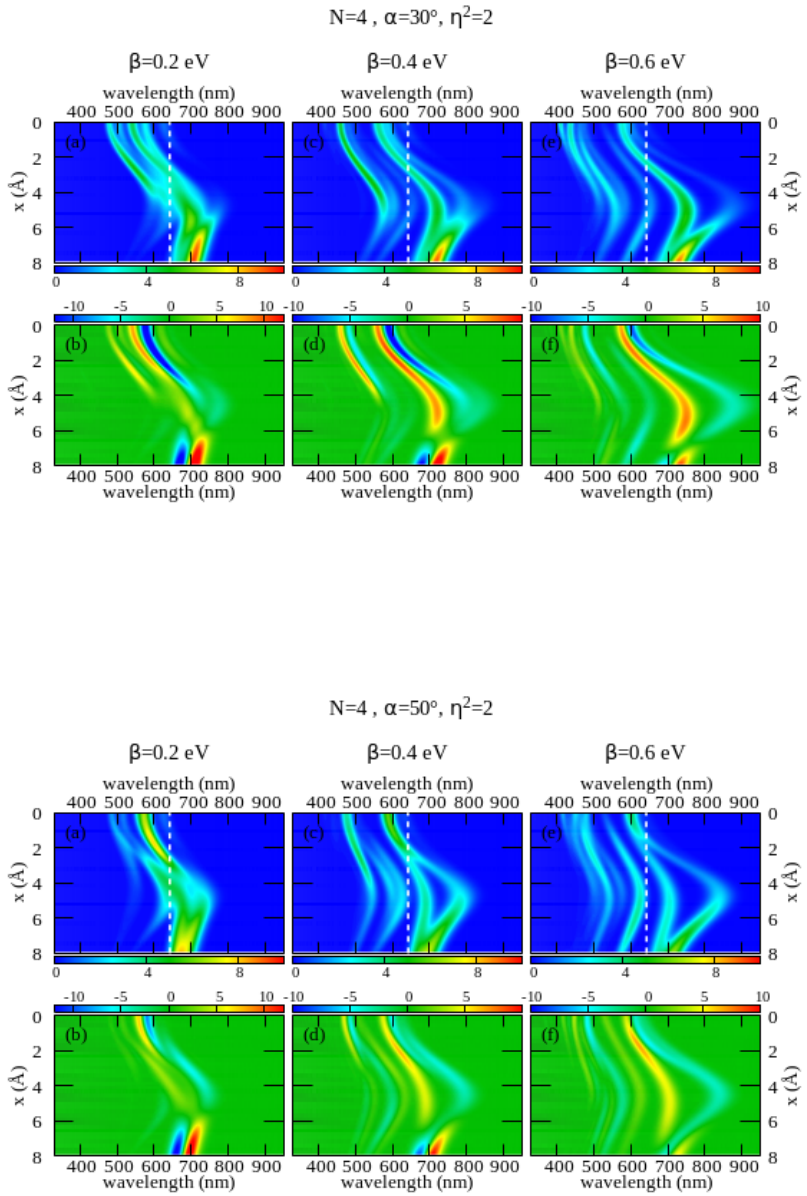

Figure S10: Results for aggregates of 4 molecules with the same molecular parameters as in Fig. 4 (main text) and for β =0.2, 0.4 and 0.6 eV with r=3.5 Å, $\eta^2 = 2$, α=30° (topmost panels) and α=50° (bottom panels).

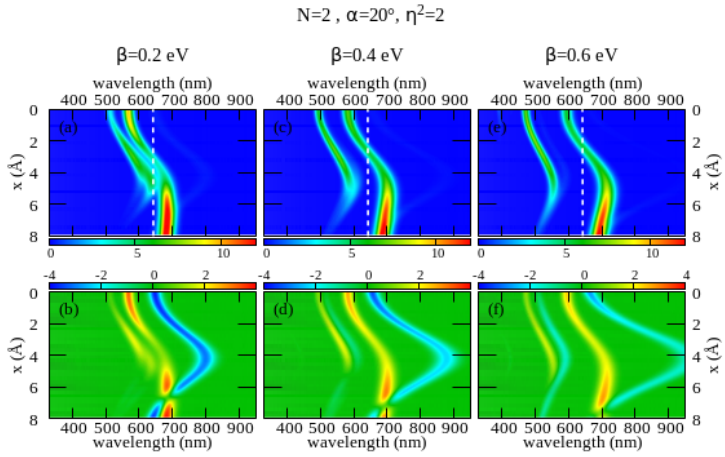

Figure S11: Results for aggregates of 2 molecules with the same molecular parameters as in Fig. 4 (main text) and for β =0.2, 0.4 and 0.6 eV with r=3.5 Å, α=20° and $\eta^2 = 2$.

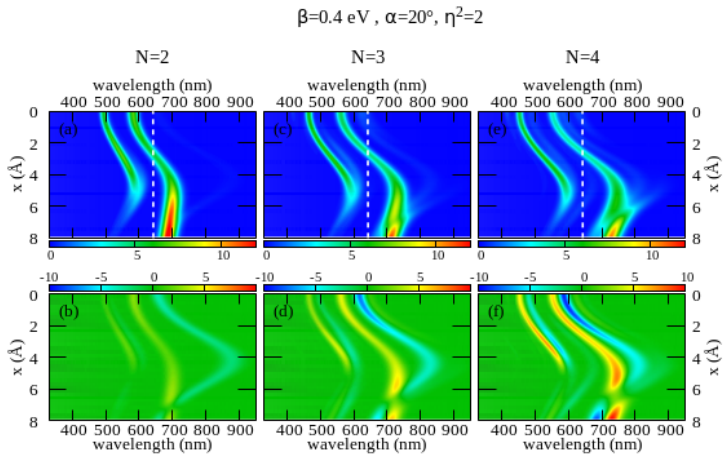

Figure S12: Results for aggregates of 2, 3 and 4 molecules with with the same molecular parameters as in Fig. 4 (main text) and for β =0.4 eV, r=3.5 Å, α=20° and $\eta^2 = 2$.

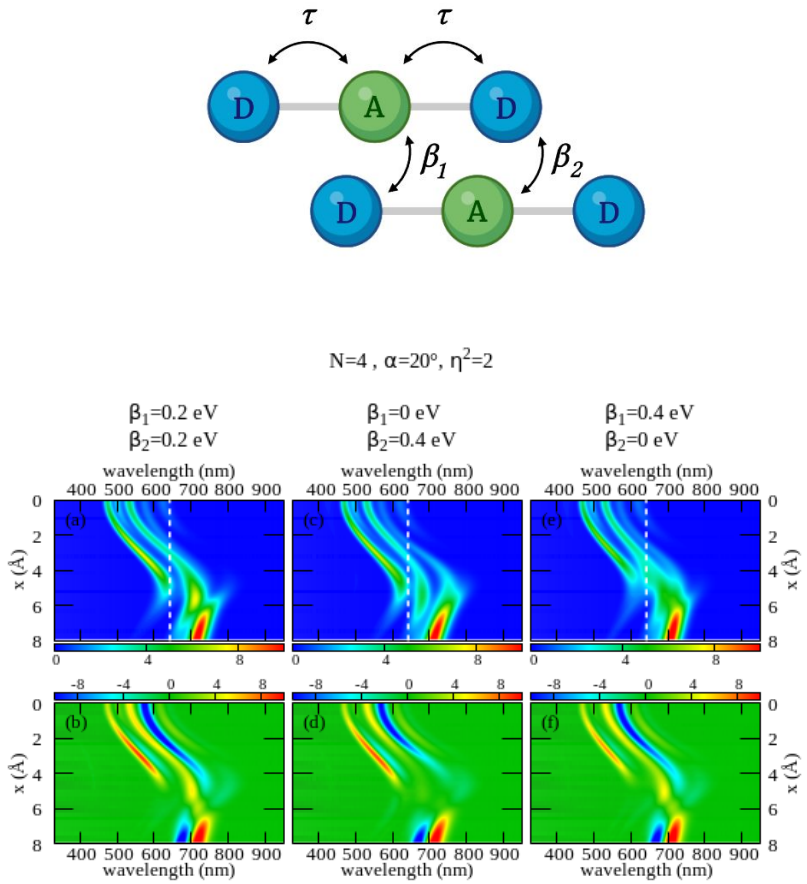

Figure S13: Results for aggregates of 4 molecules with with the same molecular parameters as in Fig. 4 (main text) and r=3.5 Å, α=20°, $\eta^2 = 2$ and imposing $\beta_1 = \beta_2 = 0.2$ eV (left panels), $\beta_1 = 0$ eV and $\beta_2 = 0.4$ eV (middle panels) and $\beta_1 = 0.4$ eV and $\beta_2 = 0$ eV (left panels).

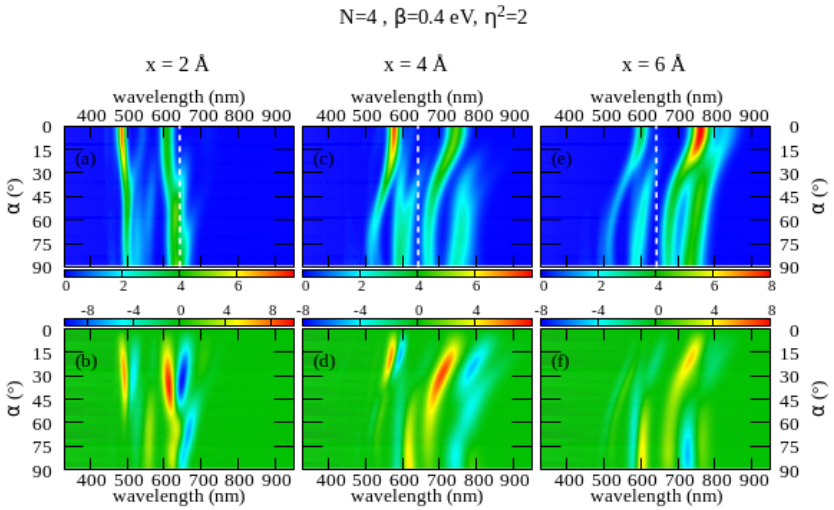

Figure S14: Results as a function of the angle α for aggregates of 4 molecules with with the same molecular parameters as in Fig. 4 (main text) and β =0.4 eV, r=3.5 Å, $\eta^2 = 2$ for different values of x.

4 Molecular dynamics simulations and time-dependent Density Functional Theory

Explicit solvent boxes were prepared as pure methanol [7] and 60:40 v/v mixture of methanol and water [8]. Simulation boxes in the two compositions were prepared and equilibrated and used as a starting point for the insertion of ProSQ-C10 according to the simulation set-up described below. For production runs in the NPT ensemble (300 K, 1 atm) Velocity Verlet algorithm was used and time step was set to 1fs, with v-rescale and Berendsen algorithms for temperature and pressure couplings, respectively, and with all bonds constrained using LINCS[9]. All simulations were pre-equilibrated for 4ns using Berendsen for both pressure and temperature coupling.

4.1 GAFF HREMDs

MD Hamiltonian replica exchange (HREMD) [10] simulations were were run using GROMACS 2020 [11] and its PLUMED plugin [12]. General AMBER Force Field (GAFF) [13] parameters were assigned using the antechamber module of AmberTools. QM calculations in g16 [14] were run to obtain RESP charges [15] at the HF/6-31G* level, calculated on previously optimized geometries at DFT-B3LYP [16] obtained by constraining planarity on the conjugated molecular core. The following simulations were run for ProSQ-C10: (a) 140ns of HREMD (12 replicas) of ProSQ-C10(S,S) tetramer in 60:40 MeOH:water (b) 140ns of HREMD (12 replicas) of ProSQ-C10(S,S) tetramer in pure MeOH (c) 60ns of HREMD (12 replicas) of ProSQ-C10(R,R) tetramer in pure MeOH. Results for ProSQ-C10 (S,S) tetramers are shown as 2D heatmaps of the center of mass (CM) distances vs. dihedral helical angle α in Fig. S15.

Simulation box size amounts to $\sim$ 50 Å corresponding to $\sim$ 1750 MeOH molecules (pure methanol simulation) or $\sim$ 1050 MeOH and 1550 water molecules (for the methanol-water 60:40 mixture), under fully periodic boundary conditions. In all cases only the trajectory of the first replica, at 300 K, was retained. In the above simulations, molecules were placed along an approximate stack in

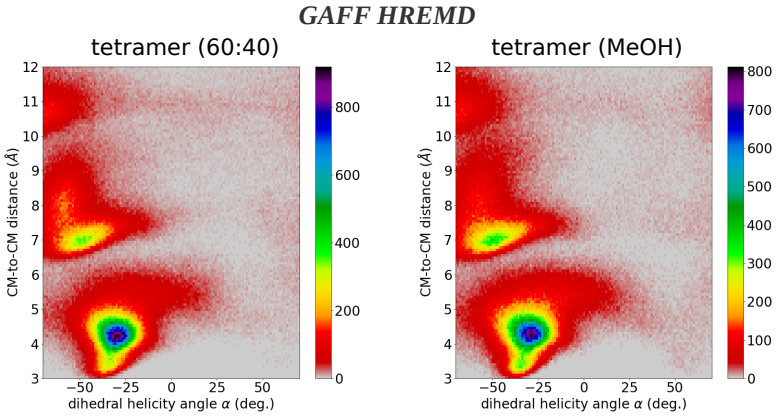

Figure S15: Results of two GAFF HREMDs on ProSQ-C10 (S,S) in methanol-water 60:40 mixtures (left) and pure methanol (right). Color plots showing the distribution of α (x axis, in degree), defined as in Fig. 3, main text) and of the distance between two center of mass (y-axis, in Å).

the starting geometry, before relaxation and equilibration. Further simulations in pure water (tot extra HREMD simulation time: 220 ns), as well as starting from different input structures (tot extra HREMD simulation time: $\sim$ 130 ns) were attempted searching for different type of aggregates and to ensure there is no bias due to the starting structure. In all cases, the same kind of helices as dominating structures were obtained (results not shown).

4.2 Modified GAFF+LCFF MDs

We manually edited some of the GAFF parameters to fix two critical issues, deriving the mod.GAFF+LCFF. First, in an attempt to improve the description of the conjugated core, we set to values for sp^2 carbon (differently from smaller value assigned automatically). This choice was motivated by the observation of several structures featuring a twisted molecular plane, not expected in term of chemical intuition. Moreover, we identify limitation of GAFF when systems exhibit long alkyl chains, as in our case. This was specifically addressed in the work by Boyd and Wilson on liquid crystals [17]. Starting from the above standard GAFF for ProSQ-C10 molecule with RESP charges, topologies were

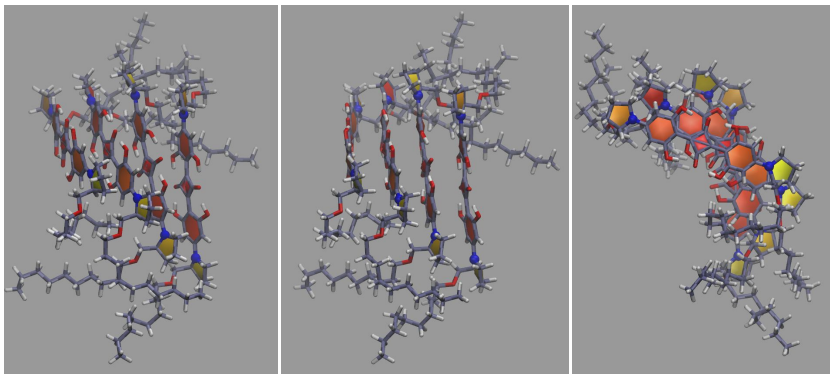

Figure S16: Sketches of a representative configuration selected along the tetramer simulated with mod. GAFF+LCFF MDs from the main right-hand helix (domain marked as A in Fig. 7 in the main text), view in three different perspectives. Rings are highlighted in colors, and nitrogen atoms represented as blue spheres.

modified accordingly, so that these mod.GAFF+LCFF MDs simulations were run of ProSQ-C10 (S,S): a) 200 ns for tetramer in Methanol:water 60:40, b1-b6) 6× 45 ns of 12-mer aggregate in 60:40 MeOH:water, c1-c2) 2× 45 ns of 24-mer aggregate in 60:40 MeOH:water.

Under fully periodic boundary conditions simulation boxes were considered with size $\sim$ 50 Å for tetramers (see above), $\sim$ 100 Å for 12-mer (9000 MeOH and 13000 water molecules approx), and $\sim$ 150 Å for 24-mer (30000 MeOH and 45000 water molecules approx). The starting structures were obtained placing the molecules onto a 2x2x3 cubic grid for 12-mer and on a 3x3x3 -3 grid for 24-mer MDs. The spacing in the grids amonted to 20 Å and moelcules where random orientated in each point of the grid. In all cases, a single aggregate is obtained after the first few ns of dynamics, often already between the minimization and the pre-equilibration phase.

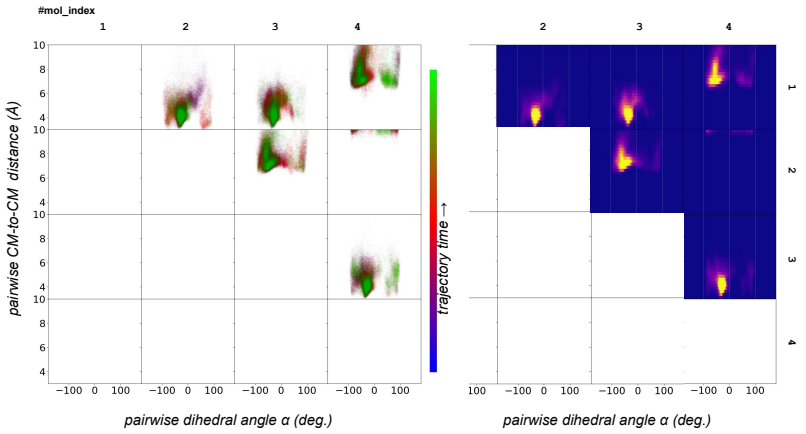

Figure S17: 2D distributions along dihedral angle α (x axis) and distance between two center of masses (y-axis) from the tetramer mod.GAFF+LCFF MDs for each molecular pair separately. Left: datapoints are shown according to the their time-occurrence during the simulation. Right, distributions of the same pairwise quantities shown as 2D color-maps on the overall trajectory.

4.3 Analysis of MD trajectories

Analysis on MDs trajectories obtained by Gromacs [11] were performed by employing python module MDAnalysis [18, 19]. The geometrical parameters were extracted, as schematically shown in Fig. S18, by selecting 4 atoms that represent the shape of the system: two carbon atoms of the squarainic core connected to oxygens (C1 and C3) and the two carbons Ca on the external vertex of the aromatic rings, connected to the two nitrogens (C14 and C8). By representing with $\vec{R}_A$ the coordinates of atom/point A, we can then define a set of geometrical derived quantities. Specifically, we define the molecular center of mass (CM) $\vec{R}_{CM} = \frac{1}{2}(\vec{R}_{C1} + \vec{R}_{C3})$, and the average plane, defined by the normal to the two axis: $\vec{a}(C1, C3)$ and $\vec{a}(C8, C14)$ as a proxy for the average molecular plane A. We also define the two molecular arms as vector connecting molecular CM to the Ca atoms: $\vec{v}(CM, C8)$ and $v(\vec{CM}, C14)$. Moreover, for the dimer we can define the angle *alpha*, defined in Fig. 3 main text, as the dihedral angle (Ca,CM,CM',Ca') where primed index refers to the second molecule, and Ca and Ca' refer to the either C8 or C14 atoms that determines the closest inter-

molecular Ca pair. All other quantities appearing in Fig. S19, including x and r (see Fig. 3, main text) were derived from the above quantisties, implementing point-to-plane distances and projections. Dealing with dimers, it is possible to compute two values for x and r, the employed value is then the average of the two. In figure S18 a sketch of some of these quantities is shown. In all cases, the first 10 ns of simulations were excluded from the analysis.

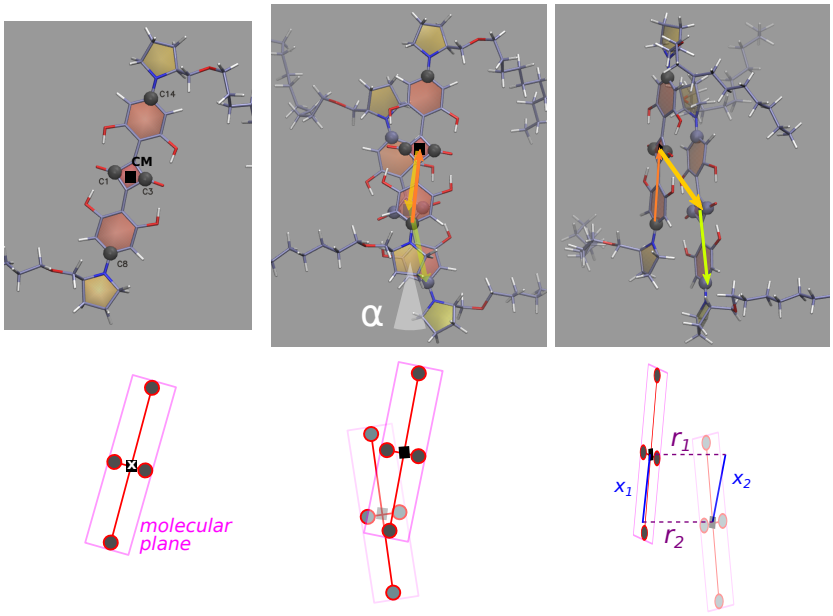

Figure S18: Top panels: example of a molecular structure of squaraine with highlighted atoms used for references and the center of mass (CM) marked as black square (left), molecular structure of a dimer with 3 vectors highlighted used to compute the dihedral angle α: $\vec{v}(Ca, CM)$ (orange), $\vec{v}(CM, CM')$ (yellow) and $\vec{v}(CM', Ca')$ (lime green), from top (middle) and side view (right). Bottom panels: sketch of the molecular frame used to define the molecular plane (left), and a possible dimer arrangement from top (middle). Side view of the same dimer with the definition of distances between CM and projection of CM', labeled as x_1 and x_2 and used to compute the displacement $x = \frac{1}{2}(x_1 + x_2)$ and the distance between the plane and such projection r_1 and r_2, used to define the plane distance $r = \frac{1}{2}(r_1 + r_2)$.

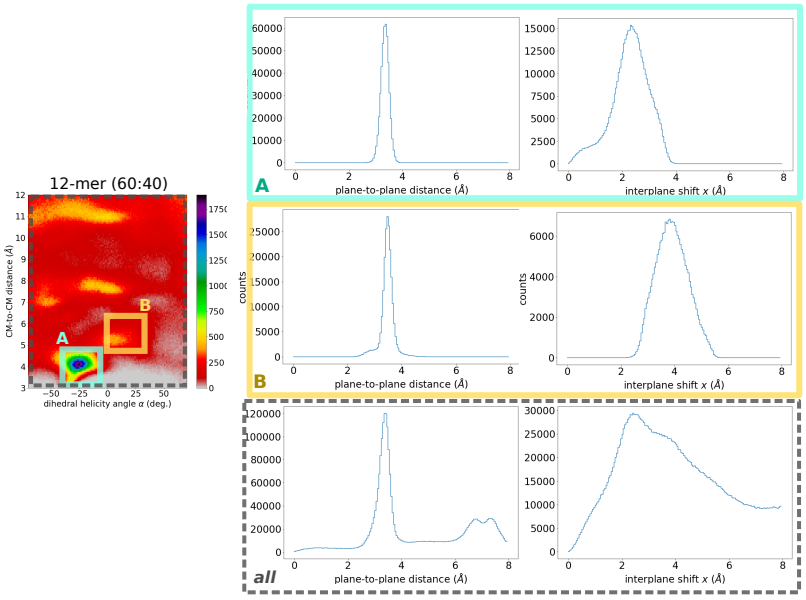

Figure S19: Panel on the right: distributions of geometrical quantities according to the region A of the right-handed helix (cyan contour), the region B of the left-handed helix (orange contour) vs. the whole region (dashed gray contour). The heatmaps on the left, is the same as Fig. T1: pairwise helical dihedral angle equivalent to α (x axis) and distance between two center of masses (y-axis) in ProSQ-C10 (S,S) 12-mer simulated with mod.GAFF+LCFF MDs.

4.4 Selection of representative dimer structures: clustering

The selection of representative dimers was only performed on MD simulations of 12-mers. From the complete pairwise information across all the 6 replicas (excluding the first portion of the trajectories as above), we first identify nearest-neighbours (i.e. pairs of molecules that spend in contact at least a fraction of the trajectory). On this ensemble of dimeric structures, the following four pairwise geometrical variables were used for clustering: r (CM-to-CM distance: same of Fig. 7b - central panel, y-axis), α (dihedral helicity: same of Fig. 7b - central panel, x-axis), angle between two average planes $\pi(A, A')$ as well as the shift x. The large numbers of point was then filtered based on the r distance by setting a cut-off at 8 Å, and 1 point each 4 was sampled in order to further reduce the number of points to 310206. On such 4-dimensional space we applied a density-peak based clustering [20], as to select the most representative dimeric structures across all 12-mers simulations. We set the threshold for merging clusters to Z =2.8, as to obtain 66 clusters. Only the 20 clusters having at least 3000 points were further considered - accounting for 90 % of the total sample. Among these, 5 were identified having a population p larger than 5%: Table S1 lists also the geometric properties of each of the representative dimers Dj - as selected by clustering to be the most representative from the sample of MD trajectory snapshots.

	p	r (d_{CM}) Å	α deg.	π deg.	x Å
D3	6.59050	5.3514	7.00	0.95	3.8990
D9	29.25685	4.3529	-25.24	-8.29	2.5778
D13	8.50822	6.3853	-50.42	177.6	5.5300
D14	8.92582	4.5537	29.47	170.44	2.9849
D19	11.60745	4.1436	-19.90	170.54	2.0967

Table S1: Populations and geometrical parameters relevant to the five representative dimers

4.5 Structure refinement and TDDFT calculations

The representative dimeric structures were then processed in order to compute excitation energies with (Time Dependent) Density functional Theory, (TD)-DFT. The 5 dimers (D3, D9, D13, D14 and D19) as extracted from above procedure rely on a classical potential and hence must be refined. We then processed the 5 dimers using `orca 5.0.2` [21] structures according to the following protocol:

1. from both molecules of dimer structures Dj the C10 chains were pruned, as to leave only a methyl group connected to oxygens at each molecular end
2. HF-3c [22] optimization (in vacuum) restraining intermolecular contacts between pairs of C atoms (`Connectfragment` option). We selected the two intermolecular pairs of aromatic ring C atoms (that are bonded to the N atoms) as a connector for the restraint
3. PBEh-3c [23] optimization (in vacuum) with the same restraint as above
4. def2-TZVP B3LYP-D3BJ [16, 24] optimization (in vacuum) with the same restraint as above
5. final TDDFT calculations at either i. B3LYP [16] or ii. CAM-B3LYP [25] functionals. We did not take advantage of Tamm-Dancoff approximation (TDA) as we realized the simulated spectra were not reliable when employing TDA. Basis set: def2-TZVP.

Simulated absorption and CD spectra for these two functionals are reported in figure S20. In our calculations 8 excited states are included. Spectra were simulated modeling each electronic transition with a Gaussian lineshape with $\sigma = 0.05$eV.

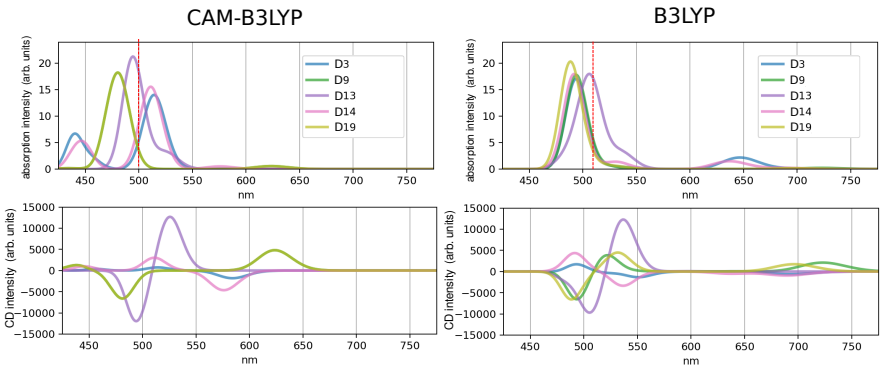

Figure S20: Simulated spectra on dimer representative structures with TDDFT at CAM-B3LYP functional (left) and B3LYP functional (right) with def2-TZVP basis set. Refined structure according to the procedure in section 4.5. Top: absorption spectra, bottom: CD spectra. Red dashed lines in the absorption spectra mark the average position of absorption maximum for corresponding monomers structures.

5 Synthesis

The synthetic route of the proline-derived squaraines (ProSQ) was adopted from the literature-known two-step, one-pot procedure.[26] As staring material, *N*-Boc-L-prolinol ((*S*)-1-Boc-2-pyrrolidinemethanol) was used as received, which was purchased from TCI, Fluorochem or chemPUR in >98 % purity and *ee* > 98 %. All other chemicals were purchased from standard suppliers and used without further purification. Solvents were purified with standard methods and, if necessary, dried according to literature procedures and stored under argon atmosphere over 4 Å molecular sieves. Reactions under inert gas conditions were performed under dry argon atmosphere with dry solvents in flame-dried glassware using *Schlenk* techniques.

NMR: ^{1}H and ^{13}C NMR were recorded at 298 K at 700 MHz and 176 MHz or 500 MHz and 125 MHz, respectively. ^{1}H NMR chemical shifts are reported on the δ scale (ppm) relative to tetramethylsilane. The residual non-deuterated solvent signal was used as the internal standard. ^{13}C NMR chemical shifts are given in δ values (ppm) relative to the deuterated solvent as the internal standard.

Mass spectrometry: electrospray ionisation (ESI) mass spectra were taken on a Orbitrap XL (*Thermo Fisher Scientific*).

UV/Vis spectroscopy: UV/Vis spectra were recorded at room temperature on a Specord 200 spectrometer (*Analytic Jena*) with 0.5 nm step size and 5 nm/s scanning speed, using 10 mm quartz cuvettes (*Hellma*). The instrument was calibrated with a reference sample in advance. UV/Vis spectra are shown as absorbance $=-\log(\text{transmission})$.

CD spectroscopy: Ellipsticity spectra were recorded on a J-810 spectro-polarimeter (*JASCO Corporation*) with 1 nm step size, a scanning speed of 200 nm/min, and a 1 nm bandwidth. An initial measurement of the pure solvent or solvent mixture was used for baseline correction. The circular dichroism (CD) spectra are shown as ellipticity in units of milli degree (mdeg) as outputted from the spectro-polarimeter. Note that CD and ellipticity are not the same values but for small quantities ellipticity = CD/2.[1]

Elemental analysis: elemental analysis was performed on a Vario EL (*Heraeus*).

All compounds were measured at least two times.

5.1 General synthesis of *N*-Boc-L-prolinyl ethers

The synthesis is based on the procedure published by *Lützen* et al. in 2017.[26] Under inert gas conditions, *N*-Boc-L-prolinol (1.00 eq.) is dissolved in *abs.* DMF (1 mL/mmol) and cooled to -15 °C in a flame-dried *Schlenk*-flask. Under vigorous stirring, sodium hydride (1.50 eq., 60 % in mineral oil) is slowly added in portions to the solution. The reaction mixture is further stirred at this temperature for 45 minutes and afterwards, the appropriate alkyl iodide (1.50 eq.) is added dropwise. The resulting suspension is stirred for 16 h during which the reaction mixture is allowed to warm up to room temperature. After complete consumption of the starting material (TLC monitoring), the reaction is quenched by adding a saturated aqueous ammonium chloride solution and diluted with ethyl acetate. The organic phase is separated and the aqueous phase is extracted three times with ethyl acetate. The combined organic phases are washed with water, brine and dried with magnesium sulfate. The solvent is removed under reduced pressure and the crude product is purified by column chromatography on silica gel (eluent cyclohexane/ethyl acetate 9:1 (v:v)). The *N*-Boc-L-prolinyl ethers are obtained as colorless oils.

5.1.1 Synthesis of *N*-Boc-L-prolinyl *n*-propyl ether

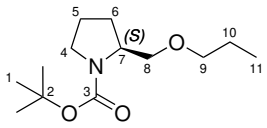

N-Boc-L-prolinol (2.01 g, 10.0 mmol) was reacted with 1-iodopropane (2.55 g, 15.0 mmol) according to the general procedure.

Yield: 1.21 g (4.98 mmol, 50 %, colorless oil)

Molecular weight: $C_{13}H_{25}NO_3$, 243.35 g/mol

^{1}H-NMR: (500 MHz, Chloroform-*d*, 298 K) δ [ppm] = 4.02-3.78 (m, 1H, H-7), 3.62-3.46 (m, 1H, H-8a), 3.46-3.11 (m, 5H, H-4, H-8b, H-9), 1.99-1.83

(m, 3H, H-5a, H-6), 1.83-1.72 (m, 1H, H-5b), 1.61-1.51 (m, 2H, H-10), 1.45 (s, 9H, H-1), 0.90 (t, 3H, H-11, $^3J_{10,11}$ = 7.4 Hz).

^{13}C-NMR: (125 MHz, Chloroform-*d*, 298 K) δ [ppm] = 154.7 (C-3), 79.3, 79.2 (C-2)*, 73.1 (C-9), 71.7, 71.0 (C-8)*, 56.6 (C-7), 47.0, 46.5 (C-4)*, 28.9, 28.1 (C-6)*, 28.7 (C-1), 23.9, 23.1 (C-5)*, 23.1 (C-10), 10.7 (C-11). Two signals can be identified that are due to rotamers.

MS (ESI(+), Dichloromethane, M = $C_{13}H_{25}NO_3$) *m/z* = 266.17 $[M+Na]^+$, 244.19 $[M+H]^+$, 188.13 $[M\text{-}C_4H_8+H]^+$, 144.14 $[M\text{-Boc}+H]^+$.

ESI HRMS: $[M+H]^+ = C_{13}H_{25}NO_3H^+$, calculated: m/z = 244.1907, found: m/z = 244.1902.

5.1.2 Synthesis of *N*-Boc-L-prolinyl *n*-butyl ether

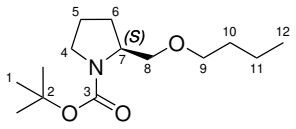

N-Boc-L-prolinol (4.06 g, 20.0 mmol) was reacted with 1-iodobutane (5.52 g, 30.0 mmol) according to the general procedure.

Yield: 2.43 g (9.43 mmol, 47 %, colorless oil)

Molecular weight: $C_{14}H_{27}NO_3$, 257.37 g/mol

^{1}H-NMR: (700 MHz, Chloroform-*d*, 298 K) δ [ppm] = 4.00-3.80 (m, 1H, H-7), 3.60-3.48 (m, 1H, H-8a), 3.48-3.37 (m, 2H, H-9), 3.37-3.17 (m, 3H, H-4, H-8b), 1.98-1.82 (m, 3H, H-5a, H-6), 1.82-1.72 (m, 1H, H-5b), 1.57-1.48 (m, 2H, H-10), 1.45 (s, 9H, H-1), 1.39-1.29 (m, 2H, H-11), 0.90 (t, 3H, H-12, $^3J_{11,12}$ = 7.5 Hz).

^{13}C-NMR: (176 MHz, Chloroform-*d*, 298 K) δ [ppm] = 154.7 (C-3), 79.3, 79.2 (C-2)*, 71.7, 71.1 (C-8)*, 71.2 (C-9), 56.6 (C-7), 47.0, 46.5 (C-4)*, 32.0 (C-10), 28.9, 28.1 (C-6)*, 28.7 (C-1), 23.9, 23.0 (C-5)*, 19.4 (C-11), 14.0 (C-12). Two signals can be identified that are due to rotamers.

MS (ESI(+), Dichloromethane, M = $C_{14}H_{27}NO_3$) *m/z* = 280.19 $[M+Na]^+$, 258.21 $[M+H]^+$, 202.14 $[M\text{-}C_4H_8+H]^+$, 144.14 $[M\text{-Boc}+H]^+$.

ESI HRMS: $[M+H]^+ = C_{14}H_{27}NO_3H^+$, calculated: $m/z = 258.2064$, found: $m/z = 258.2065$.

5.1.3 Synthesis of *N*-Boc-L-prolinyl *n*-pentyl ether

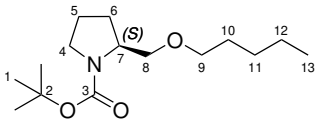

N-Boc-L-prolinol (2.02 g, 10.0 mmol) was reacted with 1-iodopentane (2.97 g, 15.0 mmol) according to the general procedure.

Yield: 1.96 g (7.22 mmol, 72 %, colorless oil)

Molecular weight: $C_{15}H_{29}NO_3$, 271.40 g/mol

^{1}H-NMR: (500 MHz, Chloroform-*d*, 298 K) δ [ppm] = 3.96-3.85 (m, 1H, H-7), 3.56-3.50 (m, 1H, H-8a), 3.49-3.35 (m, 2H, H-9), 3.35-3.23 (m, 3H, H-4, H-8b), 1.98-1.83 (m, 3H, H-5a, H-6), 1.83-1.74 (m, 1H, H-5b), 1.59-1.50 (m, 2H, H-10), 1.45 (s, 9H, H-1), 1.36-1.27 (m, 4H, H-11, H-12), 0.89 (t, 3H, H-13, $^3J_{12,13} = 7.0$ Hz).

^{13}C-NMR: (125 MHz, Chloroform-*d*, 298 K) δ [ppm] = 154.7 (C-3), 79.3 (C-2), 71.5 (C-9), 71.4 (C-8), 56.6 (C-7), 46.7 (C-4), 29.6 (C-10), 28.7 (C-1), 28.6 (C-6), 28.5 (C-11), 23.4 (C-5), 22.7 (C-12), 14.2 (C-13).

MS (ESI(+), Dichloromethane, M = $C_{15}H_{29}NO_3$) *m/z* = 565.42 $[2M+Na]^+$, 294.20 $[M+Na]^+$, 272.22 $[M+H]^+$, 216.16 $[M\text{-}C_4H_8+H]^+$, 172.17 $[M\text{-Boc}+H]^+$.

ESI HRMS: $[M+H]^+ = C_{15}H_{29}NO_3H^+$, calculated: $m/z = 272.2220$, found: $m/z = 272.2218$.

5.1.4 Synthesis of *N*-Boc-L-prolinyl *n*-hexyl ether

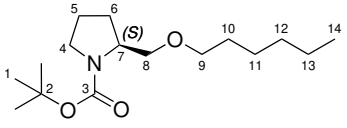

N-Boc-L-prolinyl *n*-hexyl ether was synthesized according to the literature.[26]

5.1.5 Synthesis of *N*-Boc-L-prolinyl *n*-heptyl ether

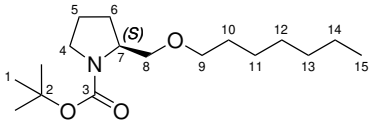

N-Boc-L-prolinol (1.01 g, 5.00 mmol) was reacted with 1-iodoheptane (3.40 g, 7.50 mmol) according to the general procedure.

Yield: 896 mg (2.99 mmol, 60 %, colorless oil)

Molecular weight: $C_{17}H_{33}NO_3$, 299.46 g/mol

^{1}H-NMR: (500 MHz, Chloroform-*d*, 298 K) δ [ppm] = 3.95-3.85 (m, 1H, H-7), 3.57-3.49 (m, 1H, H-8a), 3.48-3.36 (m, 2H, H-9), 3.36-3.22 (m, 3H, H-4, H-8b), 1.98-1.83 (m, 3H, H-5a, H-6), 1.83-1.74 (m, 1H, H-5b), 1.57-1.49 (m, 2H, H-10), 1.46 (s, 9H, H-1), 1.35-1.20 (m, 8H, H-11 to H-14), 0.87 (t, 3H, H-15, $^3J_{14,15}$ = 6.8 Hz).

^{13}C-NMR: (125 MHz, Chloroform-*d*, 298 K) δ [ppm] = 154.7 (C-3), 79.3 (C-2), 71.5 (C-9), 71.4 (C-8), 56.6 (C-7), 46.7 (C-4), 32.0, 29.3, 26.2, 22.8 (C-11 to C-14), 29.9 (C-10), 28.7 (C-1), 28.6 (C-6), 23.3 (C-5), 14.3 (C-15).

MS (ESI(+), Dichloromethane, M = $C_{17}H_{33}NO_3$) *m/z* = 621.48 $[2M+Na]^+$, 322.24 $[M+Na]^+$, 300.25 $[M+H]^+$, 244.19 $[M-C_4H_8+H]^+$, 200.20 $[M-Boc+H]^+$.

ESI HRMS: $[M+H]^+ = C_{17}H_{33}NO_3H^+$, calculated: m/z = 300.2533, found: m/z = 300.2537.

5.1.6 Synthesis of *N*-Boc-D-prolinyl *n*-heptyl ether

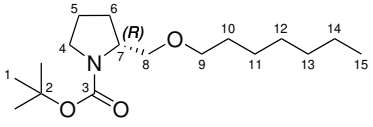

N-Boc-D-prolinol (2.01 g, 10.0 mmol) was reacted with 1-iodoheptane (1.70 g, 15.0 mmol) according to the general procedure.

Yield: 754 mg (2.52 mmol, 25 %, colorless oil)

Molecular weight: $C_{17}H_{33}NO_3$, 299.46 g/mol

All other analytical data of the (*R*,*R*)-enantiomer are in agreement with those of the (*S*,*S*)-enantiomer.

5.1.7 Synthesis of *N*-Boc-L-prolinyl *n*-octyl ether

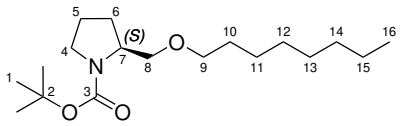

N-Boc-L-prolinol (1.01 g, 5.00 mmol) was reacted with 1-iodooctane (1.80 g, 7.50 mmol) according to the general procedure.

Yield: 997 mg (3.18 mmol, 64 %, colorless oil)

Molecular weight: $C_{18}H_{35}NO_3$, 313.48 g/mol

^{1}H-NMR: (500 MHz, Chloroform-*d*, 298 K) δ [ppm] = 3.89 (m, 1H, H-7), 3.52 (d, 1H, H-9a, $^3J_{9a,9b}$ = 7.9 Hz), 3.47-3.35 (m, 2H, H-9), 3.35-3.20 (m, 3H, H-4, H-8b), 1.97-1.82 (m, 3H, H-5a, H-6), 1.82-1.73 (m, 1H, H-5b), 1.58-1.48 (m, 2H, H-10), 1.45 (s, 9H, H-1), 1.34-1.18 (m, 10H, H-11 to H-15), 0.87 (t, 3H, H-1, $^3J_{15,16}$ = 7.1 Hz).

^{13}C-NMR: (125 MHz, Chloroform-*d*, 298 K) δ [ppm] = 154.7 (C-3), 79.2 (C-2), 71.5 (C-9), 71.5 (C-8), 56.6 (C-7), 46.7 (C-4), 32.0, 29.5, 29.4, 26.3, 23.4 (C-1 to C-15), 29.9 (C-10), 28.7 (C-1), 28.7 (C-6), 22.8 (C-5), 14.2 (C-16).

MS (ESI(+), Dichloromethane, M = $C_{18}H_{35}NO_3$) *m/z* = 336.250 $[M+Na]^+$, 314.268 $[M+H]^+$, 280.187 $[M\text{-}C_4H_8+Na]^+$, 258.206 $[M\text{-}C_4H_8+H]^+$, 214.216 $[M\text{-Boc}+H]^+$.

ESI HRMS: $[M+H]^+ = C_{18}H_{35}NO_3H^+$, calculated: m/z = 314.2690, found: m/z = 314.2685.

5.1.8 Synthesis of *N*-Boc-L-prolinyl *n*-nonyl ether

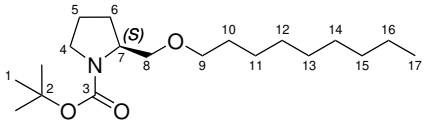

N-Boc-L-prolinol (3.02 g, 15.0 mmol) was reacted with 1-iodononane (5.72 g, 22.5 mmol) according to the general procedure.

Yield: 2.88 g (8.78 mmol, 59 %, colorless oil)

Molecular weight: $C_{19}H_{37}NO_3$, 327.51 g/mol

^{1}H-NMR: (700 MHz, Chloroform-*d*, 298 K) δ [ppm] = 3.94-3.85 (m, 1H, H-7), 3.56-3.50 (m, 1H, H-8a), 3.47-3.37 (m, 2H, H-9), 3.35-3.23 (m, 3H, H-4, H-8b), 1.97-1.83 (m, 3H, H-5a, H-6), 1.83-1.75 (m, 1H, H-5b), 1.56-1.50 (m, 2H, H-10), 1.46 (s, 9H, H-1), 1.35-1.21 (m, 12H, H-11 to H-16), 0.87 (t, 3H, H-17, $^3J_{16,17}$ = 7.1 Hz).

^{13}C-NMR: (176 MHz, Chloroform-*d*, 298 K) δ [ppm] = 154.7 (C-3), 79.3 (C-2), 71.5 (C-9), 71.4 (C-8), 56.6 (C-7), 46.7 (C-4), 32.0, 29.7, 29.6, 29.4, 26.3, 22.8 (C-11 to C-16), 29.9 (C-10), 28.7 (C-1), 28.6 (C-6), 23.3 (C-5), 14.2 (C-17).

MS (ESI(+), Dichloromethane, M = $C_{19}H_{37}NO_3$) *m/z* = 366.24 $[M+K]^+$, 350.27 $[M+Na]^+$, 328.28 $[M+H]^+$, 294.20 $[M\text{-}C_4H_8+Na]^+$, 272.22 $[M\text{-}C_4H_8+H]^+$, 228.23 $[M\text{-Boc}+H]^+$.

ESI HRMS: $[M+H]^+ = C_{19}H_{37}NO_3H^+$, calculated: m/z = 328.2846, found: m/z = 328.2833.

5.1.9 Synthesis of *N*-Boc-L-prolinyl *n*-decyl ether

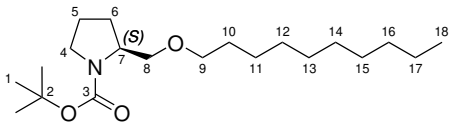

N-Boc-L-prolinol (2.01 g, 10.0 mmol) was reacted with 1-iododecane (4.02 g, 15.0 mmol) according to the general procedure.

Yield: 2.23 g (6.82 mmol, 65 %, colorless oil)

Molecular weight: $C_{20}H_{39}NO_3$, 341.54 g/mol

^{1}H-NMR: (700 MHz, Chloroform-*d*, 298 K) δ [ppm] = 3.95-3.86 (m, 1H, H-7), 3.56-3.50 (m, 1H, H-8a), 3.47-3.36 (m, 2H, H-9), 3.35-3.23 (m, 3H, H-4, H-8b), 1.97-1.83 (m, 3H, H-5a, H-6), 1.83-1.75 (m, 1H, H-5b), 1.57-1.50 (m, 2H, H-10), 1.46 (s, 9H, H-1), 1.34-1.21 (m, 14H, H-11 to H-17), 0.89 (t, 3H, H-18, $^3J_{17,18}$ = 7.1 Hz).

^{13}C-NMR: (176 MHz, Chloroform-*d*, 298 K) δ [ppm] = 154.7 (C-3), 79.3 (C-2), 71.5 (C-9), 71.4 (C-8), 56.6 (C-7), 46.8 (C-4), 32.1, 29.8, 29.7, 29.6, 29.5, 26.3 (C-11 to C-16), 29.9 (C-10), 28.7 (C-1), 28.6 (C-6), 23.4 (C-5), 22.8 (C-17), 14.3 (C-18).

MS (ESI(+), Dichloromethane, M = $C_{20}H_{39}NO_3$) *m/z* = 705.58 $[2M+Na]^+$, 364.28 $[M+Na]^+$, 342.30 $[M+H]^+$, 286.24 $[M\text{-}C_4H_8+H]^+$, 242.25 $[M\text{-Boc}+H]^+$.

ESI HRMS: $[M+H]^+ = C_{20}H_{39}NO_3H^+$, calculated: m/z = 342.3003, found: m/z = 342.3006.

5.1.10 Synthesis of *N*-Boc-L-prolinyl *n*-undecyl ether

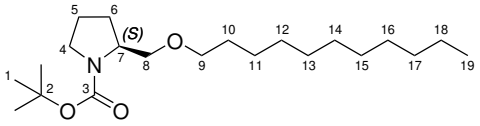

N-Boc-L-prolinol (3.02 g, 15.0 mmol) was reacted with 1-iodoundecane (6.35 g, 22.5 mmol) according to the general procedure.

Yield: 2.18 g (6.14 mmol, 41 %, colorless oil)

Molecular weight: $C_{21}H_{41}NO_3$, 355.56 g/mol

^{1}H-NMR: (500 MHz, Chloroform-*d*, 298 K) δ [ppm] = 3.94-3.85 (m, 1H, H-7), 3.55-3.49 (m, 1H, H-8a), 3.47-3.35 (m, 2H, H-9), 3.34-3.23 (m, 3H, H-4, H-8b), 1.97-1.82 (m, 3H, H-5a, H-6), 1.82-1.73 (m, 1H, H-5b), 1.57-1.49 (m, 2H, H-10), 1.45 (s, 9H, H-1), 1.34-1.18 (m, 16H, H-11 to H-18), 0.87 (t, 3H, H-19,

$^3J_{18,19}$ = 6.9 Hz).

^{13}C-NMR: (125 MHz, Chloroform-*d*, 298 K) δ [ppm] = 154.7 (C-3), 79.2 (C-2), 71.5 (C-9), 71.4 (C-8), 56.6 (C-7), 46.7 (C-4), 32.1, 29.8, 29.6, 29.5, 26.3, 22.8 (C-11 to C-18), 29.9 (C-10), 28.7 (C-1), 28.6 (C-6), 23.4 (C-5), 14.2 (C-19).

MS (ESI(+), Dichloromethane, M = $C_{21}H_{41}NO_3$) *m/z* = 394.27 $[M+K]^+$, 378.30 $[M+Na]^+$, 356.32 $[M+H]^+$, 322.24 $[M\text{-}C_4H_8+Na]^+$, 300.25 $[M\text{-}C_4H_8+H]^+$, 256.26 $[M\text{-Boc}+H]^+$.

ESI HRMS: $[M+H]^+ = C_{21}H_{41}NO_3H^+$, calculated: m/z = 356.3159, found: m/z = 356.3158.

5.1.11 Synthesis of *N*-Boc-L-prolinyl *n*-dodecyl ether

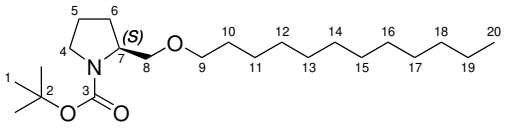

N-Boc-L-prolinol (1.01 g, 5.00 mmol) was reacted with 1-iodododecane (2.22 g, 7.50 mmol) according to the general procedure.

Yield: 2.18 g (6.14 mmol, 41 %, colorless oil, with the tendency to solidify)

Molecular weight: $C_{22}H_{43}NO_3$, 369.59 g/mol

^{1}H-NMR: (500 MHz, Chloroform-*d*, 298 K) δ [ppm] = 3.90 (m, 1H, H-7), 3.53 (dd, 1H, H-8a, $^3J_{13a,14}$ = 3.2 Hz, $^3J_{13a,13b}$ = 9.5 Hz), 3.49-3.35 (m, 2H, H-9), 3.35-3.23 (m, 3H, H-8b, H-4), 1.99-1.83 (m, 3H, H-5a, H-6), 1.83-1.73 (m, 1H, H-5b), 1.57-1.49 (m, 2H, H-10), 1.46 (s, 9H, H-1), 1.36-1.19 (m, 18H, H-11 to H-19), 0.87 (t, 3H, H-20, $^3J_{19,20}$ = 6.8 Hz).

^{13}C-NMR: (125 MHz, Chloroform-*d*, 298 K) δ [ppm] = 154.7 (C-3), 79.3 (C-2), 71.5 (C-9), 71.1 (C-8), 56.6 (C-7), 46.7 (C-4), 32.1, 29.9, 29.8, 29.8, 29.7, 29.6, 29.5, 28.9, 28.1, 26.3, 23.0 (C-6, C-10 to C-19), 28.7 (C-1), 22.8 (C-5), 14.2 (C-20).

MS (ESI(+), Dichloromethane, M = $C_{22}H_{43}NO_3$) *m/z* = 392.314 $[M+Na]^+$, 370.332 $[M+H]^+$, 314.269 $[M\text{-}C_4H_8+H]^+$, 270.279 $[M\text{-Boc}+H]^+$.

ESI HRMS: $[M+H]^+ = C_{22}H_{43}NO_3H^+$, calculated: $m/z = 370.3316$, found: $m/z = 370.3321$.

5.1.12 Synthesis of *N*-Boc-L-prolinyl *n*-hexadecyl ether

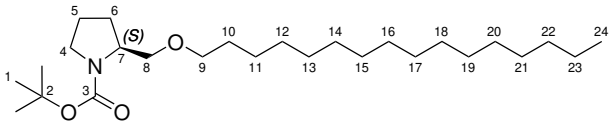

N-Boc-L-prolinyl *n*-hexadecyl ether was synthesized according to the literature.[26, 1]

5.2 General method for the Boc deprotection

The synthesis is based on the procedure published by *Lützen* et al. in 2017.[26] Under inert gas conditions and flame-dried glassware, the corresponding *N*-Boc-L-prolinyl ether (1.00 eq.) is dissolved in *abs.* dichloromethane (1 mL/mmol) and cooled to 0 °C. Under stirring, trifluoroacetic acid (10.0 eq.) is added dropwise to the solution. The reaction mixture is stirred for additional 30 minutes at 0 °C and after removing the cooling bath for 2 hours at room temperature. After dilution with dichloromethane, the mixture is poured into the same volume of ice-cold aqueous 10 % NaOH. The organic phase is separated and the aqueous phase is extracted with dichloromethane. The combined organic phases are washed with brine and dried with magnesium sulfate. The solvent is removed under reduced pressure and the obtained residue is used without further purification in the next reaction step. The products are obtained as pale yellow oils.

5.2.1 Synthesis of L-prolinyl *n*-propyl ether

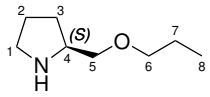

N-Boc-L-prolinyl *n*-propyl ether (1.02 g, 4.18 mmol) was deprotected according to the general procedure.

Yield: 590 mg (4.12 mmol, 99 %, pale yellow oil)

Molecular weight: $C_8H_{17}NO$, 143.23 g/mol

^{1}H-NMR: (500 MHz, Chloroform-*d*, 298 K) δ [ppm] = 6.20 (br s, 1H, NH), 3.57-3.48 (m, 2H, H-4, H-5a), 3.48-3.36 (m, 3H, H-5b, H-6), 3.18-3.03 (m, 2H, H-1), 2.00-1.78 (m, 3H, H-2, H-3a), 1.65-1.52 (m, 3H, H-3b, H-7), 0.89 (t, 3H, H-8, $^3J_{7,8}$ = 7.4 Hz).

^{13}C-NMR: (125 MHz, Chloroform-*d*, 298 K) δ [ppm] = 73.2 (C-6), 71.9, (C-5), 58.4 (C-4), 46.1 (C-1), 27.7 (C-3), 24.8 (C-2), 22.9 (C-7), 10.6 (C-8).

MS (ESI(+), Dichloromethane, M = $C_8H_{17}NO$) *m/z* = 287.27 $[2M+H]^+$, 144.14 $[M+H]^+$.

ESI HRMS: $[M+H]^+ = C_8H_{17}NOH^+$, calculated: m/z = 144.1383, found: m/z = 144.1384.

5.2.2 Synthesis of L-prolinyl *n*-butyl ether

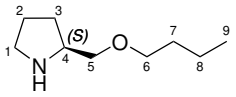

N-Boc-L-prolinyl *n*-butyl ether (2.43 g, 9.43 mmol) was deprotected according to the general procedure.

Yield: 1.01 g (6.42 mmol, 68 %, pale yellow oil)

Molecular weight: $C_9H_{19}NO$, 157.26 g/mol

^{1}H-NMR: (500 MHz, Chloroform-*d*, 298 K) δ [ppm] = 8.34 (br s, 1H, NH), 3.82-3.74 (m, 1H, H-4), 3.71-3.58 (m, 2H, H-5), 3.55-3.42 (m, 2H, H-6),

3.34-3.27 (m, 2H, H-1), 2.12-1.90 (m, 3H, H-2, H-3a), 1.88-1.77 (m, 1H, H-3b), 1.58-1.50 (m, 2H, H-7), 1.38-1.28 (m, 2H, H-8), 0.89 (t, 3H, H-9, $^3J_{8,9} = 7.4$ Hz).

^{13}C-NMR: (125 MHz, Chloroform-*d*, 298 K) δ [ppm] = 71.5 (C-6), 69.7, (C-5), 58.6 (C-4), 45.8 (C-1), 31.7 (C-7), 27.4 (C-3), 24.3 (C-2), 19.4 (C-8), 14.0 (C-9).

MS (ESI(+), Dichloromethane, M = $C_9H_{19}NO$) *m/z* = 351.28 $[2M+HCl+H]^+$, 315.30 $[2M+H]^+$, 158.15 $[M+H]^+$.

ESI HRMS: $[M+H]^+ = C_9H_{19}NOH^+$, calculated: $m/z = 158.1539$, found: $m/z = 158.1533$.

5.2.3 Synthesis of L-prolinyl *n*-pentyl ether

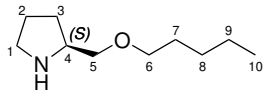

N-Boc-L-prolinyl *n*-pentyl ether (1.72 g, 6.34 mmol) was deprotected according to the general procedure.

Yield: 1.08 g (6.30 mmol, 99 %, pale yellow oil)

Molecular weight: $C_{10}H_{21}NO$, 171.28 g/mol

^{1}H-NMR: (500 MHz, Chloroform-*d*, 298 K) δ [ppm] = 3.45-3.40 (m, 3H, H-5a, H-6), 3.36-3.29 (m, 2H, H-4, H-5b), 3.30-3.21 (br s, 1H, NH), 3.05-2.88 (m, 2H, H-1), 1.90-1.80 (m, 1H, H-3a), 1.80-1.68 (m, 2H, H-2), 1.60-1.51 (m, 2H, H-7), 1.49-1.40 (m, 1H, H-3b), 1.36-1.26 (m, 4H, H-8, H-9), 0.88 (t, 3H, H-10, $^3J_{9,10} = 7.0$ Hz).

^{13}C-NMR: (125 MHz, Chloroform-*d*, 298 K) δ [ppm] = 73.7 (C-5), 71.6, (C-6), 58.1 (C-4), 46.4 (C-1), 29.5 (C-7), 28.4 (C-8), 28.0 (C-3), 25.2 (C-2), 22.7 (C-9), 14.2 (C-10).

MS (ESI(+), Dichloromethane, M = $C_{10}H_{21}NO$) *m/z* = 172.17 $[M+H]^+$.

ESI HRMS: $[M+H]^+ = C_{10}H_{21}NOH^+$, calculated: $m/z = 172.1696$, found: $m/z = 172.1693$.

5.2.4 Synthesis of L-prolinyl *n*-hexyl ether

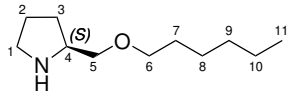

L-prolinyl *n*-hexyl ether was synthesized according to the literature.[26]

5.2.5 Synthesis of L-prolinyl *n*-heptyl ether

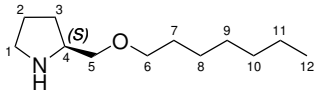

N-Boc-L-prolinyl *n*-heptyl ether (0.72 g, 2.40 mmol) was deprotected according to the general procedure.

Yield: 478 mg (2.40 mmol, quant., pale yellow oil)

Molecular weight: $C_{12}H_{25}NO$, 199.34 g/mol

^{1}H-NMR: (500 MHz, Chloroform-*d*, 298 K) δ [ppm] = 3.45-3.38 (m, 3H, H-5a, H-6), 3.36-3.28 (m, 3H, H-4, H-5b, NH), 3.05-2.87 (m, 2H, H-1), 1.93-1.80 (m, 1H, H-3a), 1.80-1.65 (m, 2H, H-2), 1.59-1.51 (m, 2H, H-7), 1.49-1.40 (m, 1H, H-3b), 1.35-1.20 (m, 8H, H-8 to H-11), 0.87 (t, 3H, H-12, $^3J_{11,12} = 6.8$ Hz).

^{13}C-NMR: (125 MHz, Chloroform-*d*, 298 K) δ [ppm] = 73.8 (C-5), 71.6, (C-6), 58.1 (C-4), 46.5 (C-1), 32.9, 29.3, 26.2, 22.8 (C-8 to C-11), 29.8 (C-7), 28.0 (C-3), 25.2 (C-2), 14.2 (C-12).

MS (ESI(+), Dichloromethane, M = $C_{12}H_{25}NO$) *m/z* = 435.37 $[2M+HCl+H]^+$, 200.20 $[M+H]^+$.

ESI HRMS: $[M+H]^+ = C_{12}H_{25}NOH^+$, calculated: $m/z = 200.2009$, found: $m/z = 200.2008$.

5.2.6 Synthesis of D-prolinyl *n*-heptyl ether

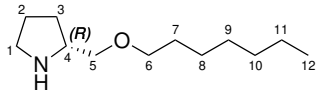

N-Boc-D-prolinyl *n*-heptyl ether (1.80 g, 6.00 mmol) was deprotected according to the general procedure.

Yield: 1.31 mg (6.00 mmol, quant., pale yellow oil)

Molecular weight: $C_{12}H_{25}NO$, 199.34 g/mol

All other analytical data of the (*R*,*R*)-enantiomer are in agreement with those of the (*S*,*S*)-enantiomer.

5.2.7 Synthesis of L-prolinyl *n*-octyl ether

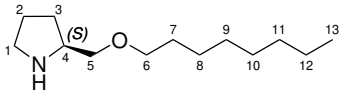

N-Boc-L-prolinyl *n*-octyl ether (888 mg, 2.83 mmol) was deprotected according to the general procedure.

Yield: 444 mg (2.08 mmol, 74 %, pale yellow oil)

Molecular weight: $C_{13}H_{27}NO$, 213.37 g/mol

^{1}H-NMR: (500 MHz, Chloroform-*d*, 298 K) δ [ppm] = 3.46-3.36 (m, 3H, H-5a, H-6), 3.36-3.28 (m, 2H, H-4, H-5b), 3.26 (br s, 1H, NH), 3.05-2.96 (m, 1H, H-1a), 2.94-2.86 (m, 1H, H-1b), 1.90-1.80 (m, 1H, H-3a), 1.80-1.67 (m, 2H, H-2), 1.60-1.49 (m, 2H, H-7), 1.49-1.38 (m, 1H, H-3b), 1.36-1.18 (m, 10H, H-8 to H-12), 0.86 (t, 3H, H-13, $^3J_{12,13}$ = 7.0 Hz).

^{13}C-NMR: (125 MHz, Chloroform-*d*, 298 K) δ [ppm] = 73.7 (C-5), 71.6 (C-6), 58.1 (C-4), 46.4 (C-1), 31.9, 29.8, 29.6, 29.4, 26.5, 22.8 (C-7 to C-12), 27.9 (C-3), 25.2 (C-2), 14.2 (C-13).

MS (ESI(+), Dichloromethane, M = $C_{13}H_{27}NO$) *m/z* = 172.17 $[M+H]^+$.

ESI HRMS: $[M+H]^+ = C_{13}H_{27}NOH^+$, calculated: m/z = 214.2165, found: m/z = 214.2165.

5.2.8 Synthesis of L-prolinyl *n*-nonyl ether

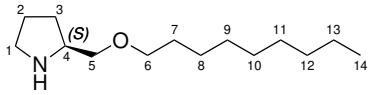

N-Boc-L-prolinyl *n*-nonyl ether (1.96 g, 5.50 mmol) was deprotected according to the general procedure.

Yield: 1.53 g (6.74 mmol, 84 %, pale yellow oil)

Molecular weight: $C_{14}H_{29}NO$, 227.39 g/mol

^{1}H-NMR: (400 MHz, Chloroform-*d*, 298 K) δ [ppm] = 4.80 (br s, 1H, NH), 3.77-3.69 (m, 1H, H-4), 3.62-3.49 (m, 2H, H-5), 3.49-3.37 (m, 2H, H-6), 3.30-3.20 (m, 2H, H-1), 2.13-1.90 (m, 3H, H-2, H-3a), 1.83-1.73 (m, 1H, H-3b), 1.57-1.49 (m, 2H, H-7), 1.34-1.19 (m, 12H, H-8 to H-13), 0.87 (t, 3H, H-14, $^3J_{13,14}$ = 6.9 Hz).

^{13}C-NMR: (125 MHz, Chloroform-*d*, 298 K) δ [ppm] = 71.8 (C-5), 70.0, (C-6), 58.7 (C-4), 45.7 (C-1), 32.0, 29.7, 29.6, 29.5, 29.4, 26.1, 22.8 (C-7 to C-13), 27.3 (C-3), 24.3 (C-2), 14.2 (C-14).

MS (ESI(+), Dichloromethane, M = $C_{14}H_{29}NO$) *m/z* = 455.46 $[2M+H]^+$, 228.23 $[M+H]^+$.

ESI HRMS: $[M+H]^+ = C_{14}H_{29}NOH^+$, calculated: m/z = 228.2322, found: m/z = 228.2310.

5.2.9 Synthesis of L-prolinyl *n*-decyl ether

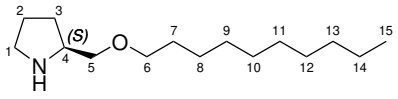

N-Boc-L-prolinyl *n*-decyl ether (1.97 g, 5.76 mmol) was deprotected according to the general procedure.

Yield: 1.39 g (5.76 mmol, quant., pale yellow oil)

Molecular weight: $C_{15}H_{31}NO$, 241.42 g/mol

^{1}H-NMR: (700 MHz, Chloroform-*d*, 298 K) δ [ppm] = 3.48-3.41 (m, 3H, H-5a, H-6), 3.41-3.33 (m, 2H, H-4, H-5b), 3.08-2.92 (m, 2H, H-1), 1.91-1.84 (m, 1H, H-3a), 1.84-1.73 (m, 1H, H-2), 1.59-1.53 (m, 2H, H-7), 1.53-1.45 (m, 1H, H-3b), 1.34-1.21 (m, 14H, H-8 to H-14), 0.87 (t, 3H, H-15, $^3J_{14,15}$ = 7.1 Hz).

^{13}C-NMR: (176 MHz, Chloroform-*d*, 298 K) δ [ppm] = 73.5 (C-5), 71.7 (C-6), 58.2 (C-4), 46.4 (C-1), 32.1, 29.8, 29.8, 29.7, 29.6, 29.5, 26.3, 22.8 (C-7 to C-14), 27.9 (C-3), 25.2 (C-2), 14.3 (C-15).

MS (ESI(+), Dichloromethane, M = $C_{15}H_{31}NO$) *m/z* = 242.25 $[M+H]^+$.

ESI HRMS: $[M+H]^+ = C_{15}H_{31}NOH^+$, calculated: m/z = 242.2478, found: m/z = 242.2480.

5.2.10 Synthesis of L-prolinyl *n*-undecyl ether

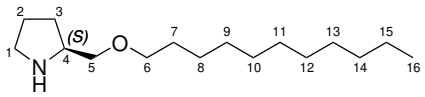

N-Boc-L-prolinyl *n*-undecyl ether (1.96 g, 5.50 mmol) was deprotected according to the general procedure.

Yield: 1.27 g (4.96 mmol, 90 %, pale yellow oil)

Molecular weight: $C_{16}H_{33}NO$, 255.45 g/mol

^{1}H-NMR: (500 MHz, Chloroform-*d*, 298 K) δ [ppm] = 4.00-3.87 (m, 1H, NH), 3.46-3.38 (m, 3H, H-5a, H-6), 3.38-3.30 (m, 2H, H-4, H-5b), 3.06-2.88 (m, 2H, H-1), 1.90-1.69 (m, 3H, H-2, H-3a), 1.58-1.50 (m, 2H, H-7), 1.50-1.42 (m, 1H, H-3b), 1.34-1.18 (m, 16H, H-8 to H-15), 0.86 (t, 3H, H-16, $^3J_{15,16}$ = 6.9 Hz).

^{13}C-NMR: (125 MHz, Chloroform-*d*, 298 K) δ [ppm] = 73.5 (C-5), 71.6 (C-6), 58.2 (C-4), 46.4 (C-1), 32.0, 29.8, 29.7, 29.7, 29.6, 29.5, 26.3, 22.8 (C-7 to C-15), 27.9 (C-3), 25.1 (C-2), 14.2 (C-16).

MS (ESI(+), Dichloromethane, M = $C_{16}H_{33}NO$) *m/z* = 256.265 $[M+H]^+$.

ESI HRMS: $[M+H]^+ = C_{16}H_{33}NOH^+$, calculated: m/z = 256.2635, found: m/z = 256.2623.

5.2.11 Synthesis of L-prolinyl *n*-dodecyl ether

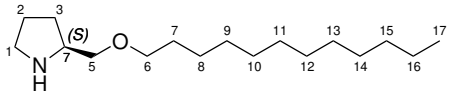

N-Boc-L-prolinyl *n*-dodecyl ether (1.09 g, 2.96 mmol) was deprotected according to the general procedure.

Yield: 787 mg (2.92 mmol, 99 %, pale yellow oil)

Molecular weight: $C_{17}H_{35}NO$, 269.47 g/mol

^{1}H-NMR: (500 MHz, Chloroform-*d*, 298 K) δ [ppm] = 4.07 (br s, 1H, NH), 3.54-3.33 (m, 5H, H-4, H-5, H-6) 3.16-2.98 (m, 2H, H-1), 2.00-1.65 (m, 3H, H-2, H-3a), 1.63-1.49 (m, 3H, H-3b, H-7), 1.36-1.17 (m, 18H, H-8 to H-16), 0.87 (t, 3H, H-17, $^3J_{16,17}$ = 6.9 Hz).

^{13}C-NMR: (125 MHz, Chloroform-*d*, 298 K) δ [ppm] = 72.5 (C-5), 71.7 (C-6), 58.3 (C-4), 46.3 (C-1), 32.1, 29.8, 29.8, 29.8, 29.8, 29.7, 29.6, 29.5, 26.2, 22.8 (C-7 to C-16), 27.8 (C-3), 25.0 (C-2), 14.3 (C-17).

MS (ESI(+), Dichloromethane, M = $C_{17}H_{35}NO$) *m/z* = 270.279 $[M+H]^+$.

ESI HRMS: $[M+H]^+ = C_{17}H_{35}NOH^+$, calculated: m/z = 270.2791, found: m/z = 270.2790.

5.2.12 Synthesis of L-prolinyl *n*-hexadecyl ether

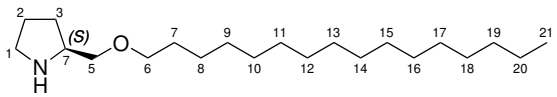

L-prolinyl *n*-hexadecyl ether was synthesized according to the literature.[26, 1]

5.3 General synthesis of squaraines

A round-bottom flask, equipped with a Dean-Stark apparatus and reflux condenser, is charged with the corresponding L-prolinyl *n*-alkyl ether (1.0 eq.) and phloroglucinol (1.00 eq.). The reactants are suspended in a mixture of toluene/1-butanol 1:1 (v/v, 10 mL/mmol) followed by degassing the mixture by 5 evacuation cycles under vigorous stirring and repressurizing with argon. The reaction mixture is refluxed under argon atmosphere for 16 hours. After cooling to room temperature, squaric acid (0.50 eq.) is added and the reaction mixture is heated to reflux for additional 16 hours. With the beginning of boiling, a sudden color change from slightly reddish over dark-green to dark-blue could be observed within minutes. The reaction mixture was slowly cooled to room temperature and stored at 4 °C overnight to promote crystallization. The intensely blue precipitate is filtered off and generously washed with methanol. The crude product is purified by column chromatography on silica gel (eluent: dichloromethane). The so-obtained deep blue solid is further purified by recrystallization from dichloromethane/methanol 1:2 (v/v) and dichloromethane/cyclohexane 1:2 (v/v). The precipitated solid was each time filtered off and washed several times with methanol. After drying under vacuum overnight, the squaraine dye is obtained as an intensively colored solid.

5.3.1 Synthesis of 2,4-Bis[4-(*S*)-(-)-2-(propyloxymethyl)-pyrrolidone-2,6-dihydroxyphenyl]squaraine (*S*,*S*)-ProSQ-C3

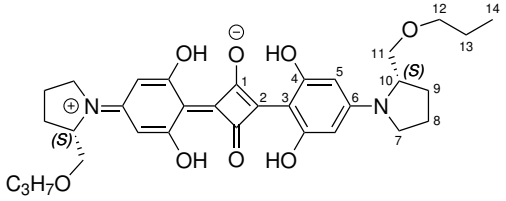

L-prolinyl *n*-propyl ether (500 mg, 3.50 mmol) was reacted according to the general procedure.

Yield: 132 mg (0.23 mmol, 13 %, deep-green solid with golden shine)

Molecular weight: $C_{32}H_{40}N_2O_8$, 580.68 g/mol

^{1}H-NMR: (700 MHz, Chloroform-*d*, 298 K) δ [ppm] = 11.01 (s, 4H, OH), 5.78 (br s, 4H, H-5), 4.09-4.04 (m, 2H, H-10), 3.55-3.49 (m, 4H, H-7a, H-11a), 3.44-3.31 (m, 8H, H-7b, H-11b, H-12), 2.17-2.06 (m, 4H, H-8a, H-9a), 2.06-1.96 (m, 4H, H-8b, H-9b), 1.61-1.54 (m, 4H, H-13), 0.92 (t, 6H, H-14, $^3J_{13,14}$ = 7.4 Hz).

^{13}C-NMR: (176 MHz, Chloroform-*d*, 298 K) δ [ppm] = 181.4 (C-2), 162.9 (C-4), 161.8 (C-1), 156.9 (C-3), 103.0 (C-6), 94.7 (C-5), 73.4 (C-12), 70.4 (C-11), 59.0 (C-10), 49.1 (C-7), 28.6 (C-9), 23.0 (C-13), 22.9 (C-8), 10.7 (C-14).

MS (ESI(+), Dichloromethane, M = $C_{32}H_{40}N_2O_8$) *m/z* = 580.28 $[M]^{\cdot+}$.

ESI HRMS: $[M]^{\cdot+}$ = $C_{32}H_{40}N_2O_8{}^{\cdot+}$, calculated: m/z = 580.2779, found: m/z = 580.2776.

UV/Vis: (Chloroform) λ_{max} = 646 nm, ε = 380800 $M^{-1}cm^{-1}$

Elemental analysis: $C_{32}H_{40}N_2O_8$ calculated C: 66.19, H: 6.94, N: 4.82; found C: 65.99, H: 7.06, N: 4.74.

5.3.2 Synthesis of 2,4-Bis[4-(*S*)-(-)-2-(butyloxymethyl)-pyrrolidone-2,6-dihydroxyphenyl]squaraine (*S*,*S*)-ProSQ-C4

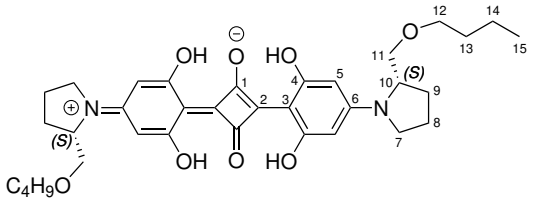

L-prolinyl *n*-butyl ether (865 mg, 5.50 mmol) was reacted according to the general procedure.

Yield: 38.2 mg (0.06 mmol, 2.3 %, ochre-brown solid)

Molecular weight: $C_{34}H_{44}N_2O_8$, 608.73 g/mol

^{1}H-NMR: (500 MHz, Chloroform-*d*, 298 K) δ [ppm] = 11.00 (s, 4H, OH), 5.77 (br s, 4H, H-5), 4.09-4.02 (m, 2H, H-10), 3.56-3.49 (m, 4H, H-7a, H-11a), 3.49-3.42 (m, 2H, H-12a), 3.42-3.35 (m, 4H, H-7b, H-12b), 3.35-3.29 (m, 2H,

H11b), 2.17-2.06 (m, 4H, H-8a, H-9a), 2.06-1.96 (m, 4H, H-8b, H-9b), 1.57-1.50 (m, 4H, H-13), 1.40-1.32 (m, 4H, H-14), 0.92 (t, 6H, H-15, $^3J_{14,15}$ = 7.4 Hz).

^{13}C-NMR: (125 MHz, Chloroform-*d*, 298 K) δ [ppm] = 181.4 (C-2), 162.8 (C-4), 161.7 (C-1), 156.9 (C-3), 103.0 (C-6), 94.7 (C-5), 71.6 (C-12), 70.4 (C-11), 59.0 (C-10), 49.1 (C-7), 31.9 (C-13), 28.6 (C-9), 22.9 (C-8), 19.5 (C-14), 14.1 (C-15).

MS (ESI(+), Dichloromethane, M = $C_{34}H_{44}N_2O_8$) *m/z* = 609.32 $[M+H]^+$.

ESI HRMS: $[M+H]^+ = C_{34}H_{44}N_2O_8H^+$, calculated: m/z = 609.3170, found: m/z = 609.3166.

UV/Vis: (Chloroform) λ_{max} = 646 nm, ε = 383400 $M^{-1}cm^{-1}$

Elemental analysis: $C_{34}H_{44}N_2O_8$ calculated C: 67.09, H: 7.29, N: 4.60; found C: 66.86, H: 7.36, N: 4.55.

5.3.3 Synthesis of 2,4-Bis[4-(*S*)-(-)-2-(pentyloxymethyl)-pyrrolidone-2,6-dihydroxyphenyl]squaraine (*S*,*S*)-ProSQ-C5

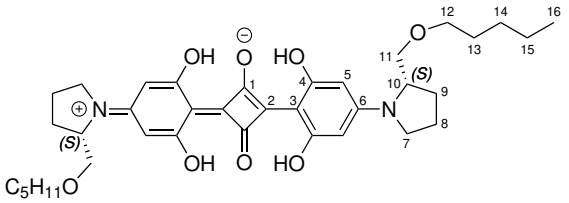

L-prolinyl *n*-pentyl ether (995 mg, 5.82 mmol) was reacted according to the general procedure.

Yield: 42 mg (0.07 mmol, 3 %, brown solid)

Molecular weight: $C_{36}H_{48}N_2O_8$, 636.79 g/mol

^{1}H-NMR: (500 MHz, Chloroform-*d*, 298 K) δ [ppm] = 11.02 (s, 4H, OH), 5.78 (br s, 4H, H-5), 4.10-4.03 (m, 2H, H-10), 3.57-3.48 (m, 4H, H-7a, H-11a), 3.48-3.42 (m, 2H, H-12a), 3.42-3.29 (m, 6H, H-7b, H-11b, H-12b), 2.18-2.06 (m, 4H, H-8a, H-9a), 2.06-1.94 (m, 4H, H-8b, H-9b), 1.61-1.50 (m, 4H, H-13), 1.38-1.26 (m, 8H, H-14, H-15), 0.90 (t, 6H, H-16, $^3J_{15,16}$ = 7.0 Hz).

^{13}C-NMR: (125 MHz, Chloroform-*d*, 298 K) δ [ppm] = 181.5 (C-2),

162.9 (C-4), 161.8 (C-1), 156.9 (C-3), 103.0 (C-6), 94.8 (C-5), 71.9 (C-12), 70.4 (C-11), 59.0 (C-10), 49.1 (C-7), 29.5 (C-13), 28.6 (C-9), 28.4 (C-14), 22.9 (C-8), 22.7 (C-15), 14.2 (C-16).

MS (ESI(+), Dichloromethane, M = $C_{36}H_{48}N_2O_8$) ***m/z*** **=** 637.35 $[M+H]^+$.

ESI HRMS: $[M+H]^+ = C_{36}H_{48}N_2O_8H^+$, calculated: $m/z = 637.3483$, found: $m/z = 637.3482$.

UV/Vis: (Chloroform) $\lambda_{max} = 646$ nm, $\varepsilon = 389300$ $M^{-1}cm^{-1}$

Elemental analysis: $C_{36}H_{48}N_2O_8 \cdot 0.3$ MeOH calculated C: 67.45, H: 7.67, N: 4.33; found C: 67.42, H: 7.68, N: 4.33.

5.3.4 Synthesis of 2,4-Bis[4-(*S*)-(-)-2-(hexyloxymethyl)-pyrrolidone-2,6-dihydroxyphenyl]squaraine (*S*,*S*)-ProSQ-C6

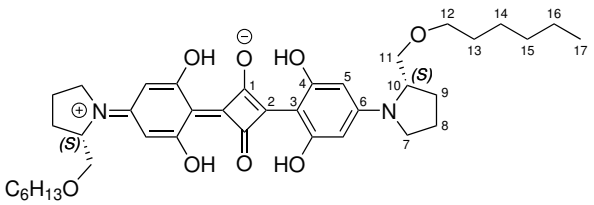

(*S*,*S*)-ProSQ-C6 was synthesized according to the literature.[26]

5.3.5 Synthesis of 2,4-Bis[4-(*S*)-(-)-2-(heptyloxymethyl)-pyrrolidone-2,6-dihydroxyphenyl]squaraine (*S*,*S*)-ProSQ-C7

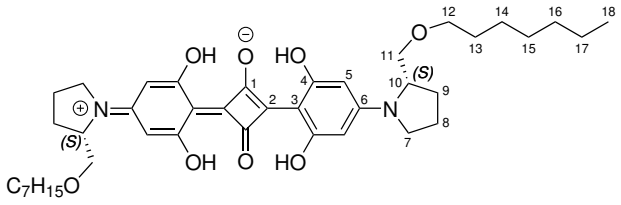

L-prolinyl *n*-heptyl ether (399 mg, 2.00 mmol) was reacted according to the general procedure.

Yield: 147 mg (0.21 mmol, 21 %, red solid)

Molecular weight: $C_{40}H_{56}N_2O_8$, 692.89 g/mol

^{1}H-NMR: (500 MHz, Chloroform-*d*, 298 K) δ [ppm] = 11.00 (s, 4H, OH), 5.77 (br s, 4H, H-5), 4.08-4.03 (m, 2H, H-10), 3.55-3.48 (m, 4H, H-7a, H-11a), 3.47-3.42 (m, 2H, H-12a), 3.40-3.34 (m, 4H, H-7b, H-12b), 3.34-3.30 (m, 2H, H-11b), 2.16-2.05 (m, 4H, H-8a, H-9a), 2.05-1.95 (m, 4H, H-8b, H-9b), 1.59-1.51 (m, 4H, H-13), 1.35-1.23 (m, 16H, H-14 to H-17), 0.88 (t, 6H, H-18, $^3J_{17,18}$ = 7.0 Hz).

^{13}C-NMR: (125 MHz, Chloroform-*d*, 298 K) δ [ppm] = 181.4 (C-2), 162.8 (C-4), 161.7 (C-1), 156.9 (C-3), 103.0 (C-6), 94.7 (C-5), 71.9 (C-12), 70.4 (C-11), 59.0 (C-10), 49.0 (C-7), 32.0, 29.8, 29.3, 26.2, 22.8 (C-13 to C-17), 28.6 (C-9), 22.9 (C-8), 14.2 (C-18).

MS (ESI(+), Dichloromethane, M = $C_{40}H_{56}N_2O_8$) *m/z* = 692.40 $[M]^{\cdot+}$.

ESI HRMS: $[M]^{\cdot+}$ = $C_{40}H_{56}N_2O_8H^+$, calculated: m/z = 692.4031, found: m/z = 692.4033.

UV/Vis: (Chloroform) λ_{max} = 646 nm, ε = 375400 $M^{-1}cm^{-1}$

Elemental analysis: $C_{40}H_{56}N_2O_8$ calculated C: 69.34, H: 8.15, N: 4.04; found C: 69.37, H: 8.15, N: 4.06.

5.3.6 Synthesis of 2,4-Bis[4-(*R*)-(-)-2-(heptyloxymethyl)-pyrrolidone-2,6-dihydroxyphenyl]squaraine (*R,R*)-ProSQ-C7

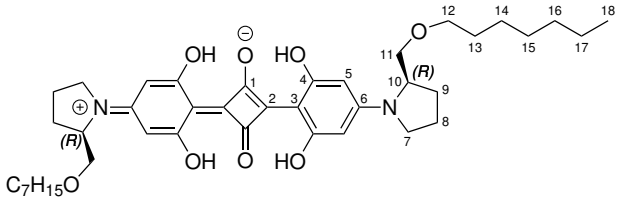

D-prolinyl *n*-heptyl ether (923 mg, 5.00 mmol) was reacted according to the general procedure.

Yield: 254 mg (0.37 mmol, 15 %, red solid)

Molecular weight: $C_{40}H_{56}N_2O_8$, 692.89 g/mol

All other analytical data of the (*R*,*R*)-enantiomer are in agreement with those of the (*S*,*S*)-enantiomer.

5.3.7 Synthesis of 2,4-Bis[4-(*S*)-(-)-2-(octyloxymethyl)-pyrrolidone-2,6-dihydroxyphenyl]squaraine (*S*,*S*)-ProSQ-C8

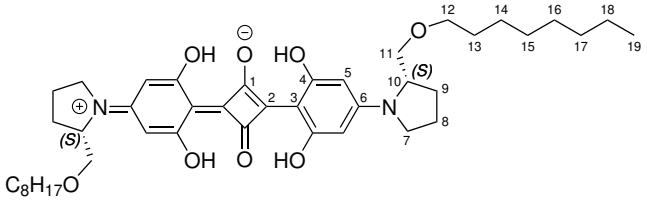

L-prolinyl *n*-octyl ether (411 mg, 1.93 mmol) was reacted according to the general procedure.

Yield: 105 mg (0.15 mmol, 17 %, red solid)

Molecular weight: $C_{42}H_{60}N_2O_8$, 720.95 g/mol

^{1}H-NMR: (500 MHz, Chloroform-*d*, 298 K) δ [ppm] = 11.02 (s, 4H, OH), 5.78 (br s, 4H, H-5), 4.12-4.00 (m, 2H, H-10), 3.61-3.48 (m, 4H, H-7a, H-11a), 3.48-3.41 (m, 2H, H-12a), 3.41-3.34 (m, 4H, H-7b, H-12b), 3.34-3.27 (m, 2H, H-11b), 2.22-2.07 (m, 4H, H-8a, H-9a), 2.07-1.91 (m, 4H, H-11b, H-8b), 1.63-1.47 (m, 4H, H-13), 1.40 1.14 (m, 20H, H-14 to H-18), 0.88 (t, 6H, H-19, $^3J_{18,19}$ = 6.6 Hz).

^{13}C-NMR: (125 MHz, Chloroform-*d*, 298 K) δ [ppm] = 181.5 (C-2), 162.9 (C-4), 161.8 (C-1), 156.9 (C-3), 103.0 (C-6), 94.8 (C-5), 71.9 (C-12), 70.4 (C-11), 59.0 (C-10), 49.1 (C-7), 32.0 (C-17), 29.8, 29.6, 29.4 (C-13, C-15, C-16), 28.6 (C-9), 26.3 (C-14), 22.9 (C-8), 22.8 (C-18), 14.3 (C-19).

MS (ESI(+), Dichloromethane, M = $C_{42}H_{60}N_2O_8$) *m/z* = 720.434 $[M]^{\cdot+}$, 577.291 $[M\text{-}C_9H_{19}O]^{\cdot+}$.

ESI HRMS: $[M]^{\cdot+} = C_{42}H_{60}N_2O_8H^{\cdot+}$, calculated: m/z = 720.4344, found: m/z = 720.4345.

UV/Vis: (Chloroform) λ_{max} = 646 nm, ε = 438000 $M^{-1}cm^{-1}$

Elemental analysis: $C_{42}H_{60}N_2O_8$ calculated C: 69.97, H: 8.39, N: 3.89; found C: 69.47, H: 8.44, N: 3.85.

5.3.8 Synthesis of 2,4-Bis[4-(*S*)-(-)-2-(nonyloxymethyl)-pyrrolidone-2,6-dihydroxyphenyl]squaraine (*S*,*S*)-ProSQ-C9

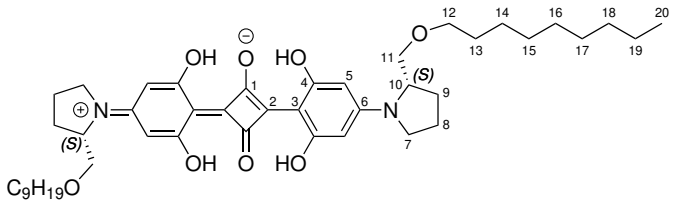

L-prolinyl *n*-nonyl ether (1.08 g, 4.75 mmol) was reacted according to the general procedure.

Yield: 456 mg (0.61 mmol, 26 %, red solid)

Molecular weight: $C_{44}H_{64}N_2O_8$, 749.00 g/mol

^{1}H-NMR: (500 MHz, Chloroform-*d*, 298 K) δ [ppm] = 11.01 (s, 4H, OH), 5.77 (br s, 4H, H-5), 4.09-4.03 (m, 2H, H-10), 3.56-3.48 (m, 4H, H-7a, H-11a), 3.48-3.42 (m, 2H, H-12a), 3.40-3.35 (m, 4H, H-7b, H-12b), 3.34-3.30 (m, 2H, H-11b), 2.16-2.06 (m, 4H, H-8a, H-9a), 2.06-1.96 (m, 4H, H-8b, H-9b), 1.57-1.51 (m, 6H, H-13), 1.36-1.19 (m, 24H, H-14 to H-19), 0.88 (t, 6H, H-20, $^3J_{19,20}$ = 7.0 Hz).

^{13}C-NMR: (125 MHz, Chloroform-*d*, 298 K) δ [ppm] = 181.4 (C-2), 162.8 (C-4), 161.7 (C-1), 156.9 (C-3), 103.0 (C-6), 94.8 (C-5), 71.9 (C-12), 70.4 (C-11), 59.0 (C-10), 49.1 (C-7), 32.0 (C-18), 29.8, 29.7, 29.6, 29.4 (C-13, C-15 to C-17), 28.6 (C-9), 26.3 (C-14), 22.9 (C-8), 22.8 (C-19), 14.3 (C-20).

MS (ESI(+), Dichloromethane, M = $C_{44}H_{64}N_2O_8$) *m/z* = 749.47 $[M]^+$

ESI HRMS: $[M]^+ = C_{44}H_{64}N_2O_8H^+$, calculated: m/z = 749.4737, found: m/z = 749.4735.

UV/Vis: (Chloroform) λ_{max} = 646 nm, ε = 367700 $M^{-1}cm^{-1}$

Elemental analysis: $C_{44}H_{64}N_2O_8$ calculated C: 70.56, H: 8.61, N: 3.74; found C: 70.73, H: 8.69, N: 3.72.

5.3.9 Synthesis of 2,4-Bis[4-(*S*)-(-)-2-(decyloxymethyl)-pyrrolidone-2,6-dihydroxyphenyl]squaraine (*S*,*S*)-ProSQ-C10

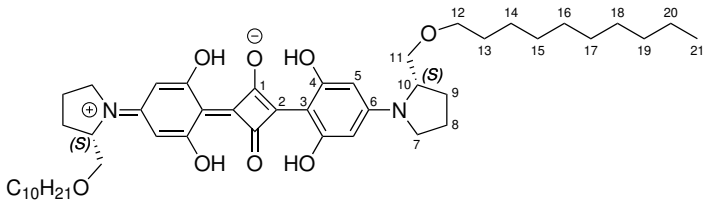

L-prolinyl *n*-decyl ether (1.10 g, 4.55 mmol) was reacted according to the general procedure.

Yield: 271 mg (0.35 mmol, 15 %, red solid)

Molecular weight: $C_{46}H_{68}N_2O_8$, 777.06 g/mol

^{1}H-NMR: (500 MHz, Chloroform-*d*, 298 K) δ [ppm] = 11.02 (s, 4H, OH), 5.78 (br s, 4H, H-5), 4.10-4.03 (m, 2H, H-10), 3.57-3.48 (m, 4H, H-7a, H-11a), 3.48-3.41 (m, 2H, H-12a), 3.41-3.29 (m, 6H, H-7b, H-11b, H-12b), 2.17-2.06 (m, 4H, H-8a, H-9a), 2.06-1.96 (m, 4H, H-8b, H-9b), 1.59-1.50 (m, 4H, H-13), 1.36-1.20 (m, 28H, H-14 to H-20), 0.88 (t, 6H, H-21, $^3J_{20,21}$ = 7.0 Hz).

^{13}C-NMR: (125 MHz, Chloroform-*d*, 298 K) δ [ppm] = 181.5 (C-2), 162.9 (C-4), 161.8 (C-1), 156.9 (C-3), 103.0 (C-6), 94.8 (C-5), 71.9 (C-12), 70.4 (C-11), 59.0 (C-10), 49.1 (C-7), 32.1, 29.8, 29.8, 29.7, 29.6, 29.5, 26.3, 22.9 (C-13 to C-20), 28.6 (C-9), 22.9 (C-8), 14.3 (C-21).

MS (ESI(+), Dichloromethane, M = $C_{46}H_{68}N_2O_8$) *m/z* = 777.50 $[M+H]^+$

ESI HRMS: $[M]^+ = C_{46}H_{68}N_2O_8H^+$, calculated: m/z = 777.5048, found: m/z = 777.5049.

UV/Vis: (Chloroform) λ_{max} = 646 nm, ε = 361000 $M^{-1}cm^{-1}$

Elemental analysis: $C_{46}H_{68}N_2O_8$ calculated C: 71.10, H: 8.82, N: 3.61; found C: 71.27, H: 8.95, N: 3.60.

5.3.10 Synthesis of 2,4-Bis[4-(*S*)-(-)-2-(undecyloxymethyl)-pyrrolidone-2,6-dihydroxyphenyl]squaraine (*S*,*S*)-ProSQ-C11

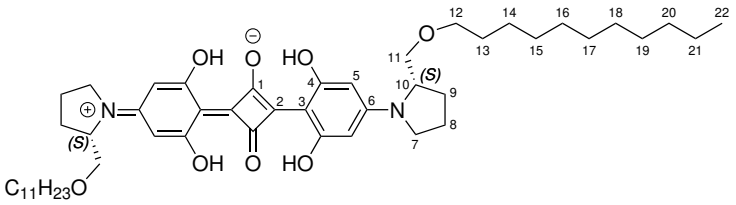

L-prolinyl *n*-undecyl ether (1.02 g, 4.00 mmol) was reacted according to the general procedure.

Yield: 165 mg (0.20 mmol, 5 %, red solid)

Molecular weight: $C_{48}H_{72}N_2O_8$, 805.11 g/mol

^{1}H-NMR: (700 MHz, Chloroform-*d*, 298 K) δ [ppm] = 11.02 (s, 4H, OH), 5.78 (br s, 4H, H-5), 4.09-4.04 (m, 2H, H-10), 3.56-3.49 (m, 4H, H-7a, H-11a), 3.47-3.42 (m, 2H, H-12a), 3.41-3.35 (m, 4H, H-7b, H-12b), 3.35-3.30 (m, 2H, H-11b), 2.16-2.07 (m, 4H, H-8a, H-9a), 2.06-1.96 (m, 4H, H-8b, H-9b), 1.58-1.52 (m, 4H, H-13), 1.34-1.23 (m, 32H, H-14 to H-21), 0.88 (t, 6H, H-22, $^3J_{21,22}$ = 7.0 Hz).

^{13}C-NMR: (176 MHz, Chloroform-*d*, 298 K) δ [ppm] = 181.5 (C-2), 162.9 (C-4), 161.8 (C-1), 156.9 (C-3), 103.0 (C-6), 94.8 (C-5), 71.9 (C-12), 70.4 (C-11), 59.0 (C-10), 49.1 (C-7), 32.1 (C-20), 29.8, 29.8, 29.8, 29.6, 29.5 (C-13, C-15 to C-19), 28.6 (C-9), 26.3 (C-14), 22.9 (C-8), 22.9 (C-21), 14.3 (C-22).

MS (ESI(+), Dichloromethane, M = $C_{48}H_{72}N_2O_8$) *m/z* = 804.53 $[M]^{\cdot+}$, 619.34 $[M\text{-}C_{12}H_{25}O]^{\cdot+}$

ESI HRMS: $[M]^+ = C_{48}H_{72}N_2O_8^{\cdot+}$, calculated: m/z = 804.5283, found: m/z = 804.5283.

UV/Vis: (Chloroform) λ_{max} = 646 nm, ε = 382000 $M^{-1}cm^{-1}$

Elemental analysis: $C_{48}H_{72}N_2O_8$ calculated C: 71.61, H: 9.01, N: 3.48; found C: 71.35, H: 9.05, N: 3.33.

5.3.11 Synthesis of 2,4-Bis[4-(*S*)-(-)-2-(dodecyloxymethyl)-pyrrolidone-2,6-dihydroxyphenyl]squaraine (*S*,*S*)-ProSQ-C12

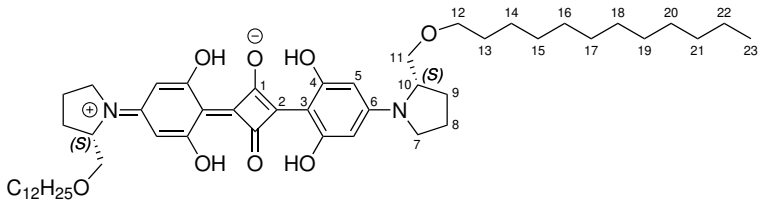

L-prolinyl *n*-dodecyl ether (719 mg, 2.67 mmol) was reacted according to the general procedure.

Yield: 226 mg (0.27 mmol, 22 %, violet solid)

Molecular weight: $C_{50}H_{76}N_2O_8$, 833.17 g/mol

^{1}H-NMR: (500 MHz, Chloroform-*d*, 298 K) δ [ppm] = 11.02 (s, 4H, OH), 5.78 (br s, 4H, H-5), 4.10-4.01 (m, 2H, H-10), 3.57-3.48 (m, 4H, H-7a, H-11a), 3.48-3.41 (m, 2H, H-12a), 3.41-3.35 (m, 4H, H-7b, H-12b), 3.35-3.29 (m, 2H, H-11b), 2.20-2.07 (m, 4H, H-8a, H-9a), 2.07-1.94 (m, 4H, H-7b, H-9b), 1.61-1.48 (m, 4H, H-13), 1.37-1.16 (m, 36H, H-14 to H-22), 0.88 (t, 6H, H-23, $^3J_{22,23}$ = 7.0 Hz).

^{13}C-NMR: (125 MHz, Chloroform-*d*, 298 K) δ [ppm] = 181.5 (C-2), 162.9 (C-4), 161.8 (C-1), 156.9 (C-3), 103.0 (C-6), 94.8 (C-5), 71.9 (C-12), 70.4 (C-11), 59.0 (C-10), 49.1 (C-7), 32.1 (C-21), 29.8, 29.8, 29.8, 29.8, 29.8, 29.6, 29.5 (C-13, C-16 to C-20), 28.6 (C-9), 26.3 (C-14), 22.9 (C-8), 22.8 (C-22), 14.3 (C-23).

MS (ESI(+), Dichloromethane, M = $C_{50}H_{76}N_2O_8$) *m/z* = 832.56 $[M]^{\cdot+}$

ESI HRMS: $[M]^+$ = $C_{50}H_{76}N_2O_8^{\cdot+}$, calculated: m/z = 832.5596, found: m/z = 832.5597.

UV/Vis: (Chloroform) λ_{max} = 646 nm, ε = 408000 $M^{-1}cm^{-1}$

Elemental analysis: $C_{50}H_{76}N_2O_8$ calculated C: 72.08, H: 9.19, N: 3.36; found C: 71.92, H: 9.30, N: 3.22.

5.3.12 Synthesis of 2,4-Bis[4-(*S*)-(-)-2-(hexadecyloxymethyl)-pyrrolidone-2,6-dihydroxyphenyl]squaraine (*S*,*S*)-ProSQ-C16

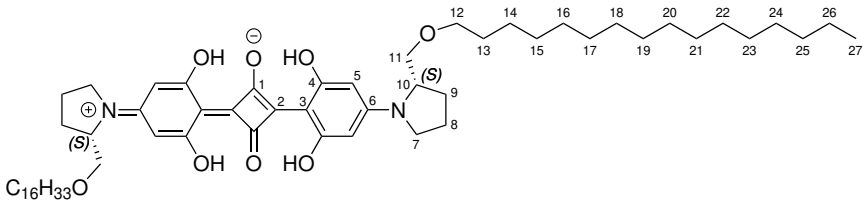

(*S*,*S*)-ProSQ-C16 was synthesized according to the literature.[26, 1]

References

[1] Matthias Schulz et al. "Giant intrinsic circular dichroism of prolinol-derived squaraine thin films". In: *Nat. Commun.* 9.2413 (2018), p. 2413.

[2] Kasha, M. "Energy Transfer Mechanism and the Molecular Exciton Model for Molecular Aggregates". In: *Radiat. Res.* 3 (1964), pp. 317–331.

[3] Spano, F. C. "The Spectral Signatures of Frenkel Polarons in H- and J-Aggregates". In: *Acc. Chem. Res.* 43.3 (2010), pp. 429–439. DOI: 10.1021/ar900233v.

[4] M. Anzola, F. Di Maiolo, and A. Painelli. "Optical spectra of molecular aggregates and crystals: testing approximation schemes". In: *Phys. Chem. Chem. Phys.* 21.36 (2019), pp. 19816–19824. DOI: 10.1039/c9cp03122g.

[5] Sabnam Kar et al. "Emergence of Chiroptical Properties in Molecular Assemblies of Phenyleneethynylenes: The Role of Quasi-degenerate Excitations". In: *J. Phys. Chem. Lett.* 9.16 (2018), pp. 4584–4590. DOI: 10.1021/acs.jpclett.8b01988.

[6] Nicholas J Hestand et al. "Confirmation of the origins of panchromatic spectra in squaraine thin films targeted for organic photovoltaic devices". In: *J. of Phys. Chem. C* 119.33 (2015), pp. 18964–18974.

[7] C. Caleman et al. “Force field benchmark of organic liquids: density, enthalpy of vaporization, heat capacities, surface tension, isothermal compressibility, volumetric expansion coefficient, and dielectric constant”. In: *J. Chem. Theory Comput.* 8 (2012), p. 61.

[8] William L. Jorgensen et al. “Comparison of simple potential functions for simulating liquid water”. In: *J. Chem. Phys.* 79.2 (1983), pp. 926–935. DOI: 10.1063/1.445869. eprint: https://doi.org/10.1063/1.445869. URL: https://doi.org/10.1063/1.445869.

[9] Berk Hess et al. “LINCS: A linear constraint solver for molecular simulations”. In: *J. Comp. Chem.* 18.12 (1997), pp. 1463–1472.

[10] Giovanni Bussi. “Hamiltonian replica exchange in GROMACS: a flexible implementation”. In: *Molecular Physics* 112.3-4 (2014), pp. 379–384. DOI: 10.1080/00268976.2013.824126. eprint: https://doi.org/10.1080/00268976.2013.824126. URL: https://doi.org/10.1080/00268976.2013.824126.

[11] David Van Der Spoel et al. “GROMACS: Fast, flexible, and free”. In: *J. Comp. Chem.* 26.16 (2005), pp. 1701–1718. DOI: https://doi.org/10.1002/jcc.20291. eprint: https://onlinelibrary.wiley.com/doi/pdf/10.1002/jcc.20291. URL: https://onlinelibrary.wiley.com/doi/abs/10.1002/jcc.20291.

[12] Gareth A. Tribello et al. “PLUMED 2: New feathers for an old bird”. In: *Computer Physics Communications* 185.2 (2014), pp. 604–613. ISSN: 0010-4655. DOI: https://doi.org/10.1016/j.cpc.2013.09.018. URL: https://www.sciencedirect.com/science/article/pii/S0010465513003196.

[13] J. Wang et al. “Development and Testing of a General Amber Force Field”. In: *J. Comput. Chem.* 25 (2004), p. 1157.

[14] M. J. Frisch et al. *GaussianË16 Revision C.01*. Gaussian Inc. Wallingford CT. 2016.

[15] C. I. Bayly et al. “A Well-Behaved Electrostatic Potential Based Method Using Charge Restraints for Deriving Atomic Charges: the RESP Model”. In: *J. Phys. Chem.* 97 (1993), p. 10269.

[16] P. J. Stephens et al. “Ab Initio Calculation of Vibrational Absorption and Circular Dichroism Spectra Using Density Functional Force Fields”. In: *J. Phys. Chem.* 98.45 (1994), pp. 11623–11627. DOI: 10.1021/j100096a001. eprint: https://doi.org/10.1021/j100096a001. URL: https://doi.org/10.1021/j100096a001.

[17] Nicola Jane Boyd and Mark R. Wilson. “Validating an optimized GAFF force field for liquid crystals: TNI predictions for bent-core mesogens and the first atomistic predictions of a dark conglomerate phase”. In: *Phys. Chem. Chem. Phys.* 20 (3 2018), pp. 1485–1496. DOI: 10.1039/C7CP07496D. URL: http://dx.doi.org/10.1039/C7CP07496D.

[18] Naveen Michaud-Agrawal et al. “MDAnalysis: A toolkit for the analysis of molecular dynamics simulations”. In: *J. Comp. Chem.* 32.10 (2011), pp. 2319–2327. DOI: https://doi.org/10.1002/jcc.21787. eprint: https://onlinelibrary.wiley.com/doi/pdf/10.1002/jcc.21787. URL: https://onlinelibrary.wiley.com/doi/abs/10.1002/jcc.21787.

[19] Richard J. Gowers et al. “MDAnalysis: A Python Package for the Rapid Analysis of Molecular Dynamics Simulations”. In: *Proceedings of the 15th Python in Science Conference*. Ed. by Sebastian Benthall and Scott Rostrup. 2016, pp. 98–105. DOI: 10.25080/Majora-629e541a-00e.

[20] Maria dâErrico et al. “Automatic topography of high-dimensional data sets by non-parametric density peak clustering”. In: *Information Sciences* 560 (2021), pp. 476–492. ISSN: 0020-0255. DOI: https://doi.org/10.1016/j.ins.2021.01.010. URL: https://www.sciencedirect.com/science/article/pii/S0020025521000116.

[21] Frank Neese. “Software update: The ORCA program systemâVersion 5.0”. In: *WIREs Computational Molecular Science* 12.5 (2022), e1606. DOI: https://doi.org/10.1002/wcms.1606. eprint: https://wires.onlinelibrary.wiley.com/doi/pdf/10.1002/wcms.1606. URL: https://wires.onlinelibrary.wiley.com/doi/abs/10.1002/wcms.1606.

[22] Rebecca Sure and Stefan Grimme. “Corrected small basis set Hartree-Fock method for large systems”. In: *Journal of Computational Chemistry* 34.19

(2013), pp. 1672–1685. DOI: https://doi.org/10.1002/jcc.23317. eprint: https://onlinelibrary.wiley.com/doi/pdf/10.1002/jcc.23317. URL: https://onlinelibrary.wiley.com/doi/abs/10.1002/jcc.23317.

[23] Stefan Grimme et al. "Consistent structures and interactions by density functional theory with small atomic orbital basis sets". In: *The Journal of Chemical Physics* 143.5 (2015), p. 054107. DOI: 10.1063/1.4927476. eprint: https://doi.org/10.1063/1.4927476. URL: https://doi.org/10.1063/1.4927476.

[24] Stefan Grimme, Stephan Ehrlich, and Lars Goerigk. "Effect of the damping function in dispersion corrected density functional theory". In: *Journal of Computational Chemistry* 32.7 (2011), pp. 1456–1465. DOI: https://doi.org/10.1002/jcc.21759. eprint: https://onlinelibrary.wiley.com/doi/pdf/10.1002/jcc.21759. URL: https://onlinelibrary.wiley.com/doi/abs/10.1002/jcc.21759.

[25] Takeshi Yanai, David P Tew, and Nicholas C Handy. "A new hybrid exchangeâcorrelation functional using the Coulomb-attenuating method (CAM-B3LYP)". In: *Chemical Physics Letters* 393.1 (2004), pp. 51–57. ISSN: 0009-2614. DOI: https://doi.org/10.1016/j.cplett.2004.06.011. URL: https://www.sciencedirect.com/science/article/pii/S0009261404008620.

[26] Matthias Schulz et al. "Organic photodiodes from homochiral L-proline derived squaraine compounds with strong circular dichroism". In: *Phys. Chem. Chem. Phys.* 19.10 (2017), pp. 6996–7008.

6 NMR and mass spectra

6.1 NMR spectra

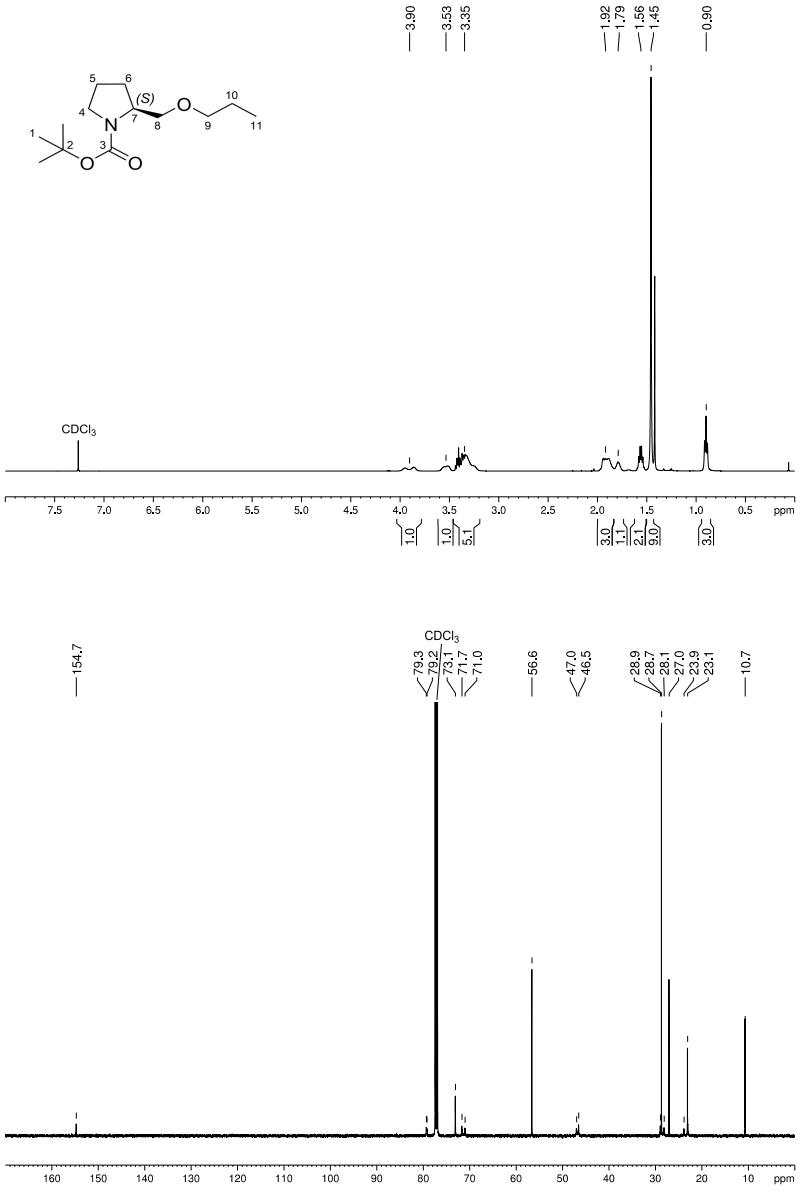

Figure S21: ^{1}H- (top, 500 MHz) and ^{13}C-NMR (bottom, 125 MHz) spectrum of *N*-Boc-L-prolinyl *n*-propyl ether; $CDCl_3$, 298 K.

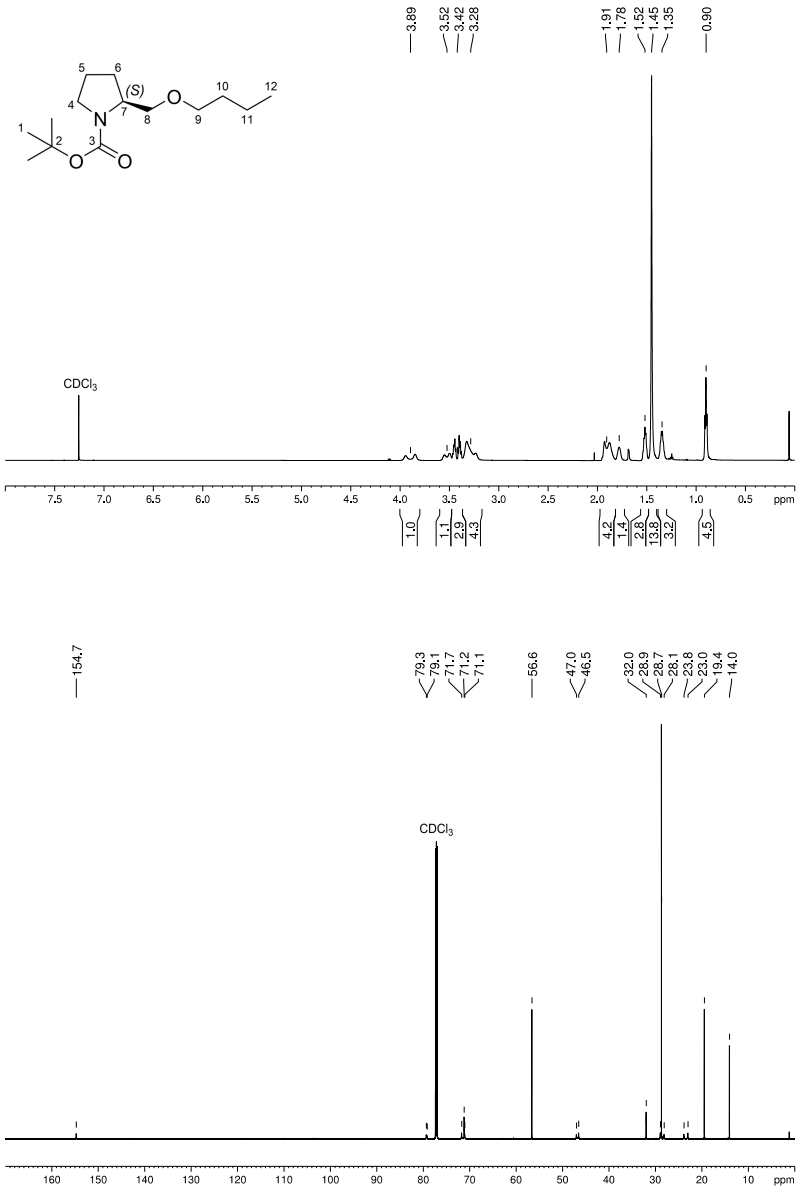

Figure S22: ^{1}H- (top, 700 MHz) and ^{13}C-NMR (bottom, 176 MHz) spectrum of *N*-Boc-L-prolinyl *n*-butyl ether; $CDCl_3$, 298 K.

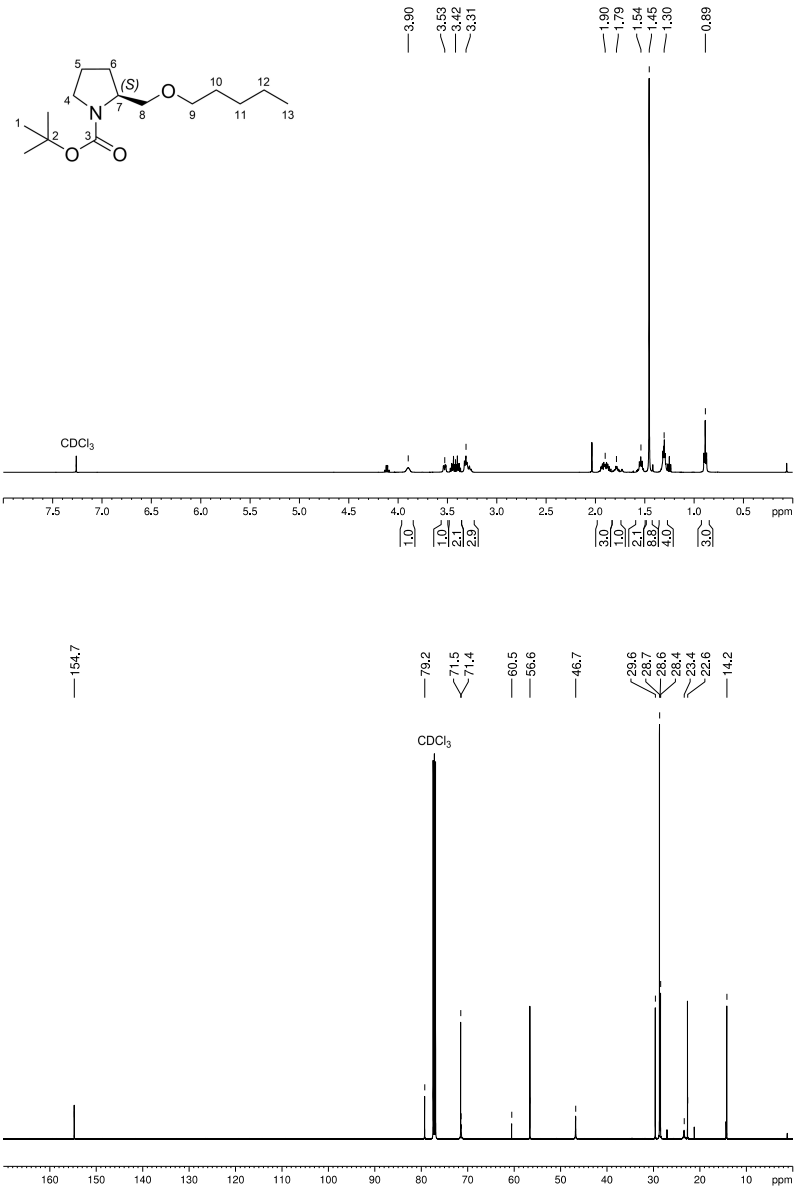

Figure S23: ^{1}H- (top, 500 MHz) and ^{13}C-NMR (bottom, 125 MHz) spectrum of *N*-Boc-L-prolinyl *n*-pentyl ether; $CDCl_3$, 298 K.

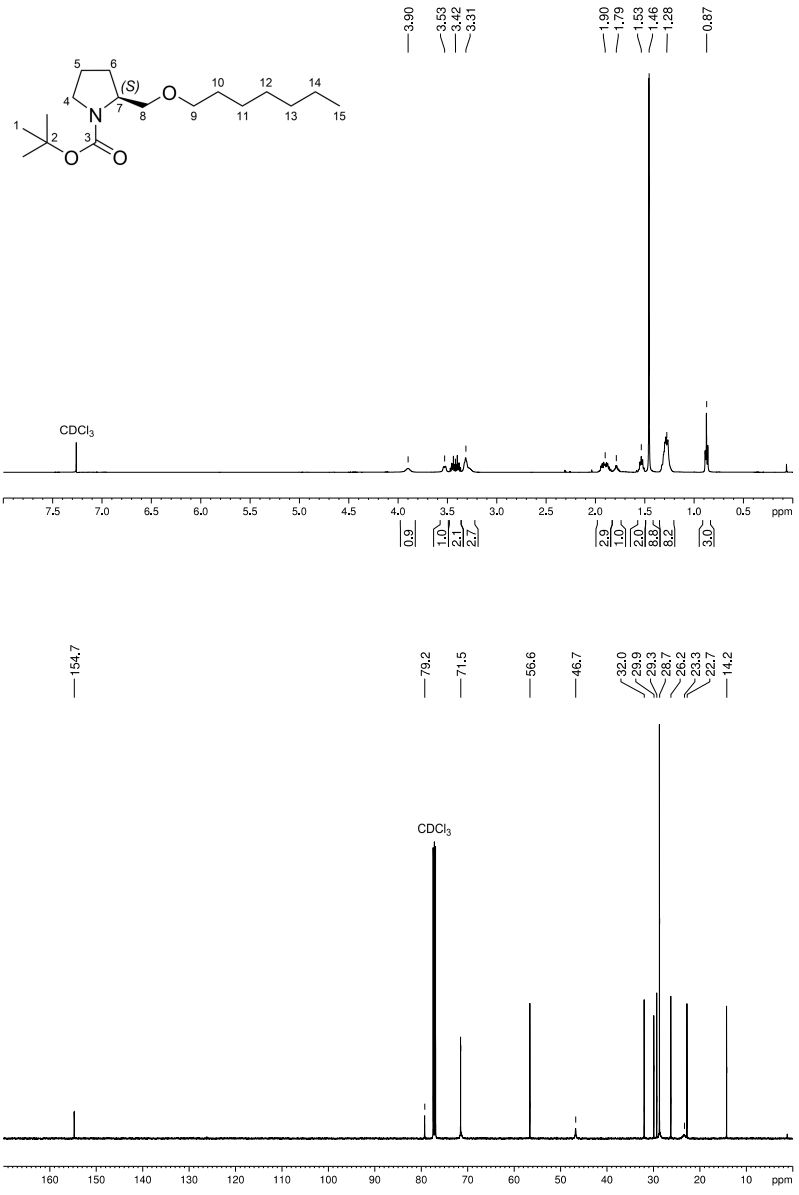

Figure S24: ^{1}H- (top, 500 MHz) and ^{13}C-NMR (bottom, 125 MHz) spectrum of *N*-Boc-L-prolinyl *n*-heptyl ether; $CDCl_3$, 298 K.

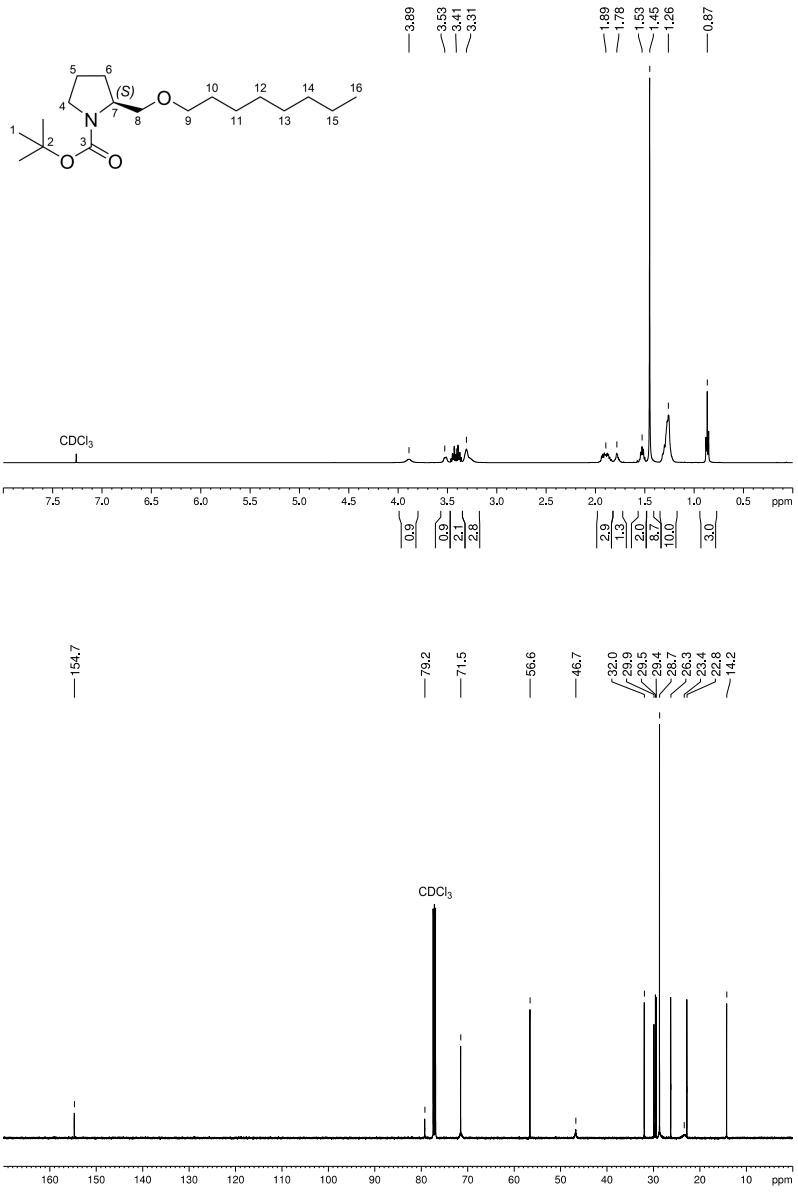

Figure S25: ^{1}H- (top, 500 MHz) and ^{13}C-NMR (bottom, 125 MHz) spectrum of *N*-Boc-L-prolinyl *n*-octyl ether; $CDCl_3$, 298 K.

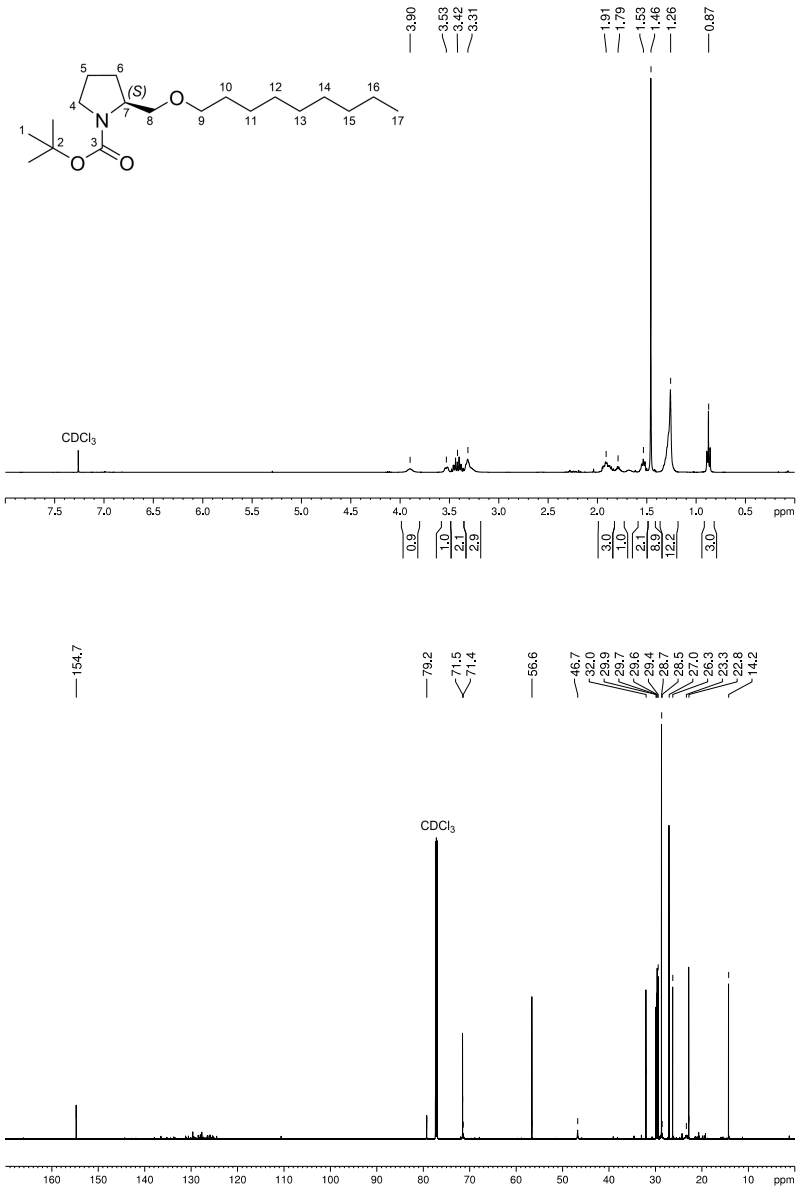

Figure S26: ^{1}H- (top, 700 MHz) and ^{13}C-NMR (bottom, 176 MHz) spectrum of *N*-Boc-L-prolinyl *n*-nonyl ether; $CDCl_3$, 298 K.

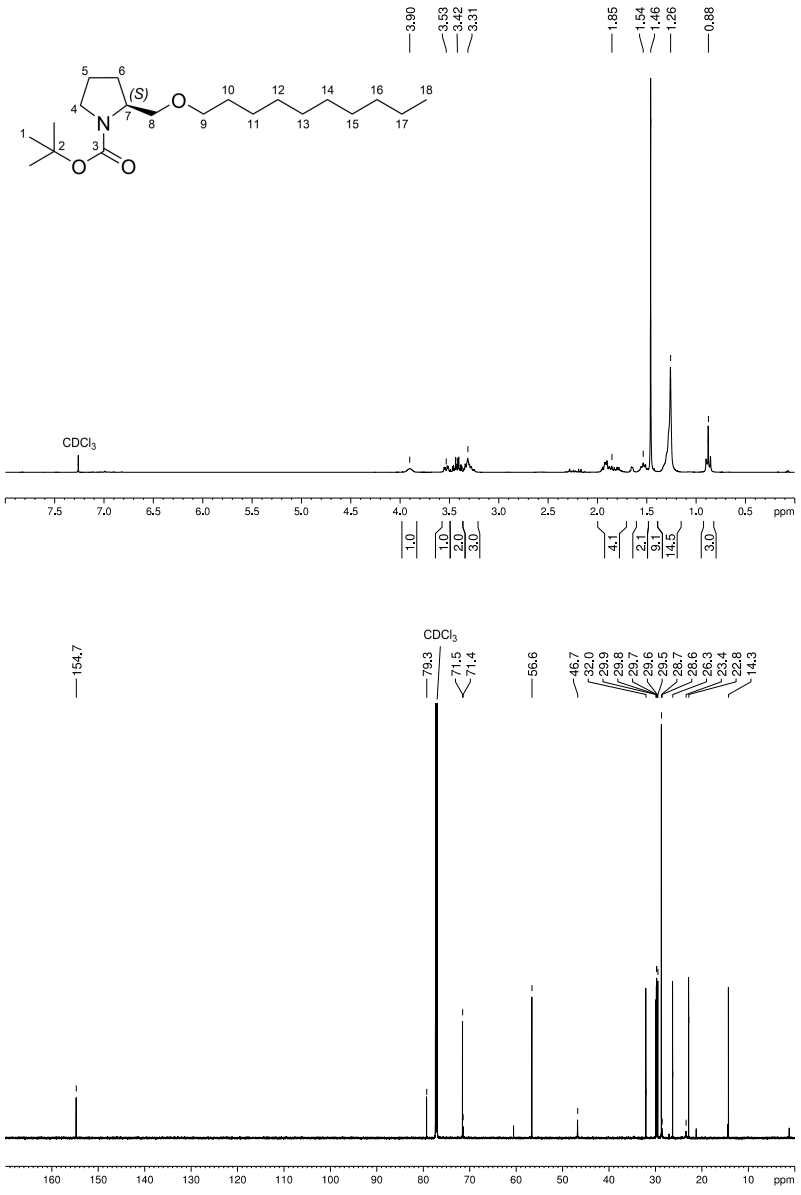

Figure S27: ^{1}H- (top, 700 MHz) and ^{13}C-NMR (bottom, 176 MHz) spectrum of *N*-Boc-L-prolinyl *n*-decyl ether; $CDCl_3$, 298 K.

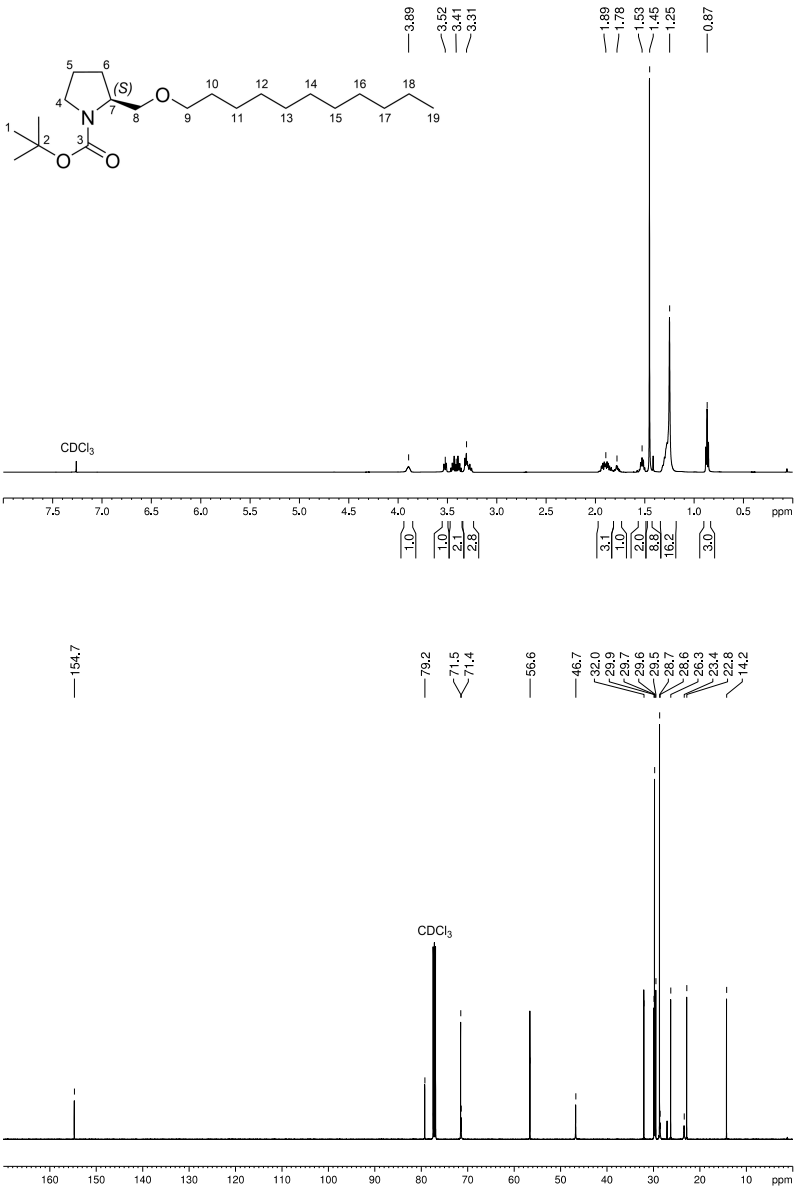

Figure S28: ^{1}H- (top, 500 MHz) and ^{13}C-NMR (bottom, 125 MHz) spectrum of *N*-Boc-L-prolinyl *n*-undecyl ether; $CDCl_3$, 298 K.

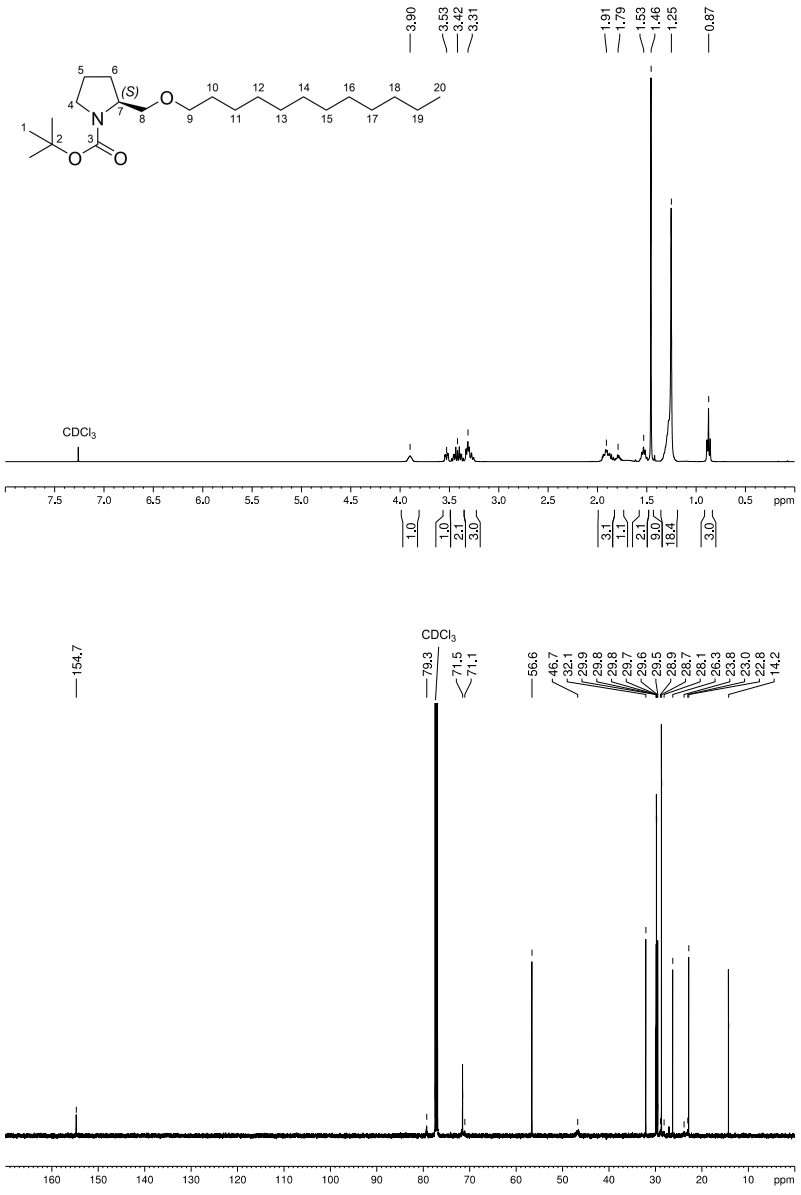

Figure S29: ^{1}H- (top, 400 MHz) and ^{13}C-NMR (bottom, 125 MHz) spectrum of *N*-Boc-L-prolinyl *n*-dodecyl ether; $CDCl_3$, 298 K.

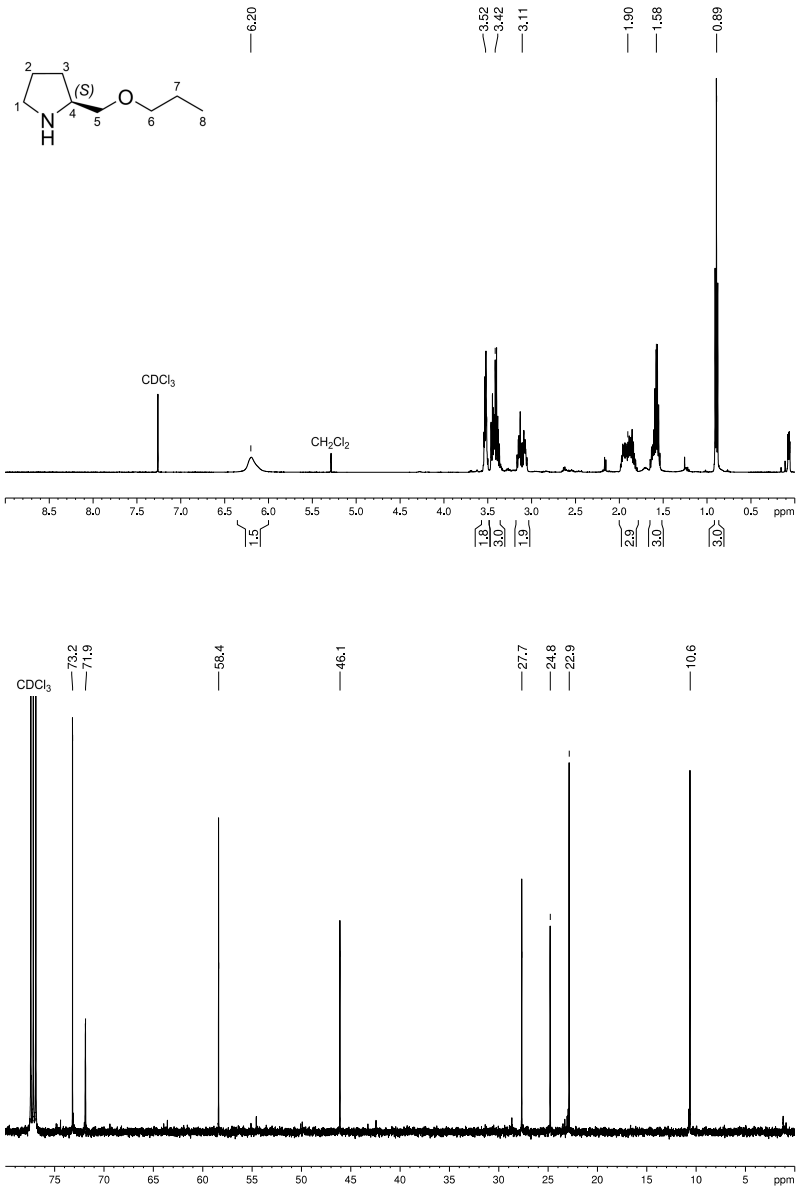

Figure S30: ^{1}H- (top, 500 MHz) and ^{13}C-NMR (bottom, 125 MHz) spectrum of L-prolinyl *n*-propyl ether; $CDCl_3$, 298 K.

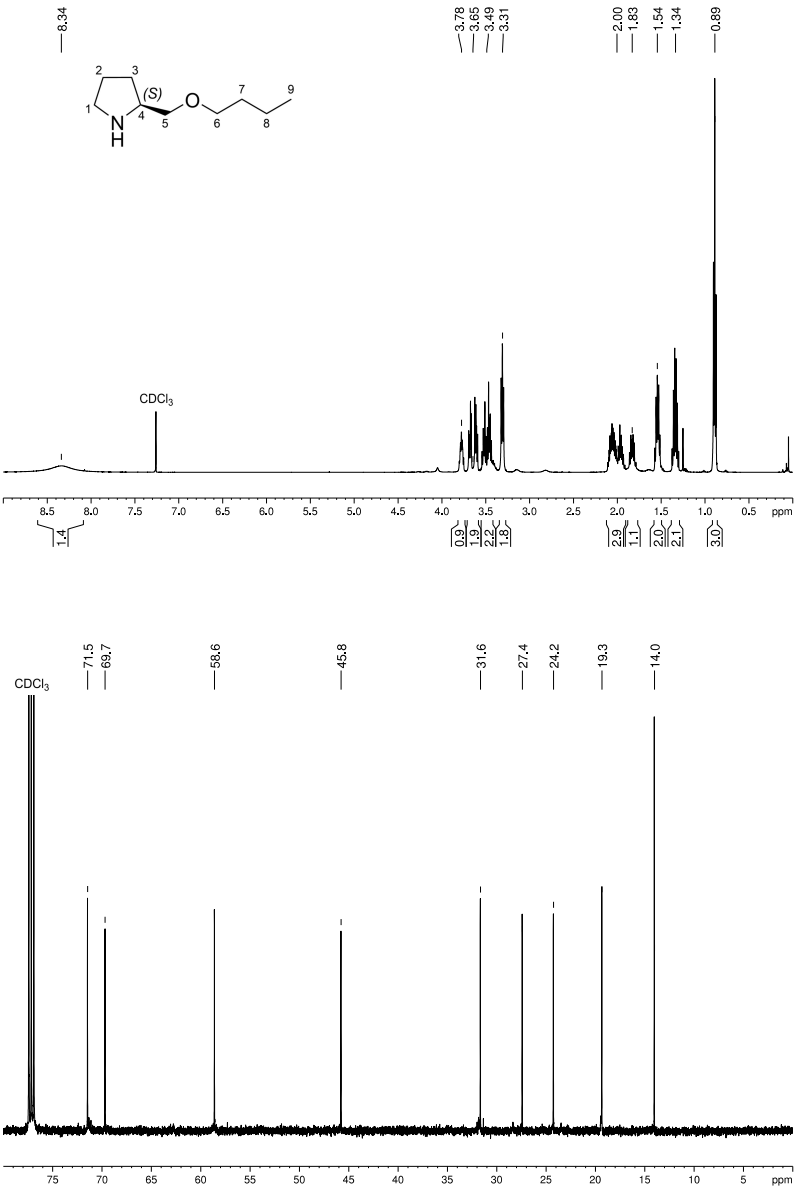

Figure S31: ^{1}H- (top, 500 MHz) and ^{13}C-NMR (bottom, 125 MHz) spectrum of L-prolinyl *n*-butyl ether; $CDCl_3$, 298 K.

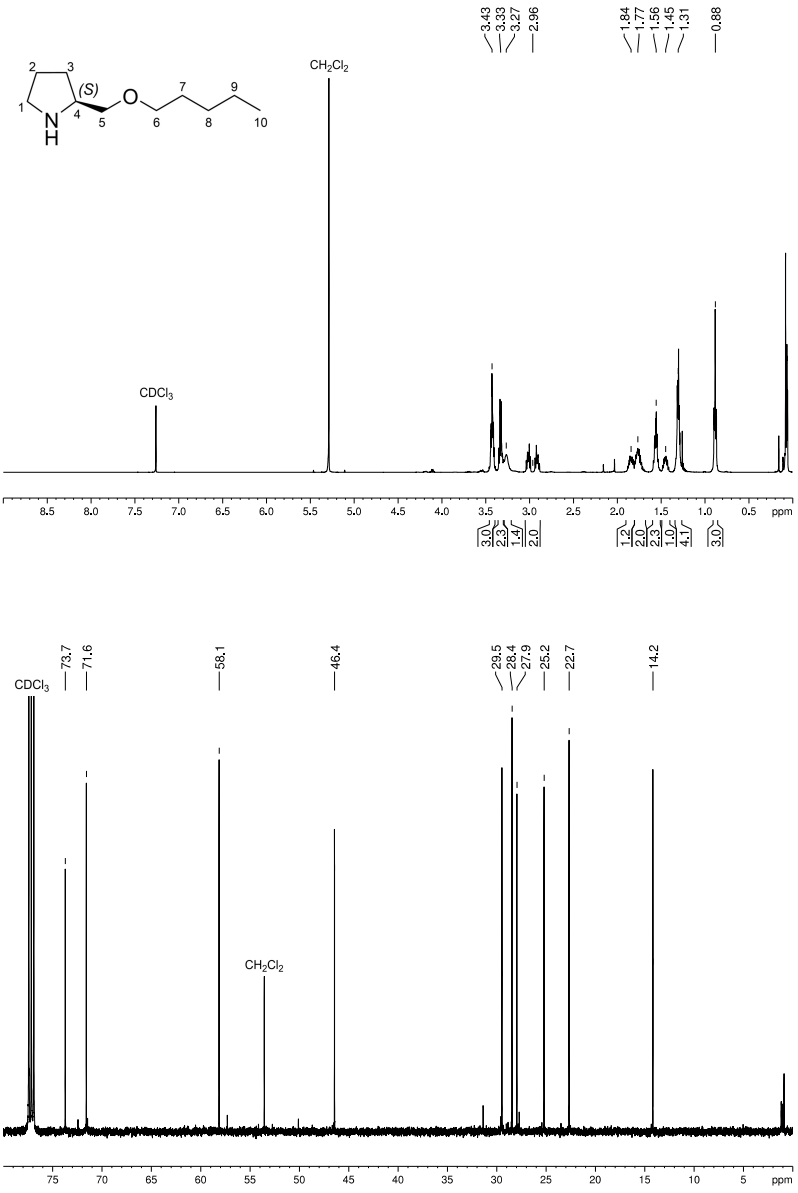

Figure S32: ^{1}H- (top, 500 MHz) and ^{13}C-NMR (bottom, 125 MHz) spectrum of L-prolinyl *n*-pentyl ether; $CDCl_3$, 298 K.

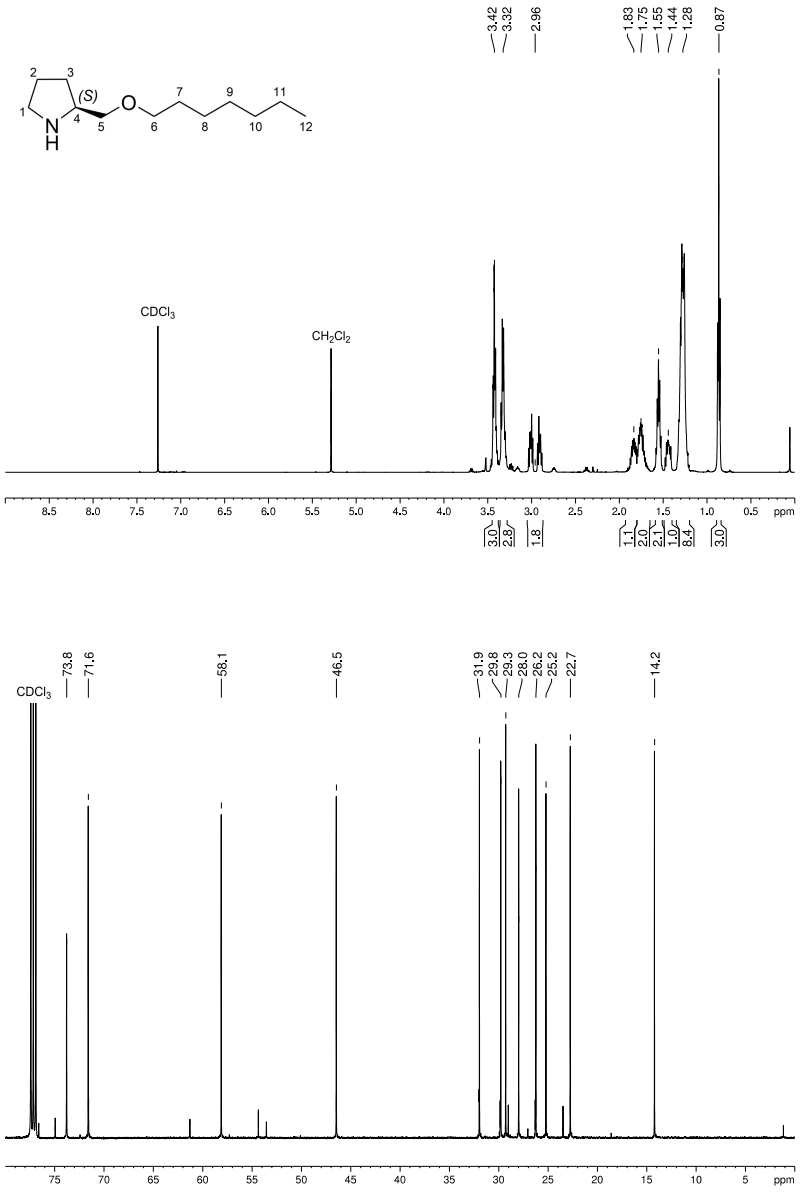

Figure S33: ^{1}H- (top, 500 MHz) and ^{13}C-NMR (bottom, 125 MHz) spectrum of L-prolinyl *n*-heptyl ether; $CDCl_3$, 298 K.

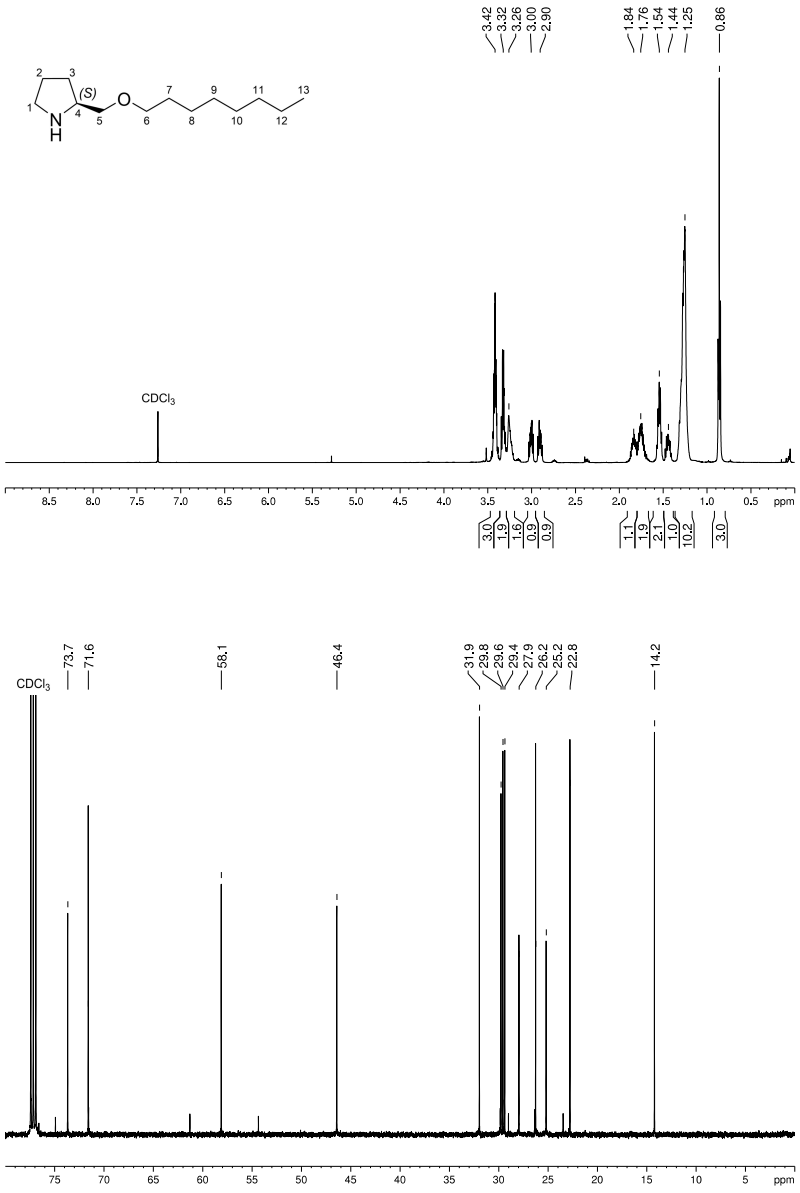

Figure S34: ^{1}H- (top, 500 MHz) and ^{13}C-NMR (bottom, 125 MHz) spectrum of L-prolinyl *n*-octyl ether; $CDCl_3$, 298 K.

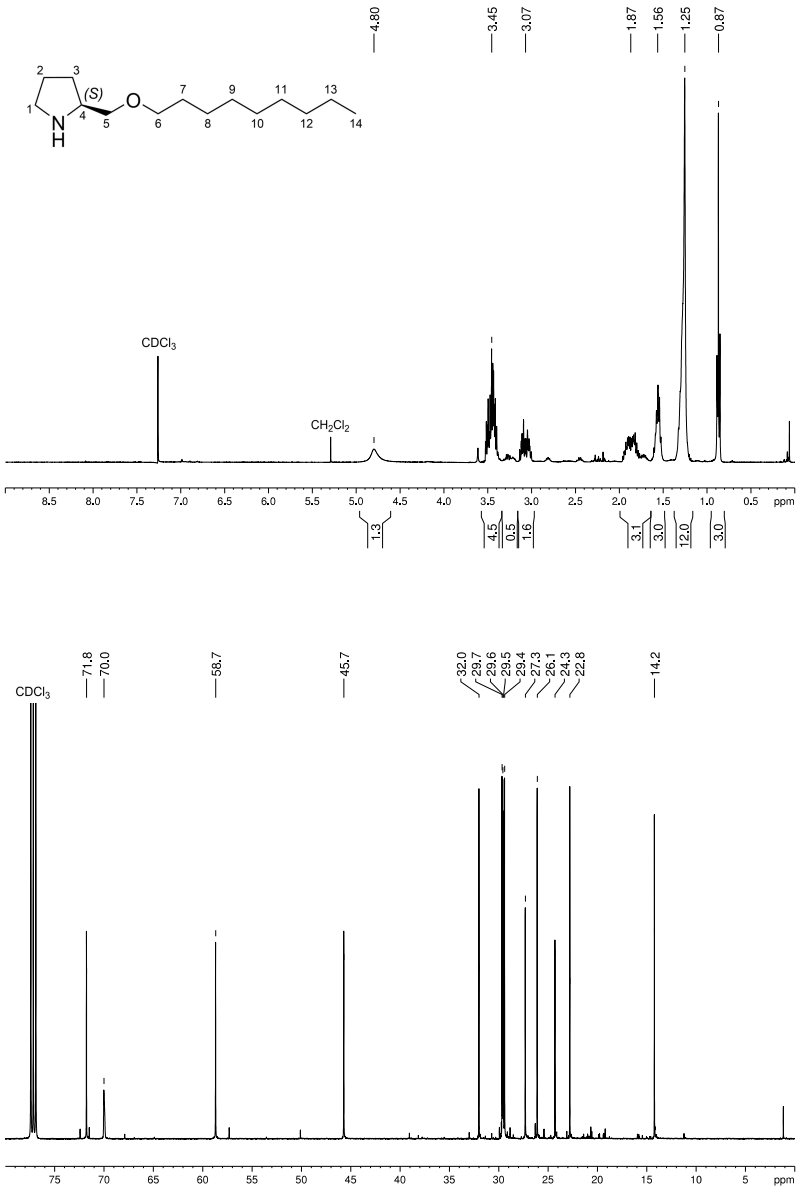

Figure S35: ^{1}H- (top, 400 MHz) and ^{13}C-NMR (bottom, 176 MHz) spectrum of L-prolinyl *n*-nonyl ether; $CDCl_3$, 298 K.

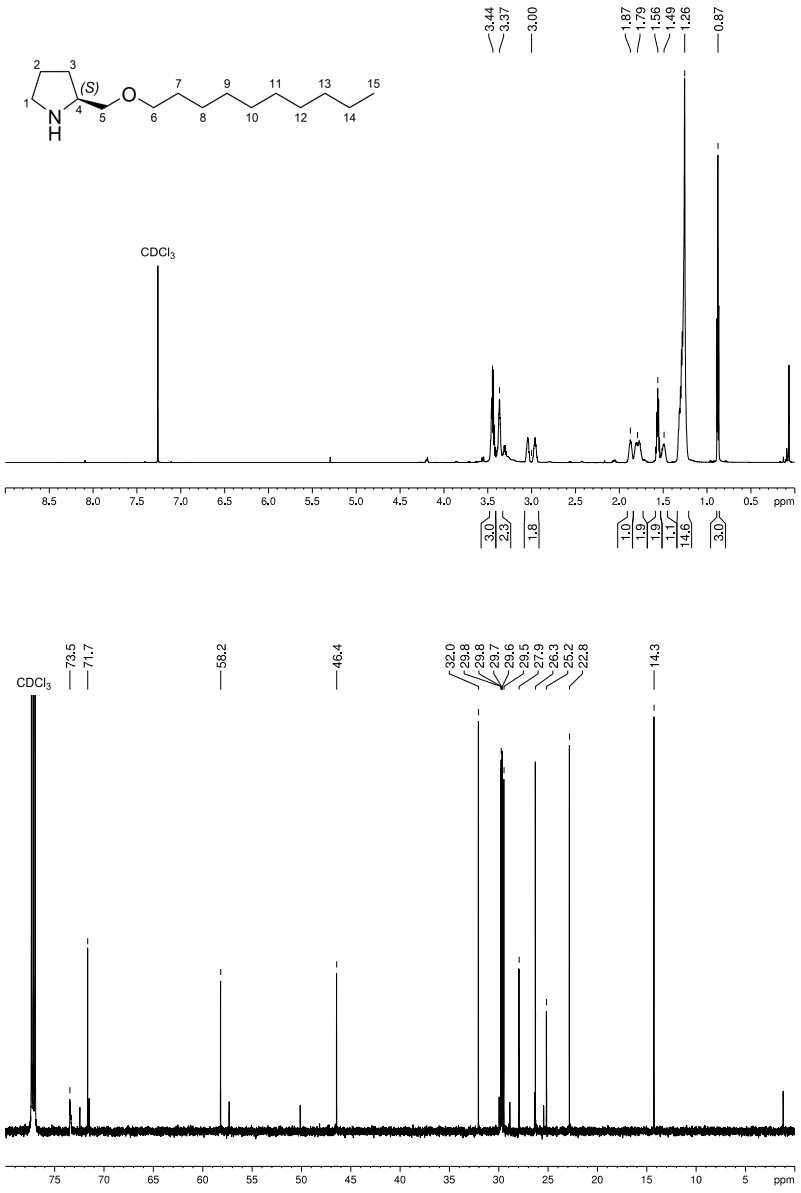

Figure S36: ^{1}H- (top, 700 MHz) and ^{13}C-NMR (bottom, 176 MHz) spectrum of L-prolinyl *n*-decyl ether; $CDCl_3$, 298 K.

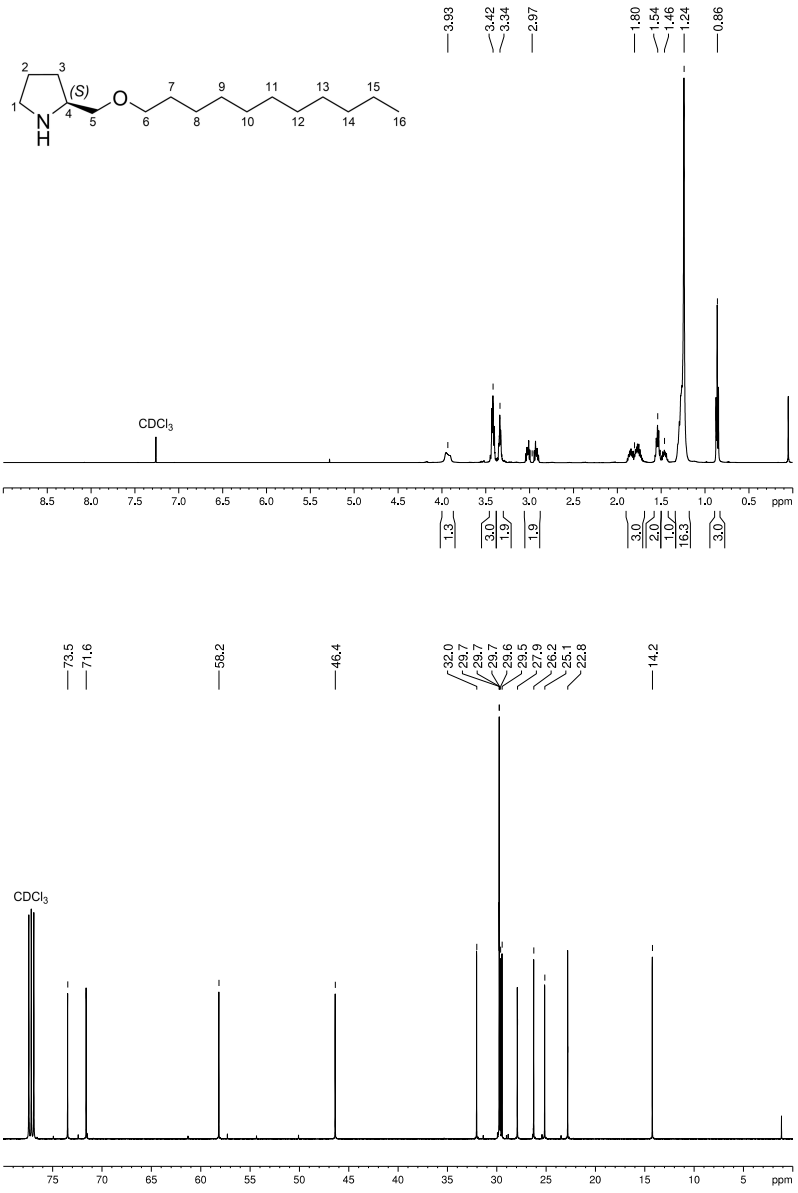

Figure S37: ^{1}H- (top, 500 MHz) and ^{13}C-NMR (bottom, 125 MHz) spectrum of L-prolinyl *n*-undecyl ether; $CDCl_3$, 298 K.

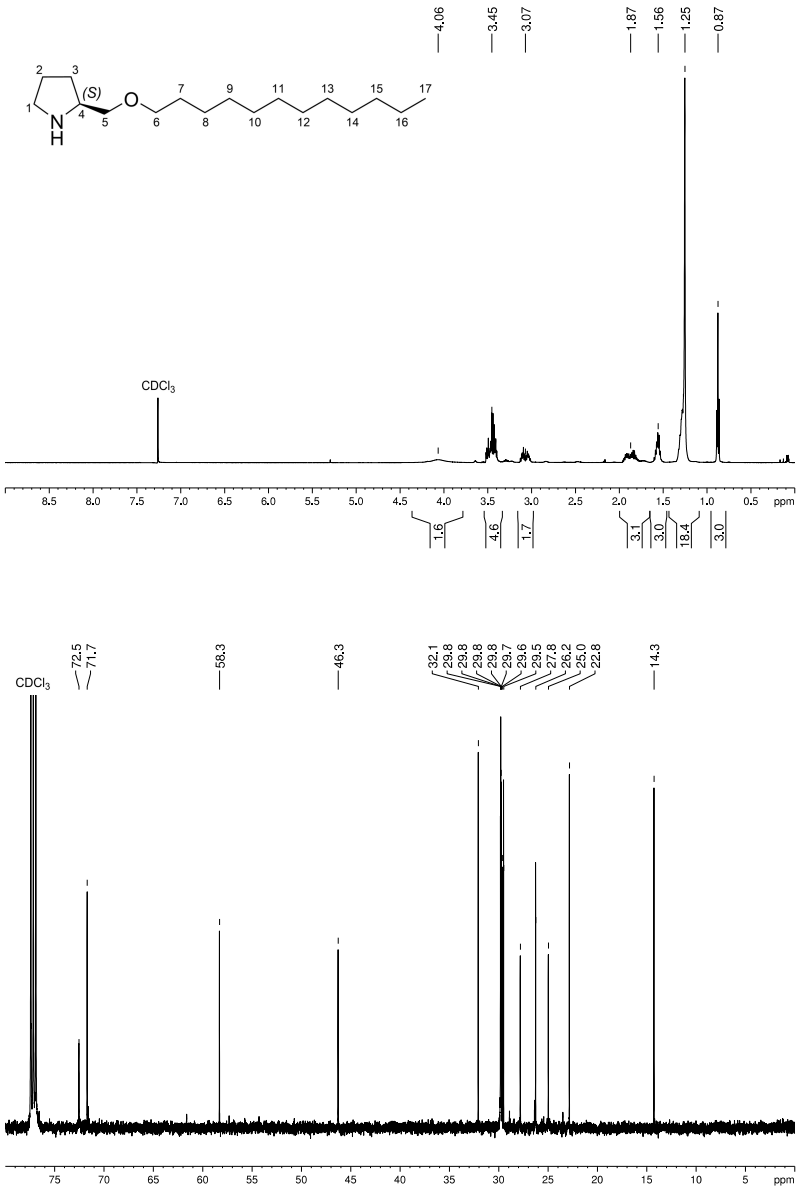

Figure S38: ^{1}H- (top, 500 MHz) and ^{13}C-NMR (bottom, 125 MHz) spectrum of L-prolinyl *n*-dodecyl ether; $CDCl_3$, 298 K.

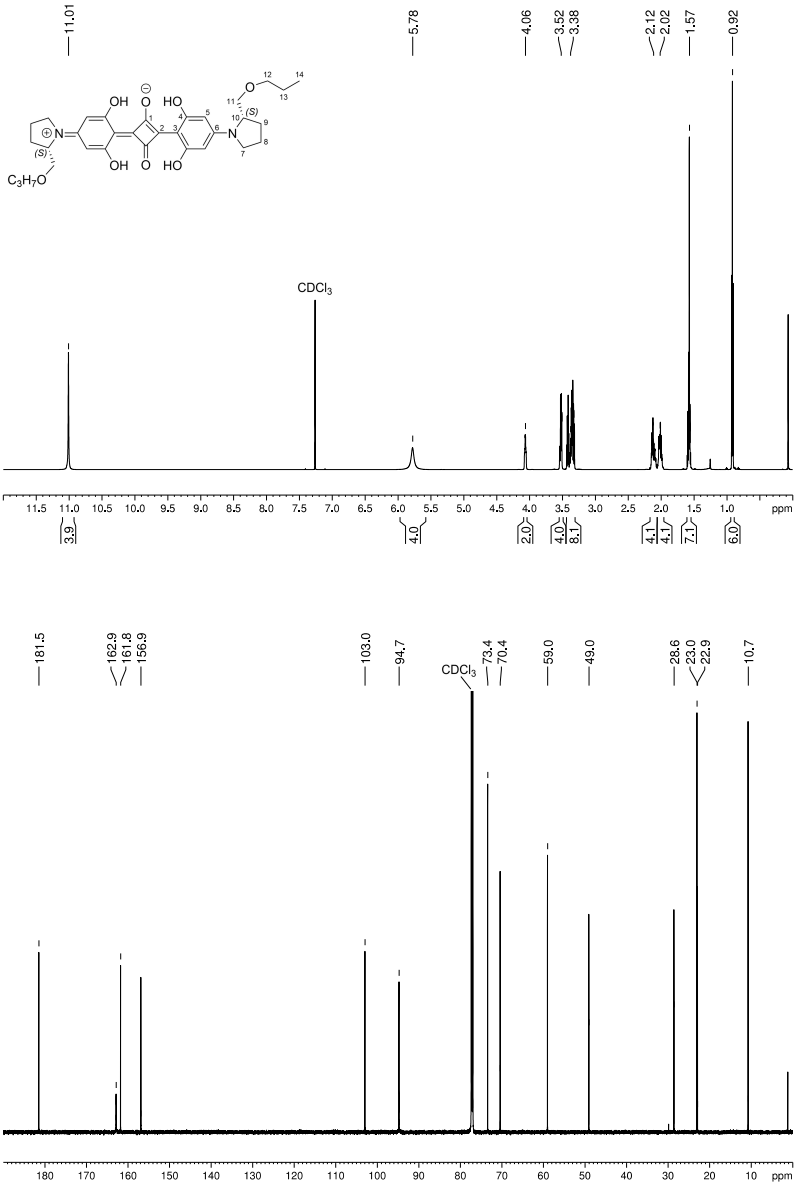

Figure S39: ^{1}H- (top, 700 MHz) and ^{13}C-NMR (bottom, 176 MHz) spectrum of (*S*,*S*)-ProSQ-C3; $CDCl_3$, 298 K.

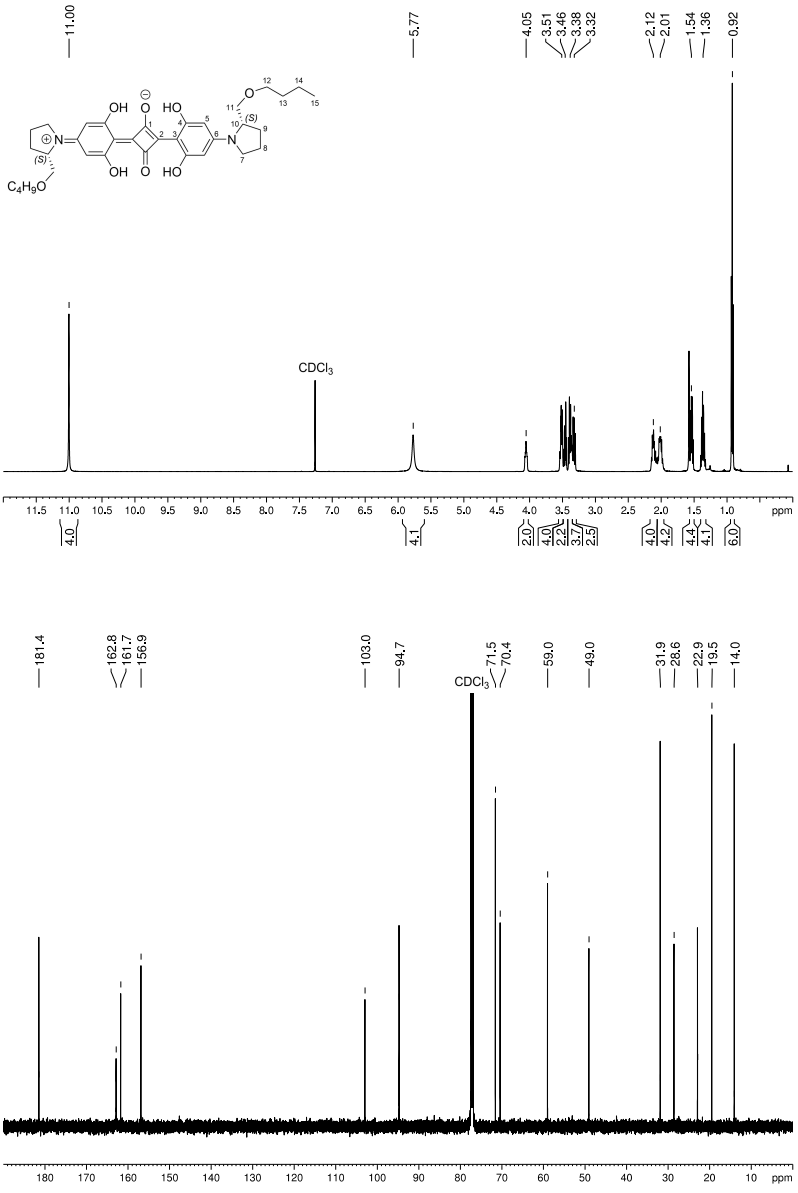

Figure S40: ^{1}H- (top, 500 MHz) and ^{13}C-NMR (bottom, 125 MHz) spectrum of (*S*,*S*)-ProSQ-C4; $CDCl_3$, 298 K.

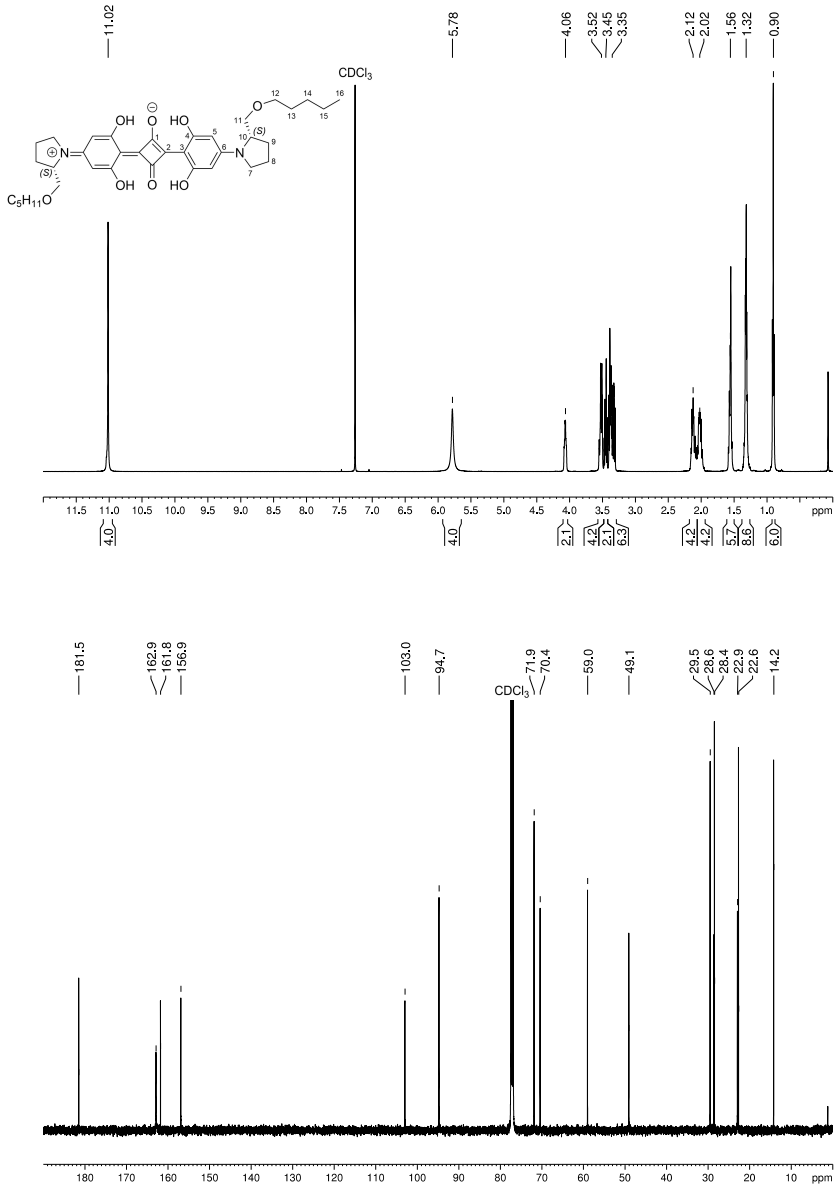

Figure S41: ^{1}H- (top, 500 MHz) and ^{13}C-NMR (bottom, 125 MHz) spectrum of (*S*,*S*)-ProSQ-C5; $CDCl_3$, 298 K.

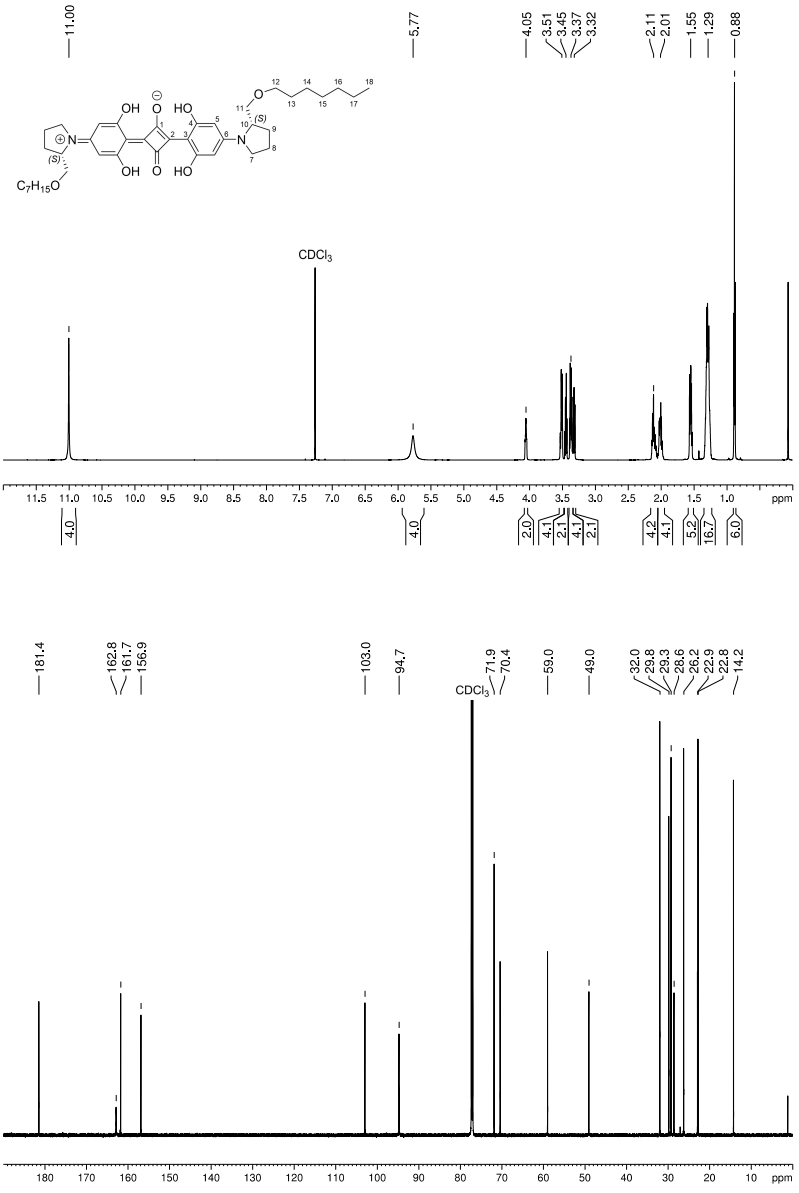

Figure S42: ^{1}H- (top, 500 MHz) and ^{13}C-NMR (bottom, 125 MHz) spectrum of (*S*,*S*)-ProSQ-C7; $CDCl_3$, 298 K.

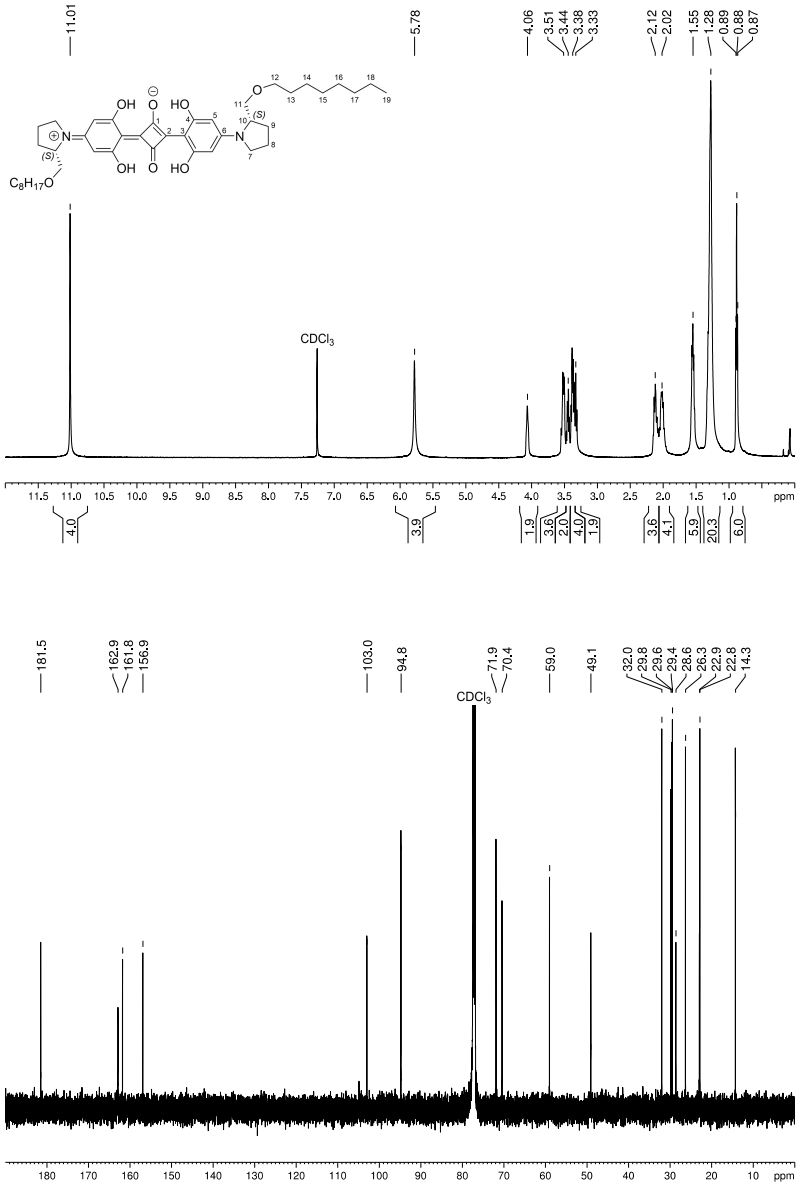

Figure S43: ^{1}H- (top, 500 MHz) and ^{13}C-NMR (bottom, 125 MHz) spectrum of (*S*,*S*)-ProSQ-C8; $CDCl_3$, 298 K.

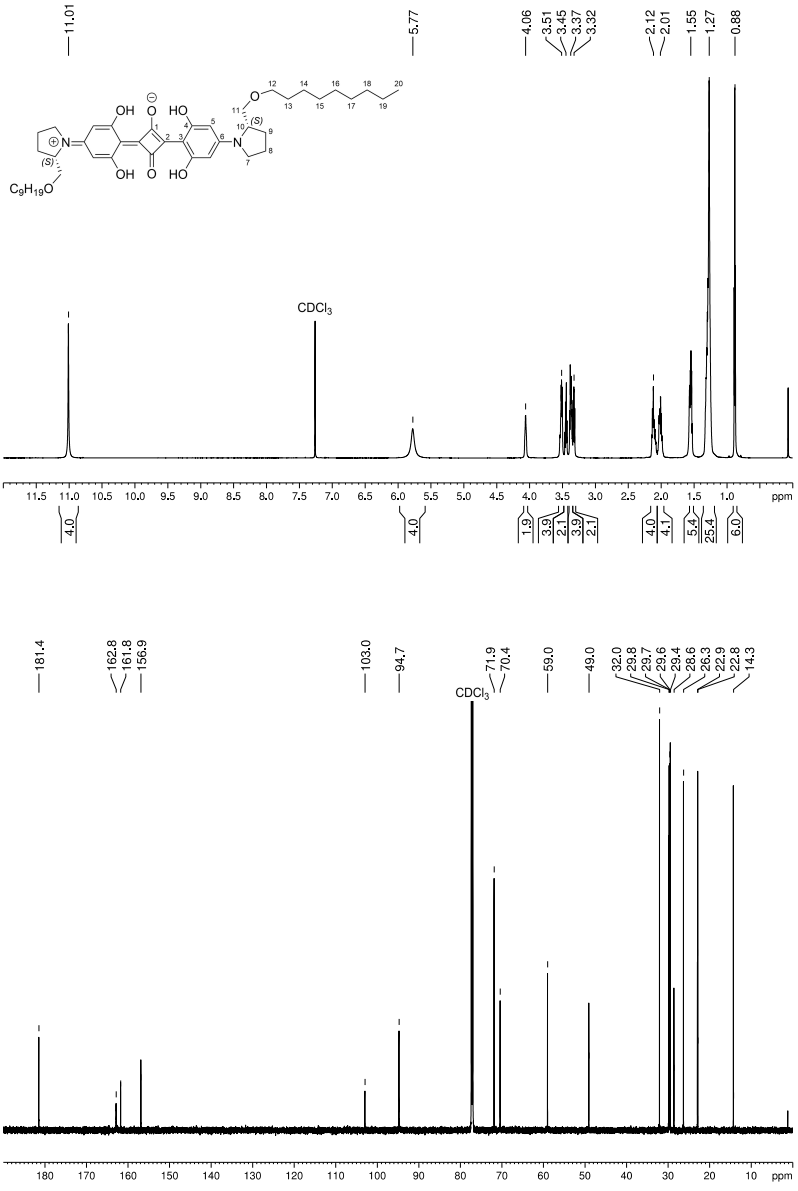

Figure S44: ^{1}H- (top, 500 MHz) and ^{13}C-NMR (bottom, 176 MHz) spectrum of (*S*,*S*)-ProSQ-C9; $CDCl_3$, 298 K.

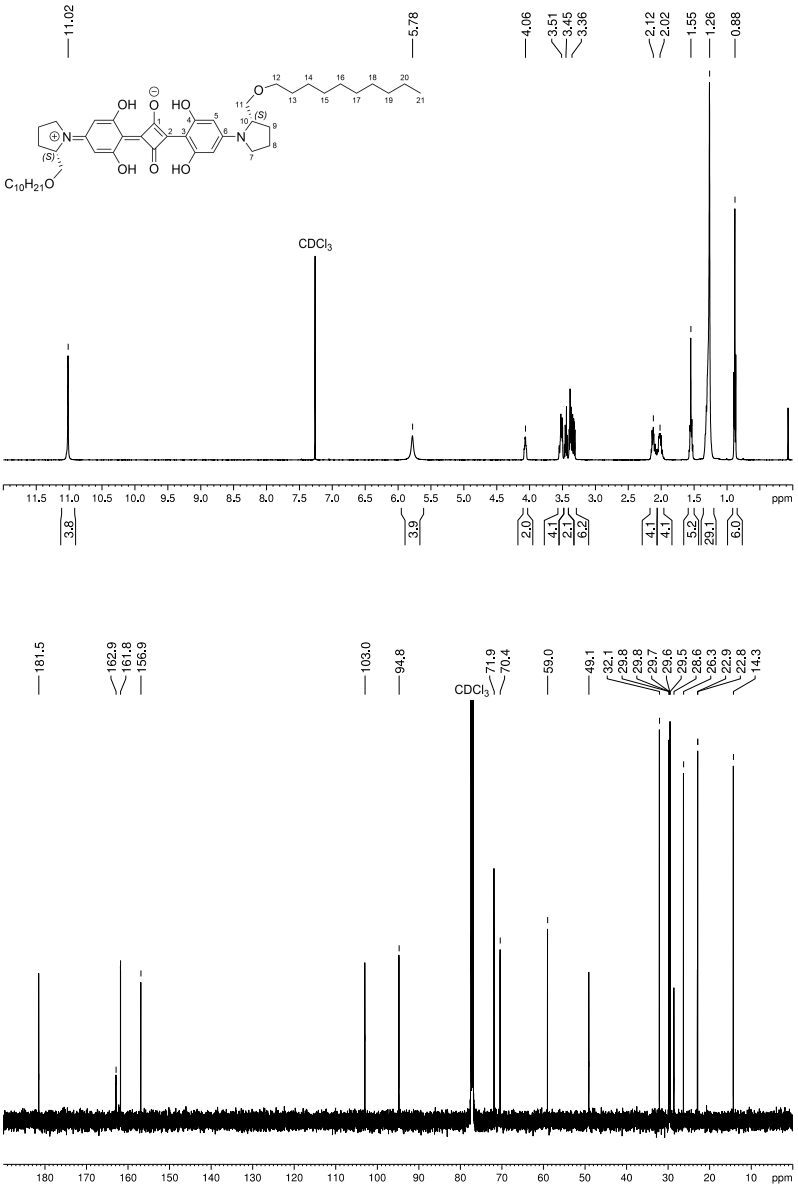

Figure S45: ^{1}H- (top, 500 MHz) and ^{13}C-NMR (bottom, 125 MHz) spectrum of (*S*,*S*)-ProSQ-C10; $CDCl_3$, 298 K.

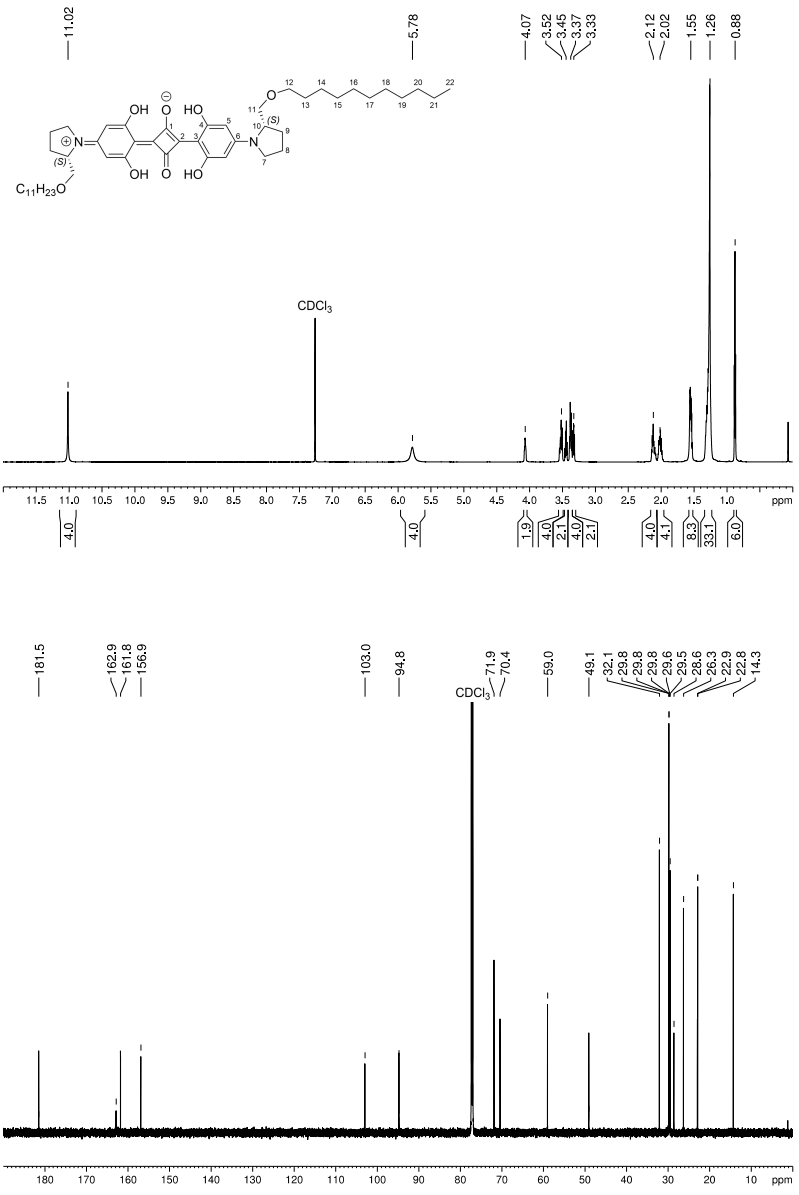

Figure S46: ^{1}H- (top, 700 MHz) and ^{13}C-NMR (bottom, 176 MHz) spectrum of (*S*,*S*)-ProSQ-C11; $CDCl_3$, 298 K.

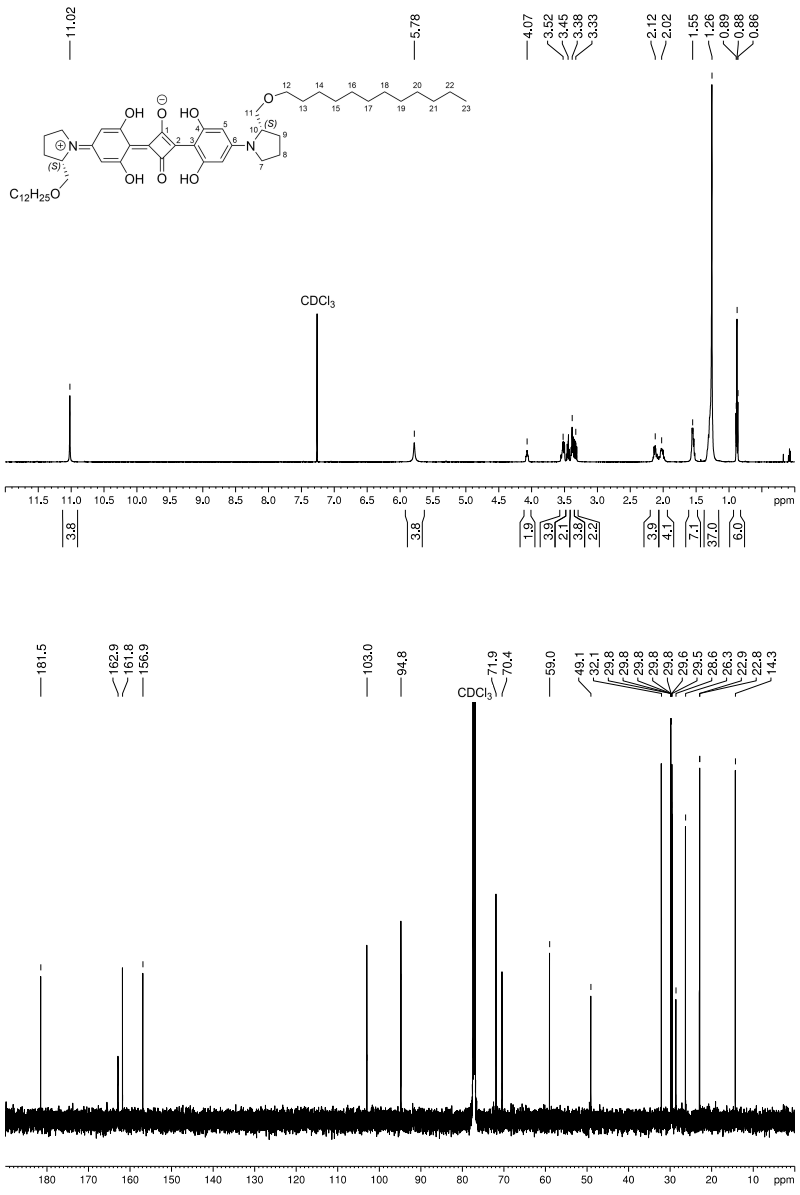

Figure S47: ^{1}H- (top, 500 MHz) and ^{13}C-NMR (bottom, 125 MHz) spectrum of (*S*,*S*)-ProSQ-C12; $CDCl_3$, 298 K.

6.2 Mass spectra

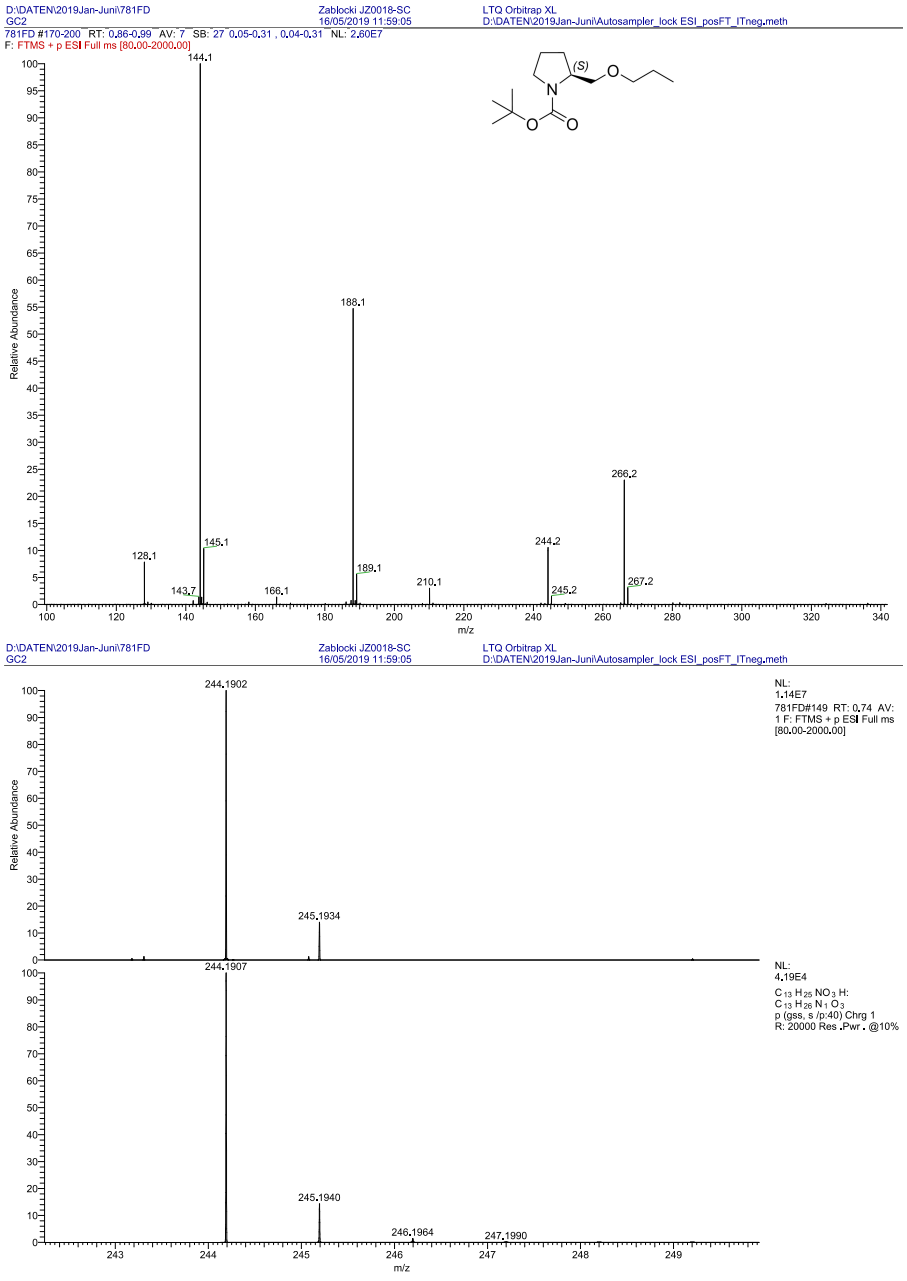

Figure S48: ESI(+) Mass spectra of *N*-Boc-L-prolinyl *n*-propyl ether

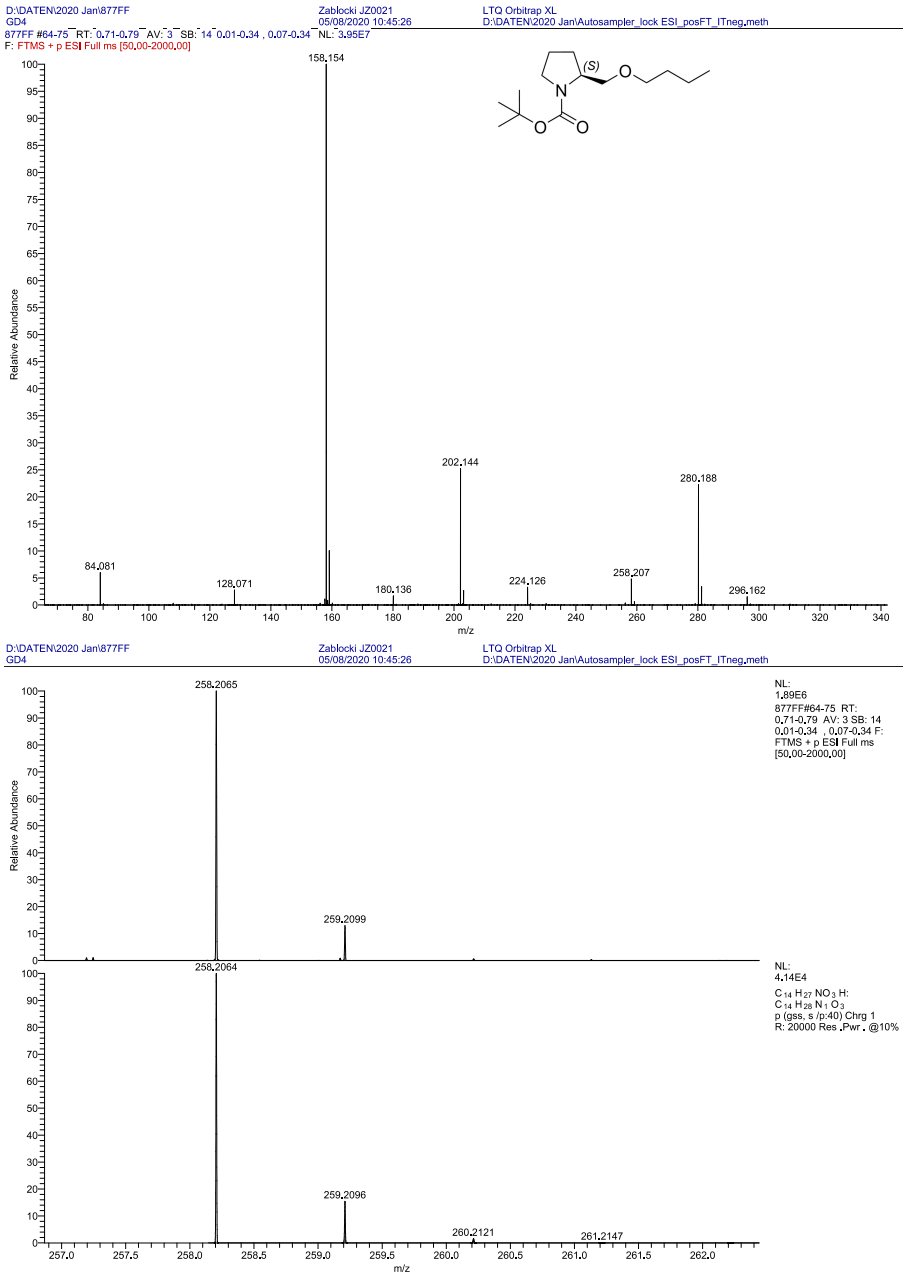

Figure S49: ESI(+) Mass spectra of *N*-Boc-L-prolinyl *n*-butyl ether

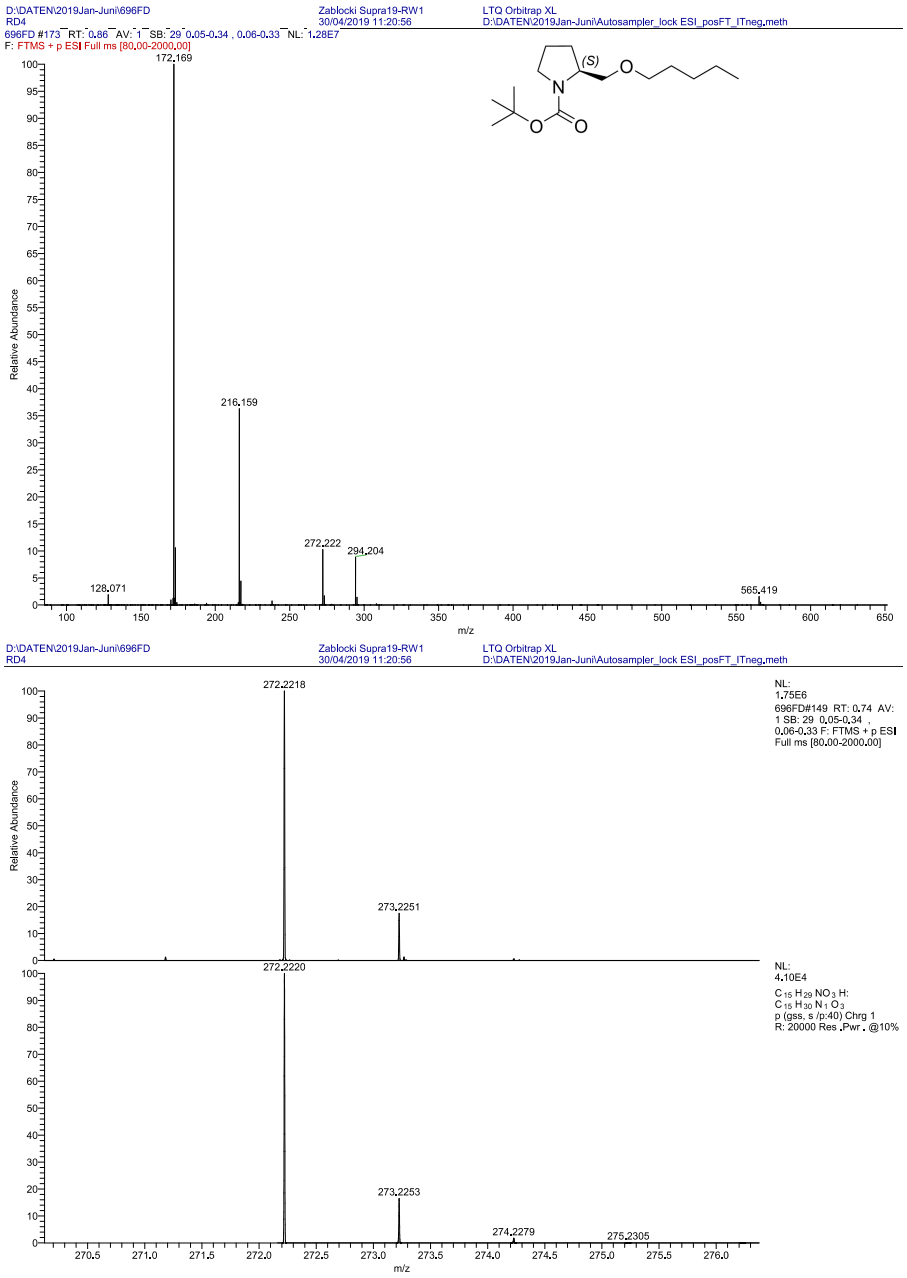

Figure S50: ESI(+) Mass spectra of *N*-Boc-L-prolinyl *n*-pentyl ether

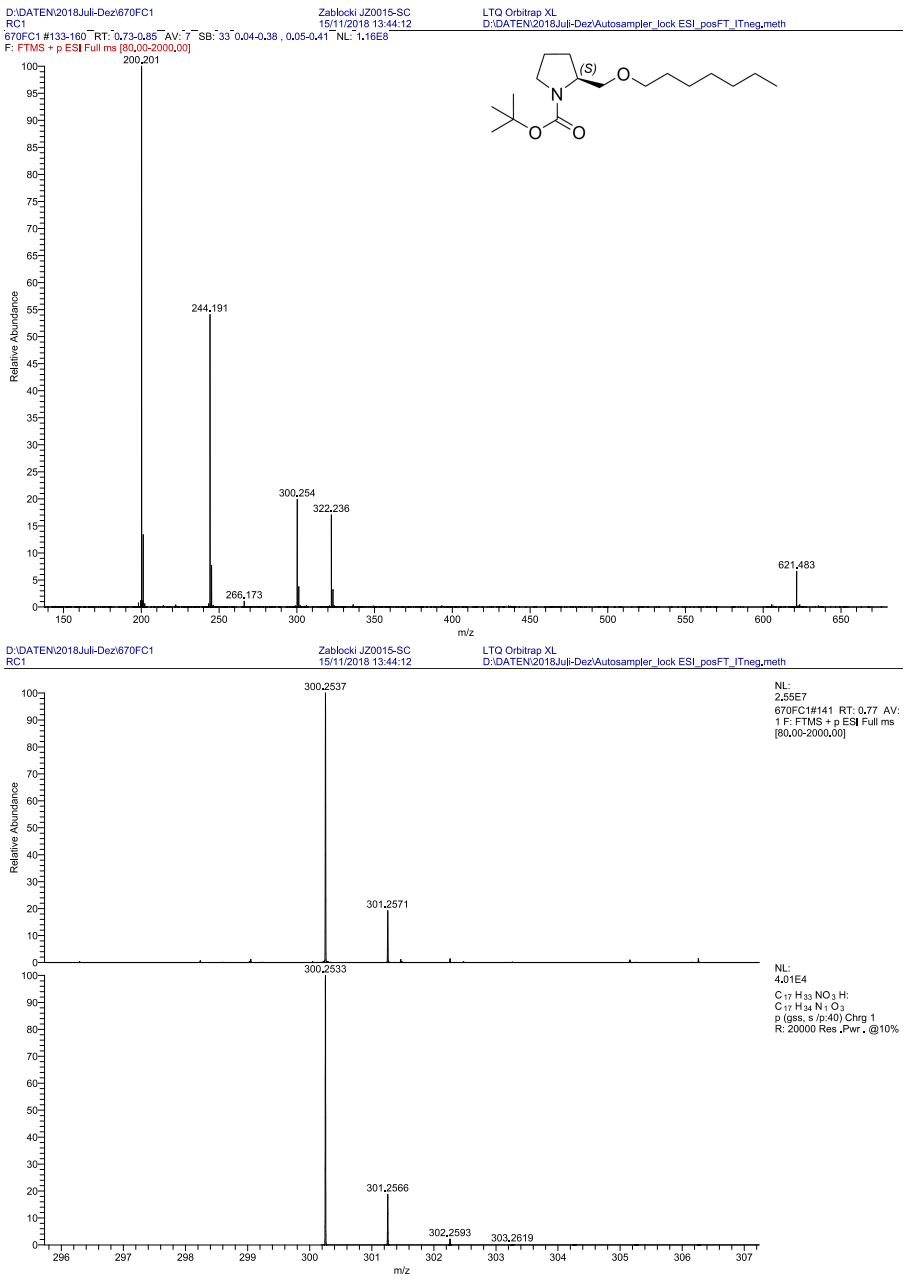

Figure S51: ESI(+) Mass spectra of *N*-Boc-L-prolinyl *n*-heptyl ether

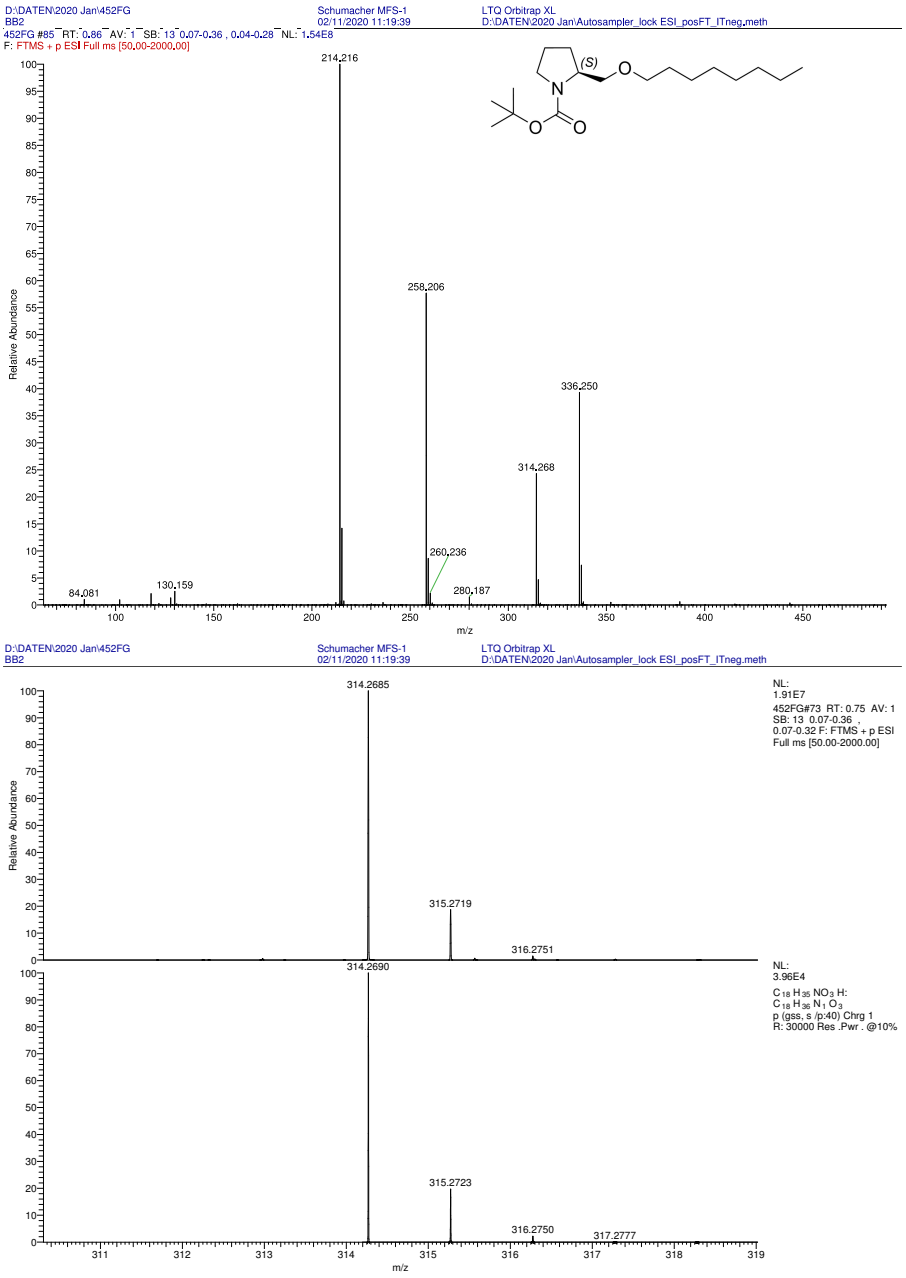

Figure S52: ESI(+) Mass spectra of *N*-Boc-L-prolinyl *n*-octyl ether

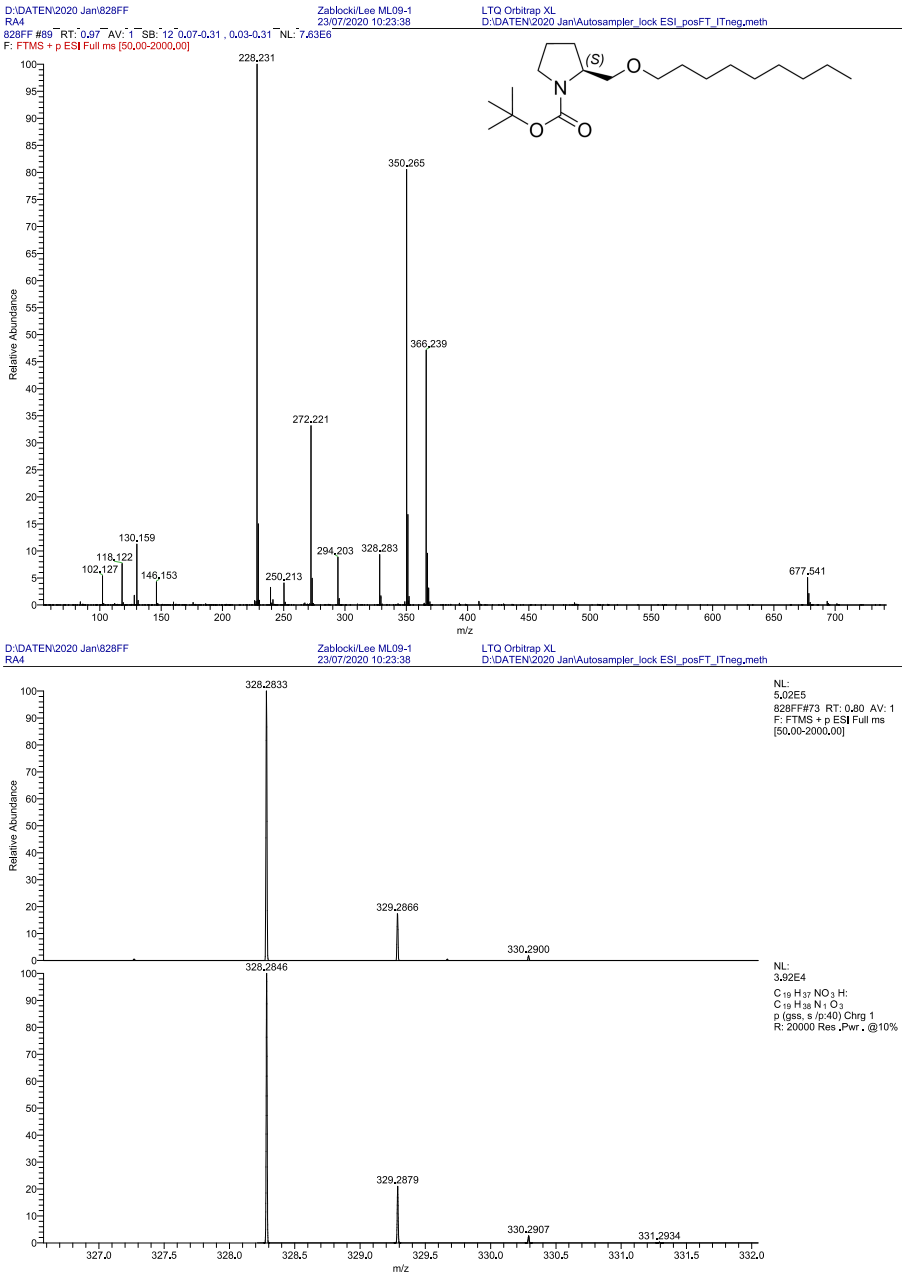

Figure S53: ESI(+) Mass spectra of *N*-Boc-L-prolinyl *n*-nonyl ether

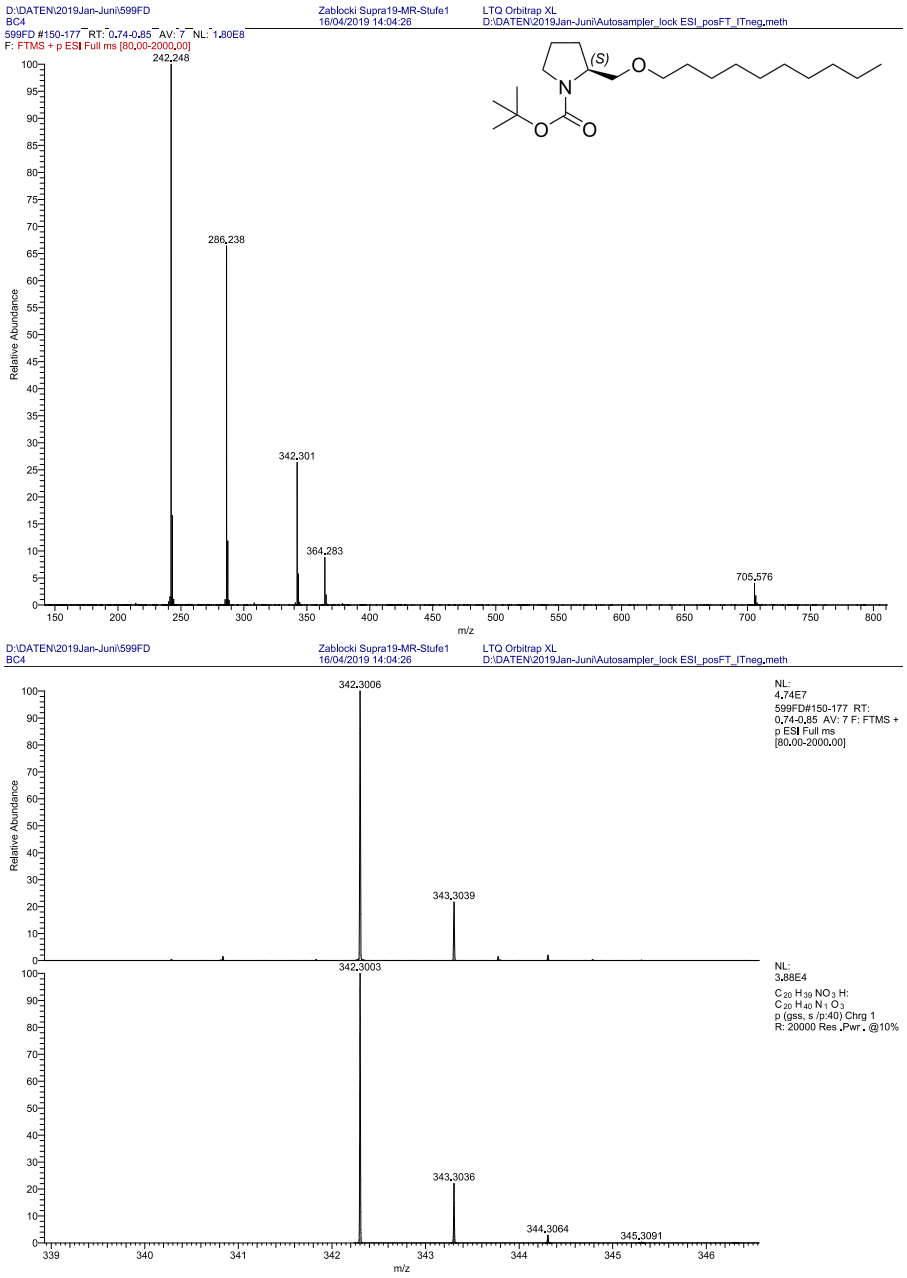

Figure S54: ESI(+) Mass spectra of *N*-Boc-L-prolinyl *n*-decyl ether

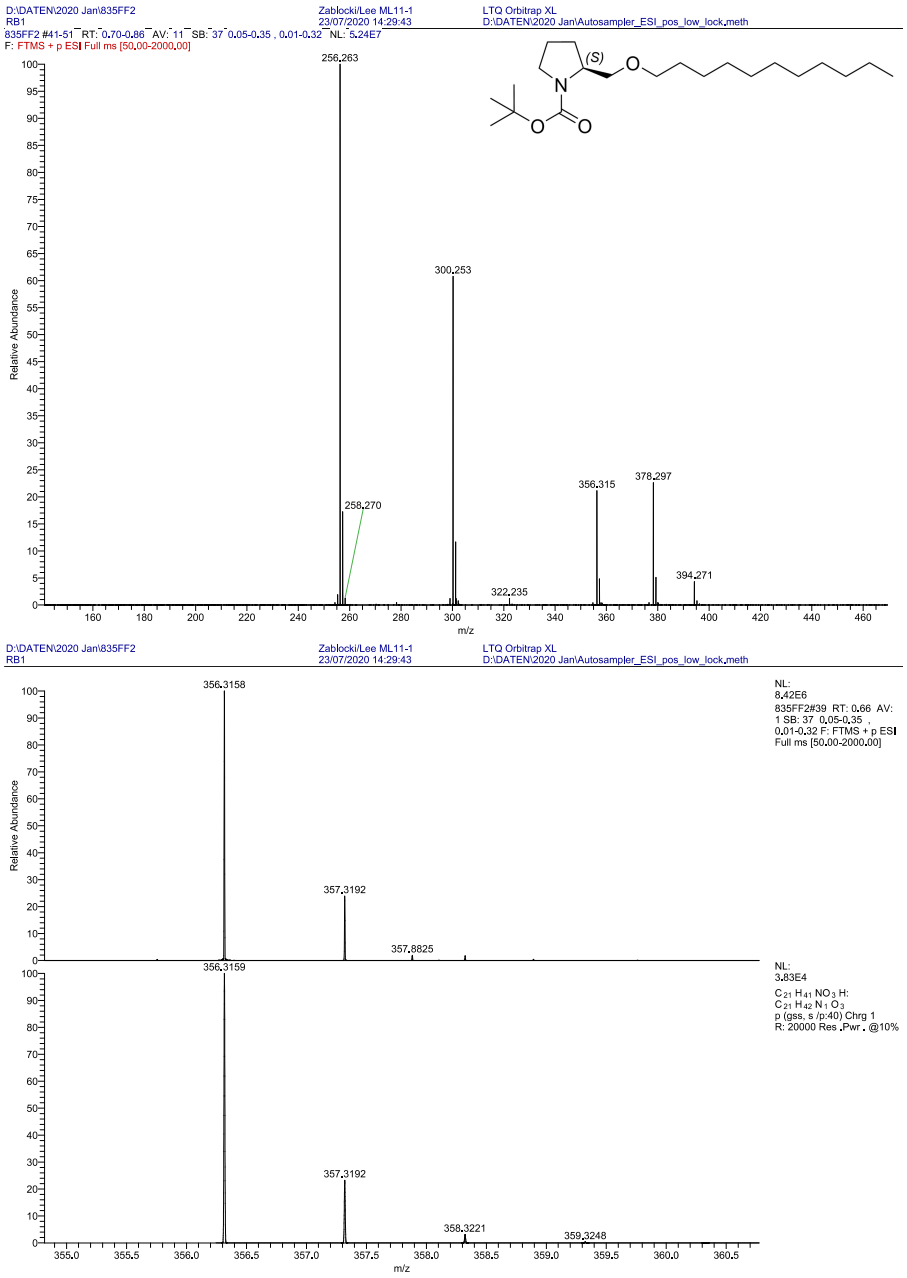

Figure S55: ESI(+) Mass spectra of *N*-Boc-L-prolinyl *n*-undecyl ether

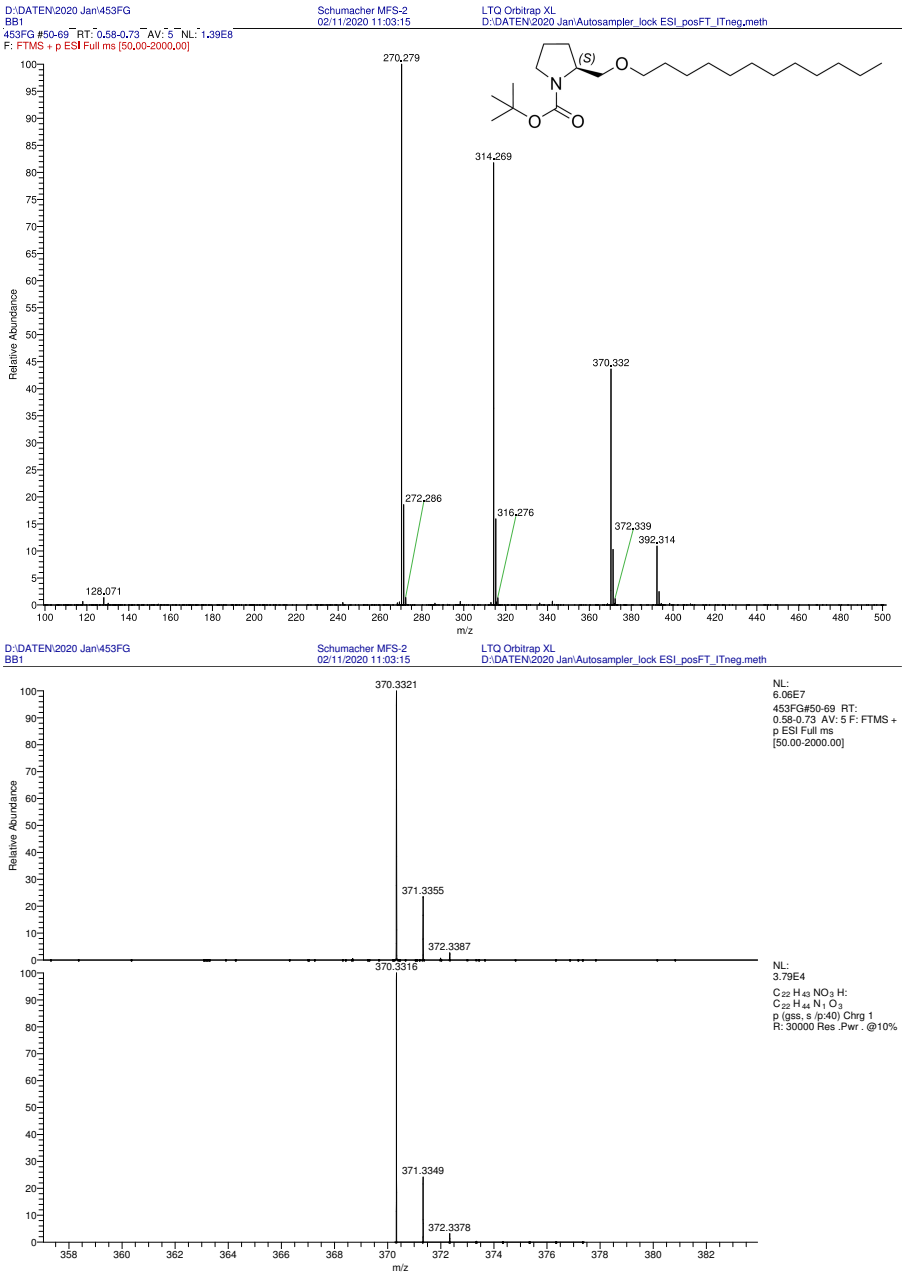

Figure S56: ESI(+) Mass spectra of *N*-Boc-L-prolinyl *n*-dodecyl ether

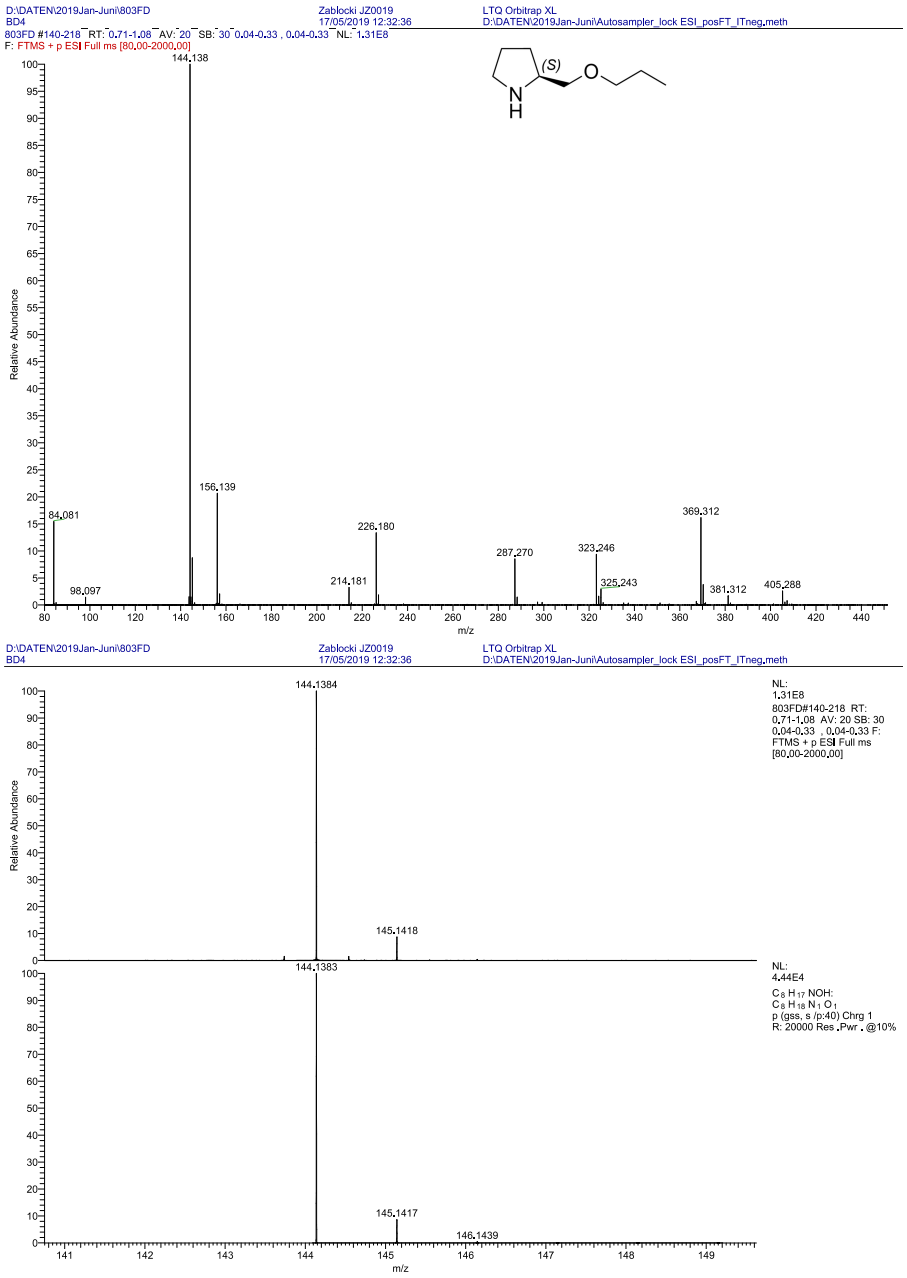

Figure S57: ESI(+) Mass spectra of L-prolinyl *n*-propyl ether

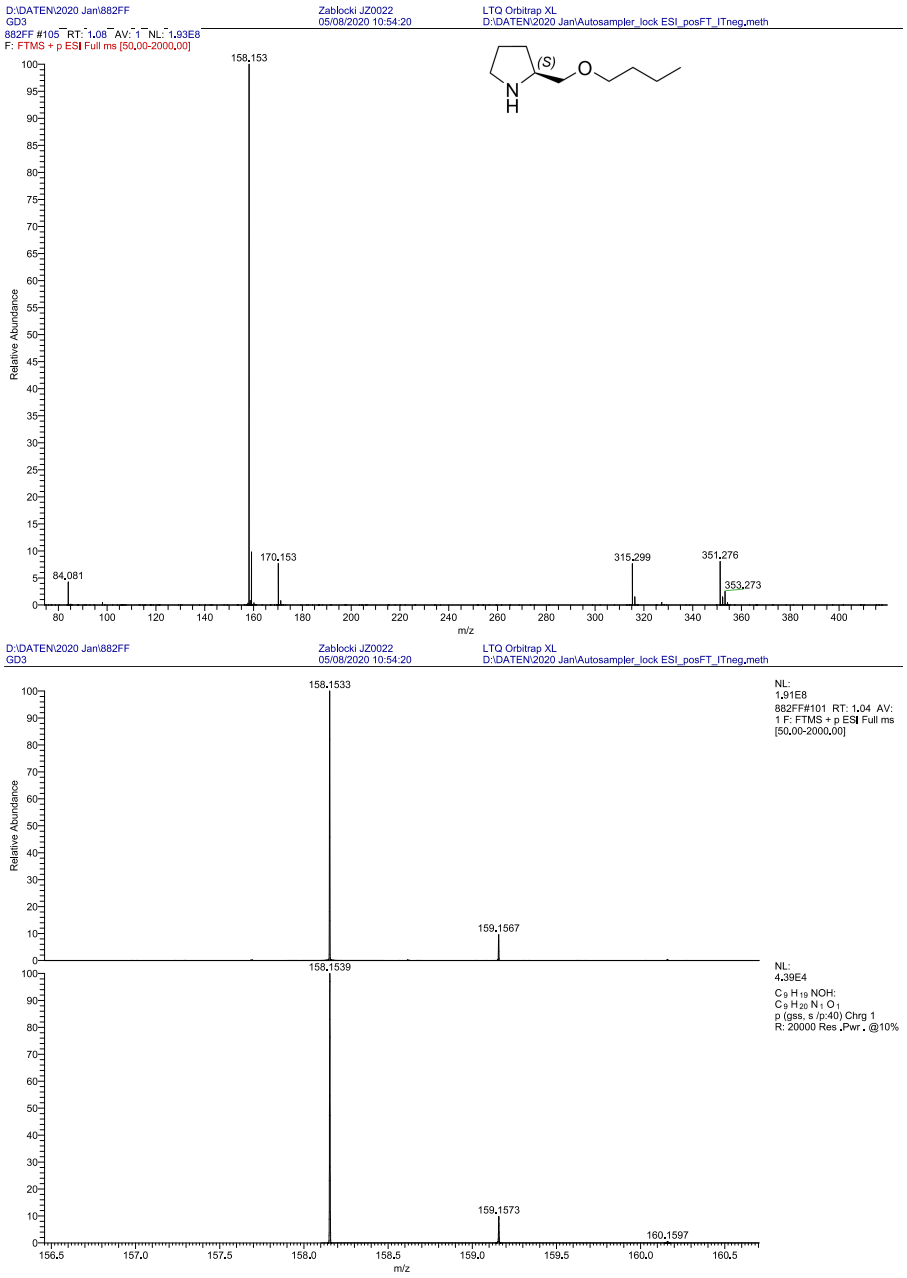

Figure S58: ESI(+) Mass spectra of L-prolinyl *n*-butyl ether

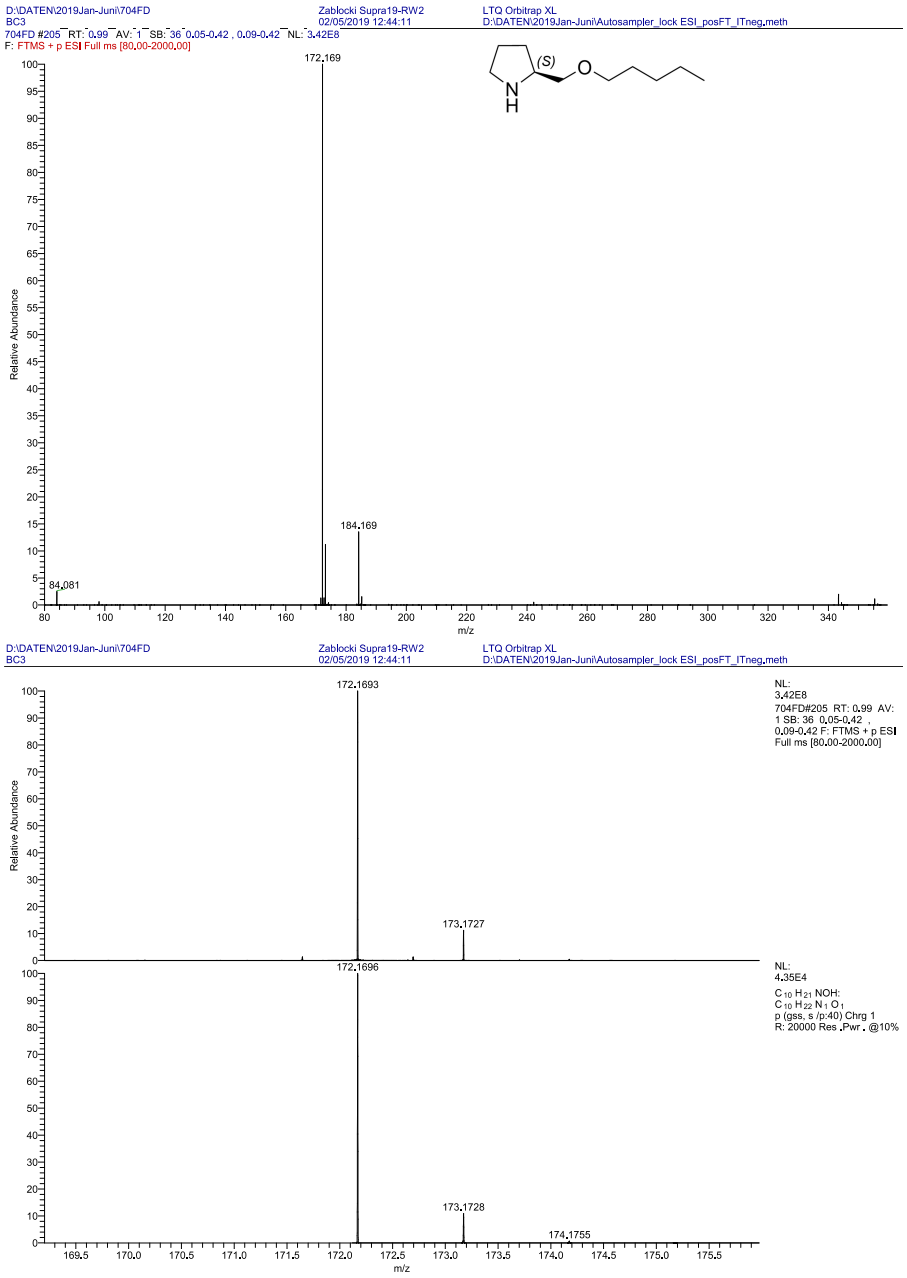

Figure S59: ESI(+) Mass spectra of L-prolinyl *n*-pentyl ether

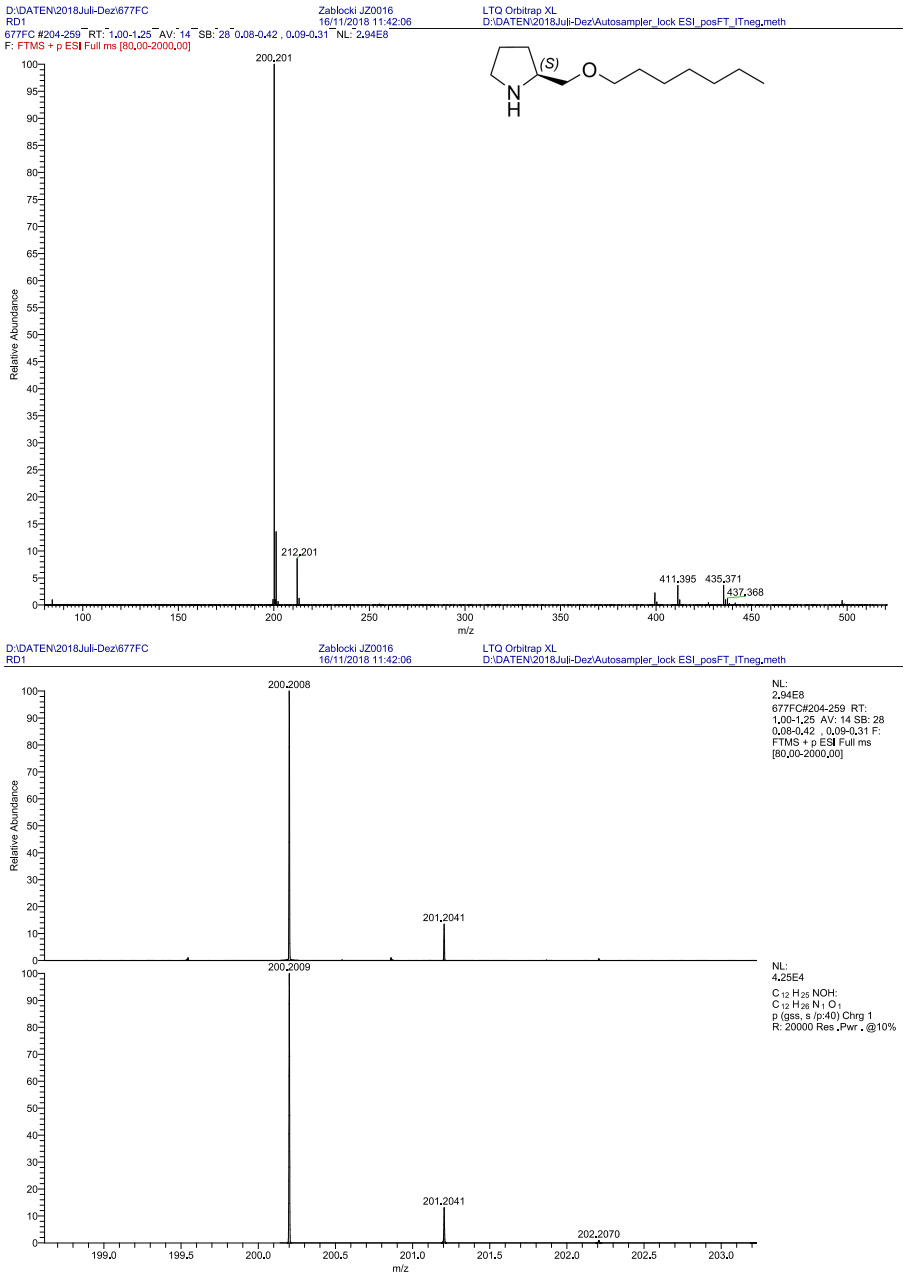

Figure S60: ESI(+) Mass spectra of L-prolinyl *n*-heptyl ether

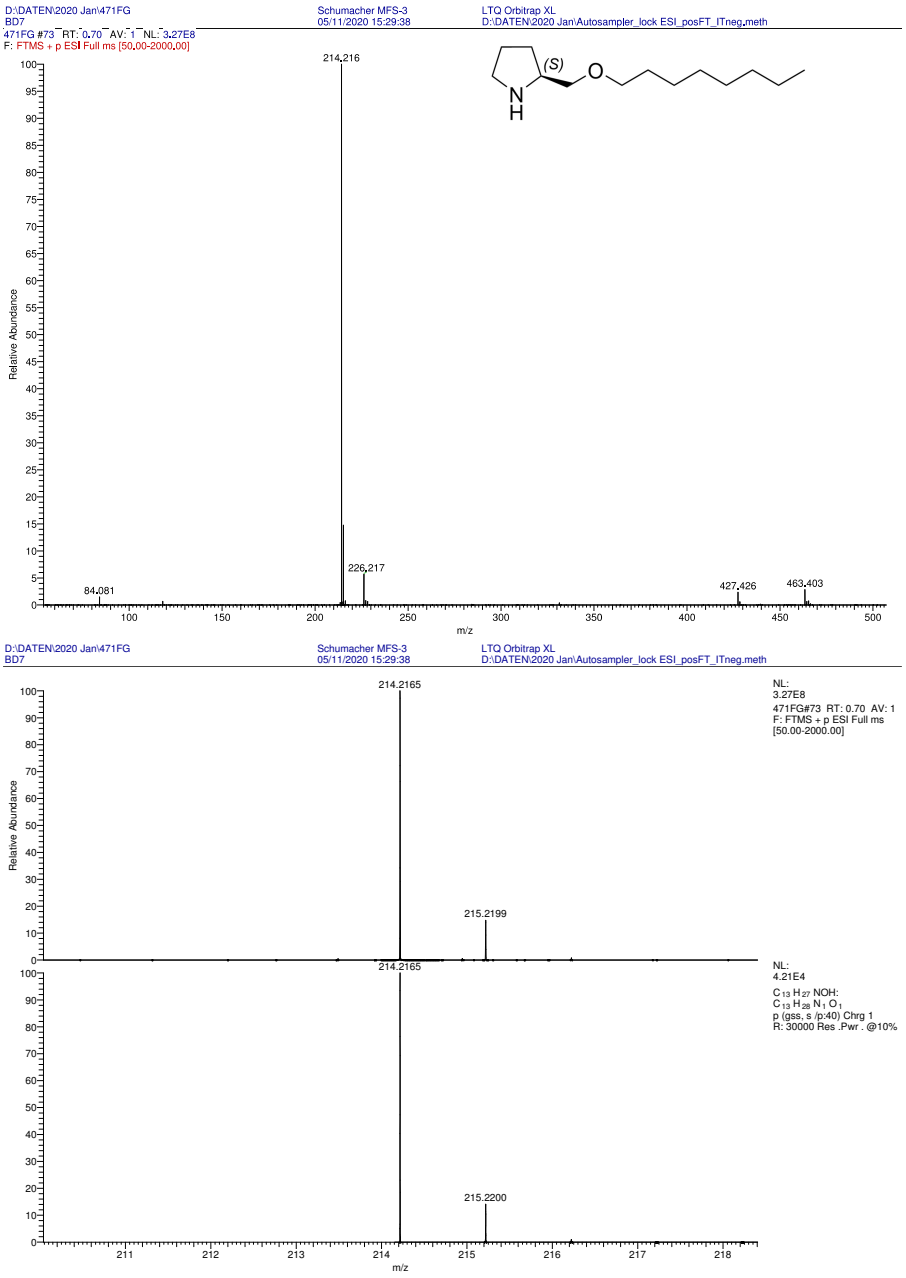

Figure S61: ESI(+) Mass spectra of L-prolinyl *n*-octyl ether

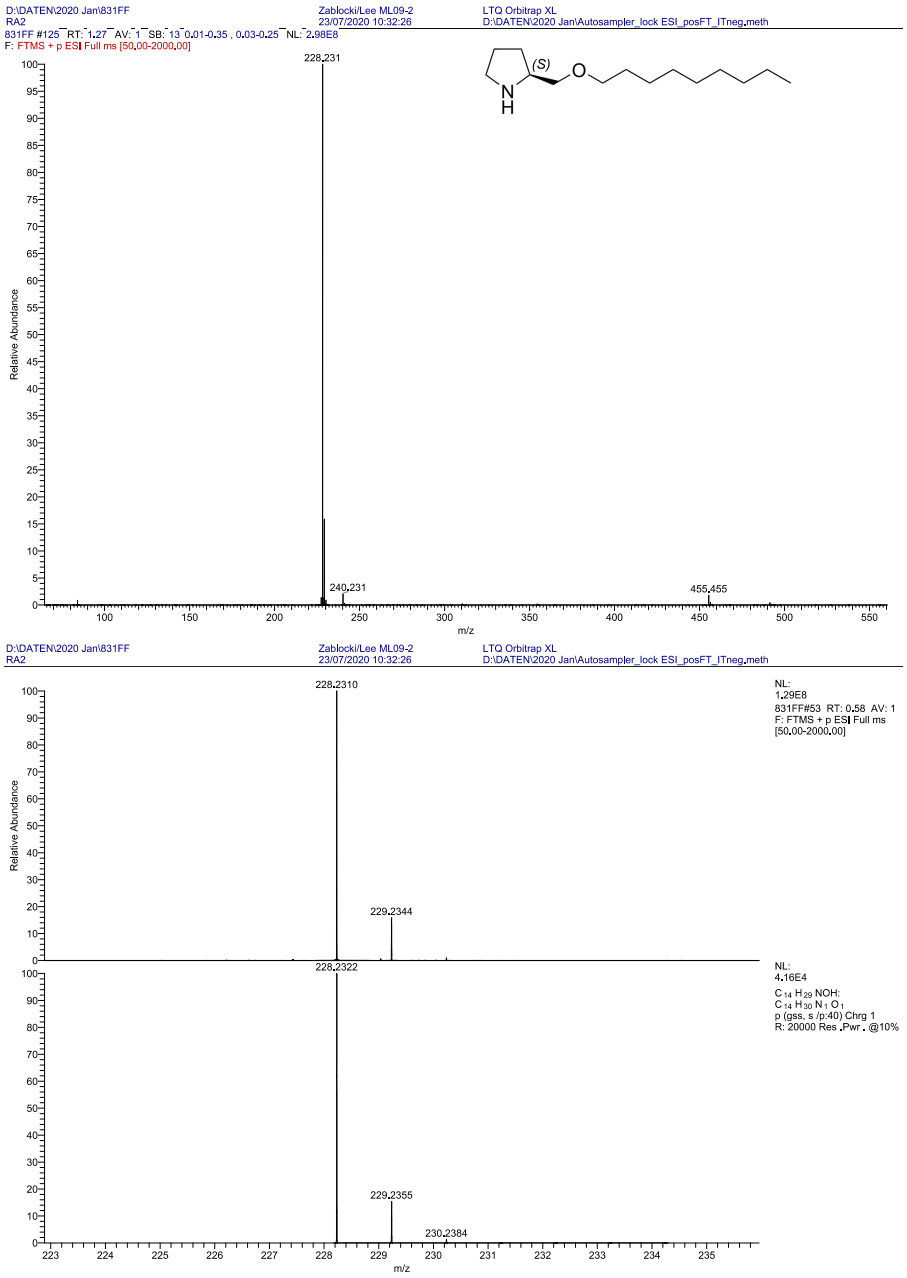

Figure S62: ESI(+) Mass spectra of L-prolinyl *n*-nonyl ether

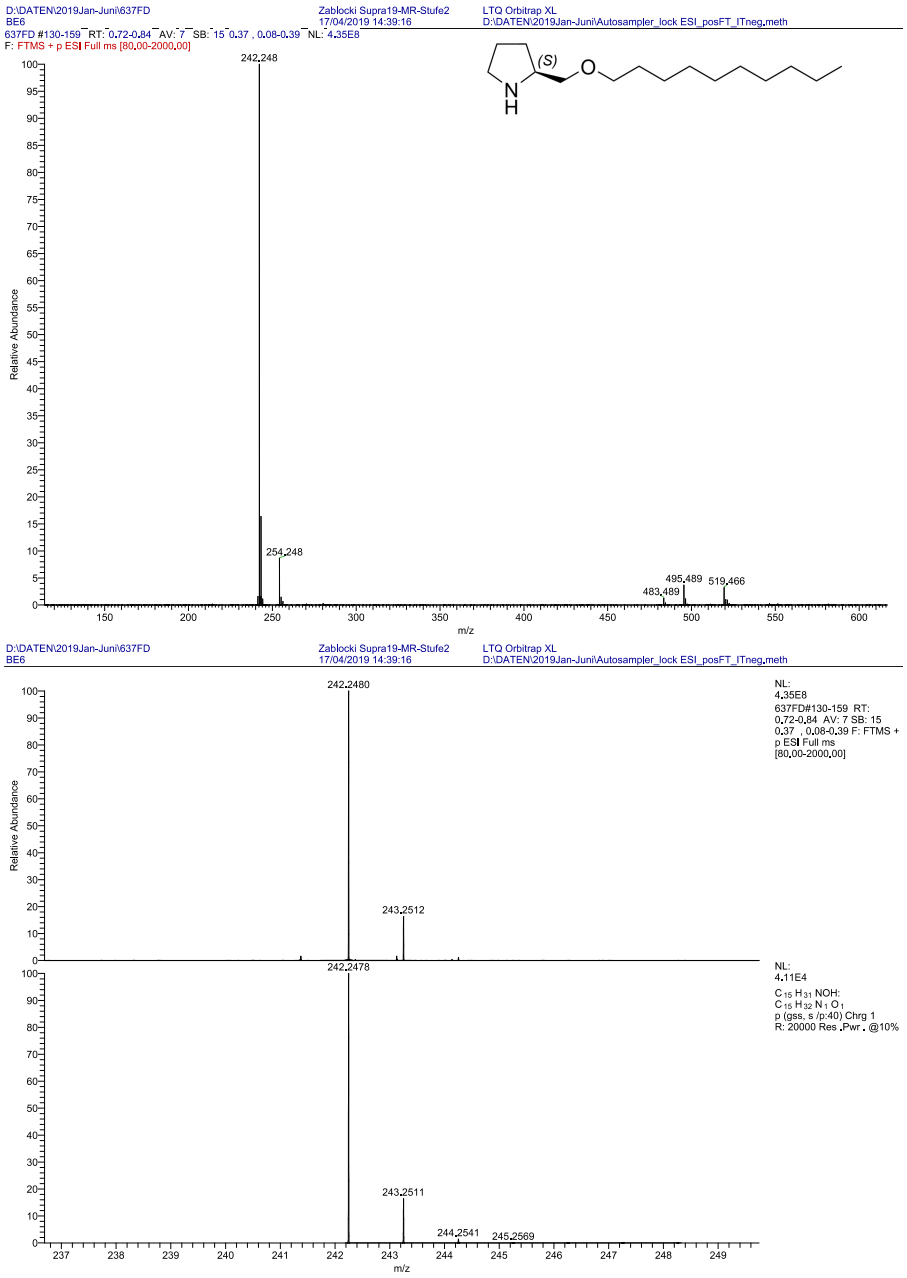

Figure S63: ESI(+) Mass spectra of L-prolinyl n-decyl ether

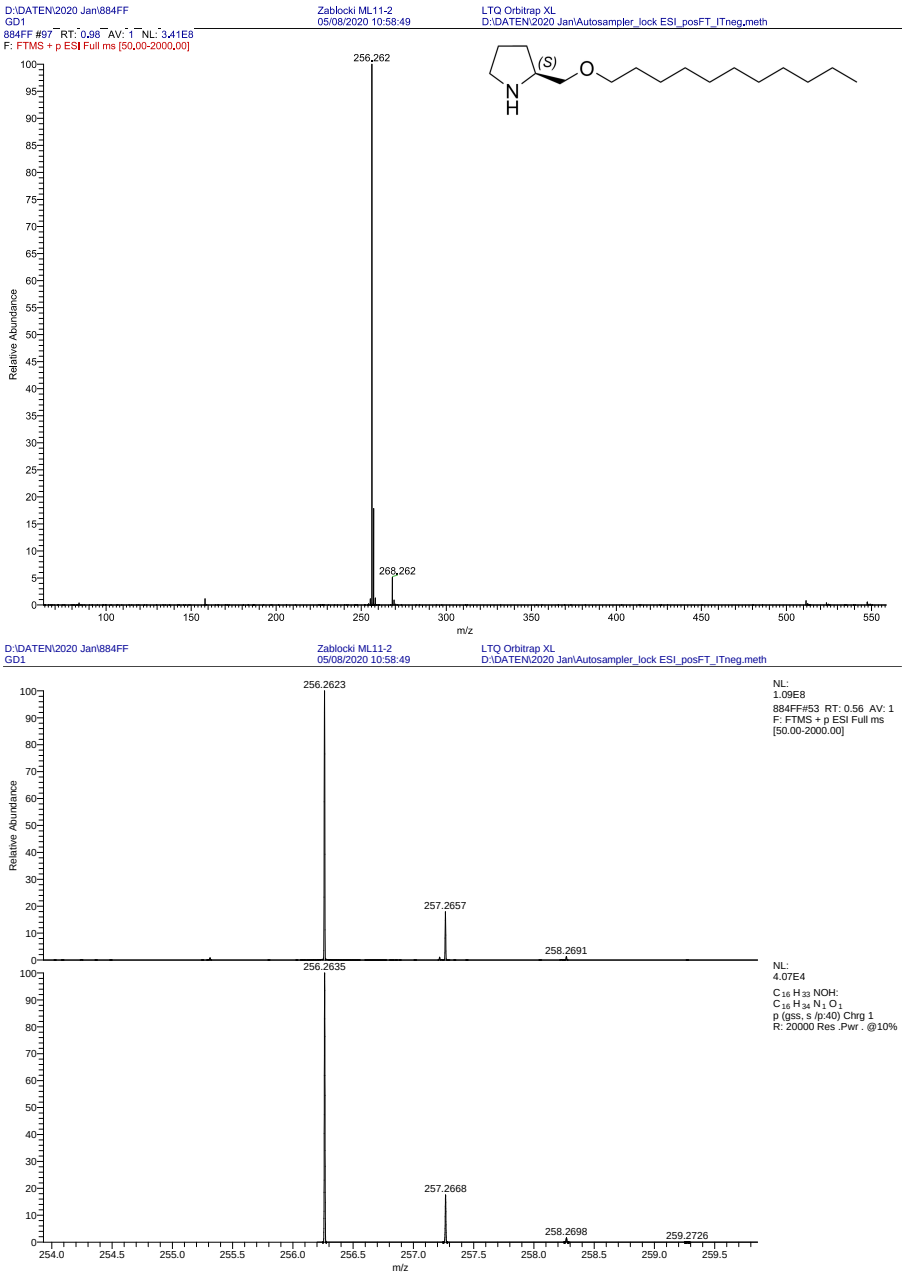

Figure S64: ESI(+) Mass spectra of L-prolinyl *n*-undecyl ether

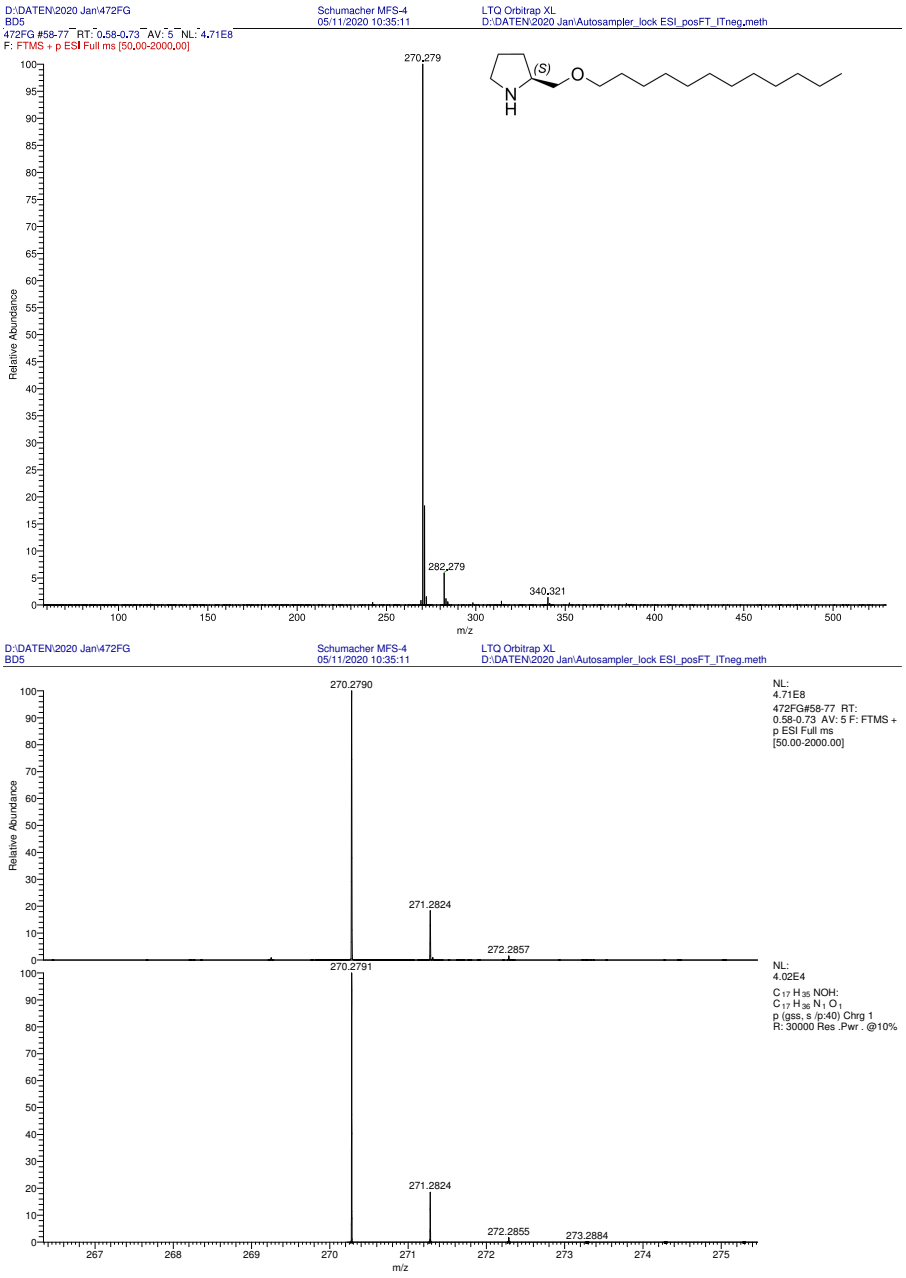

Figure S65: ESI(+) Mass spectra of L-prolinyl *n*-dodecyl ether

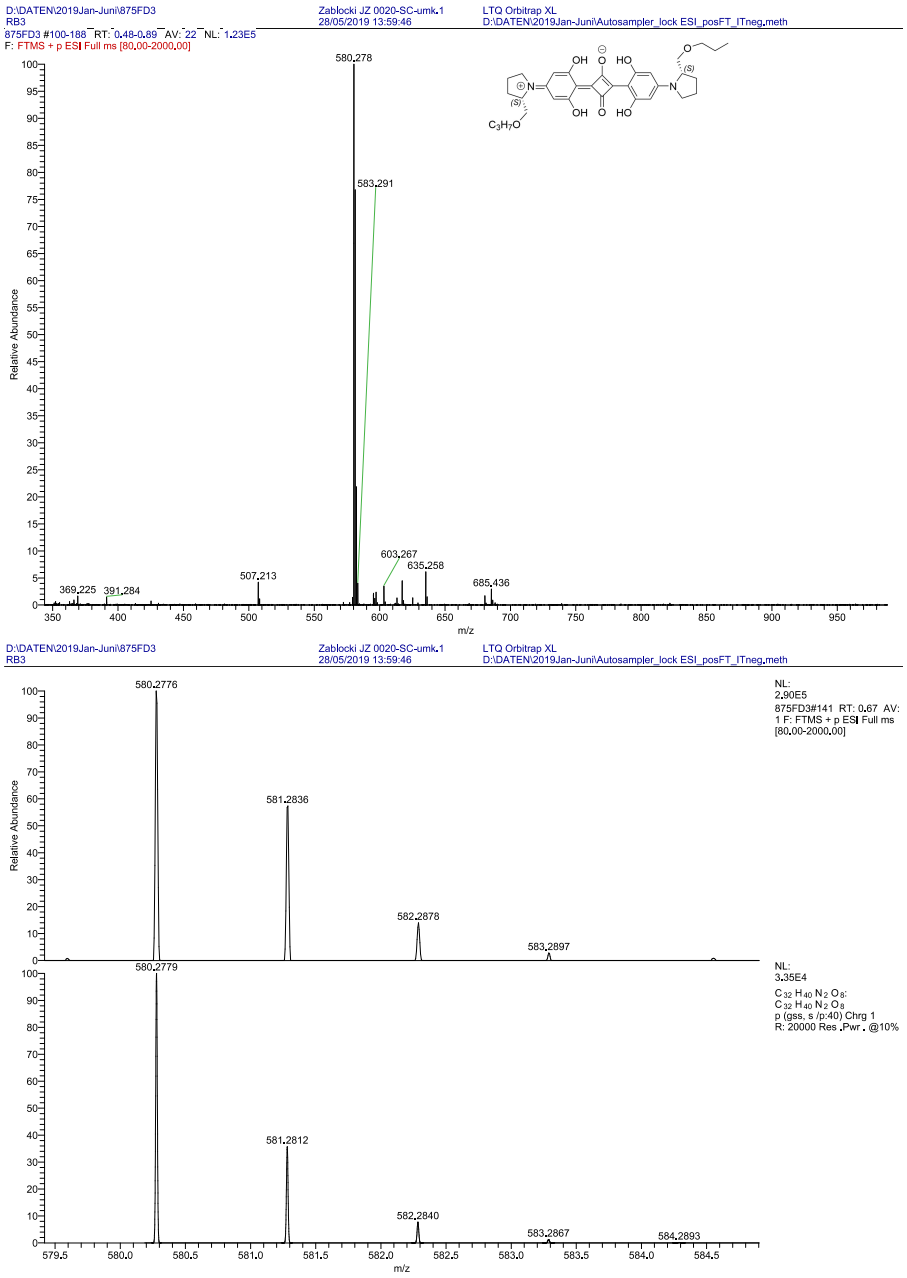

Figure S66: ESI(+) Mass spectra of (*S*,*S*)-ProSQ-C3

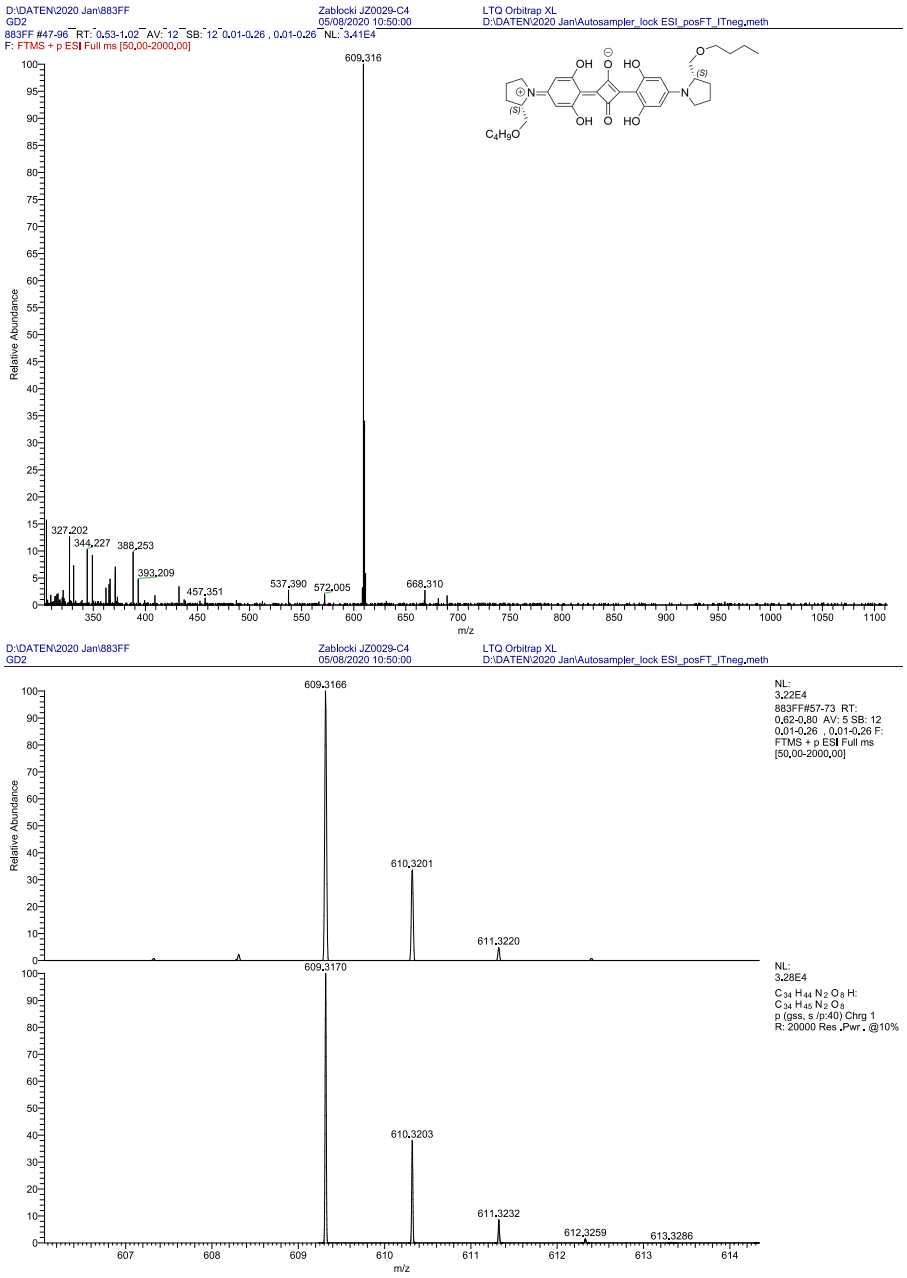

Figure S67: ESI(+) Mass spectra of (*S*,*S*)-ProSQ-C4

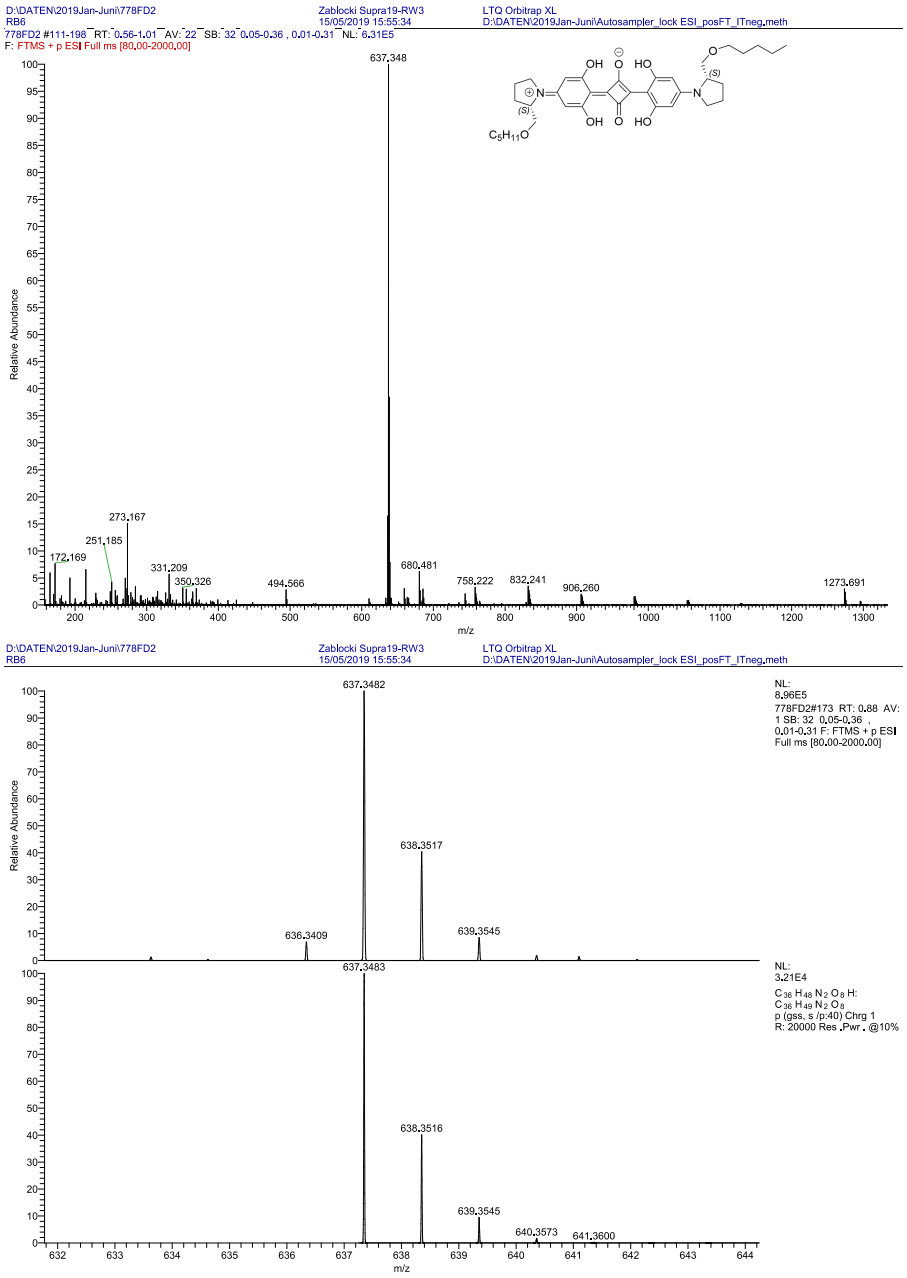

Figure S68: ESI(+) Mass spectra of (*S*,*S*)-ProSQ-C5

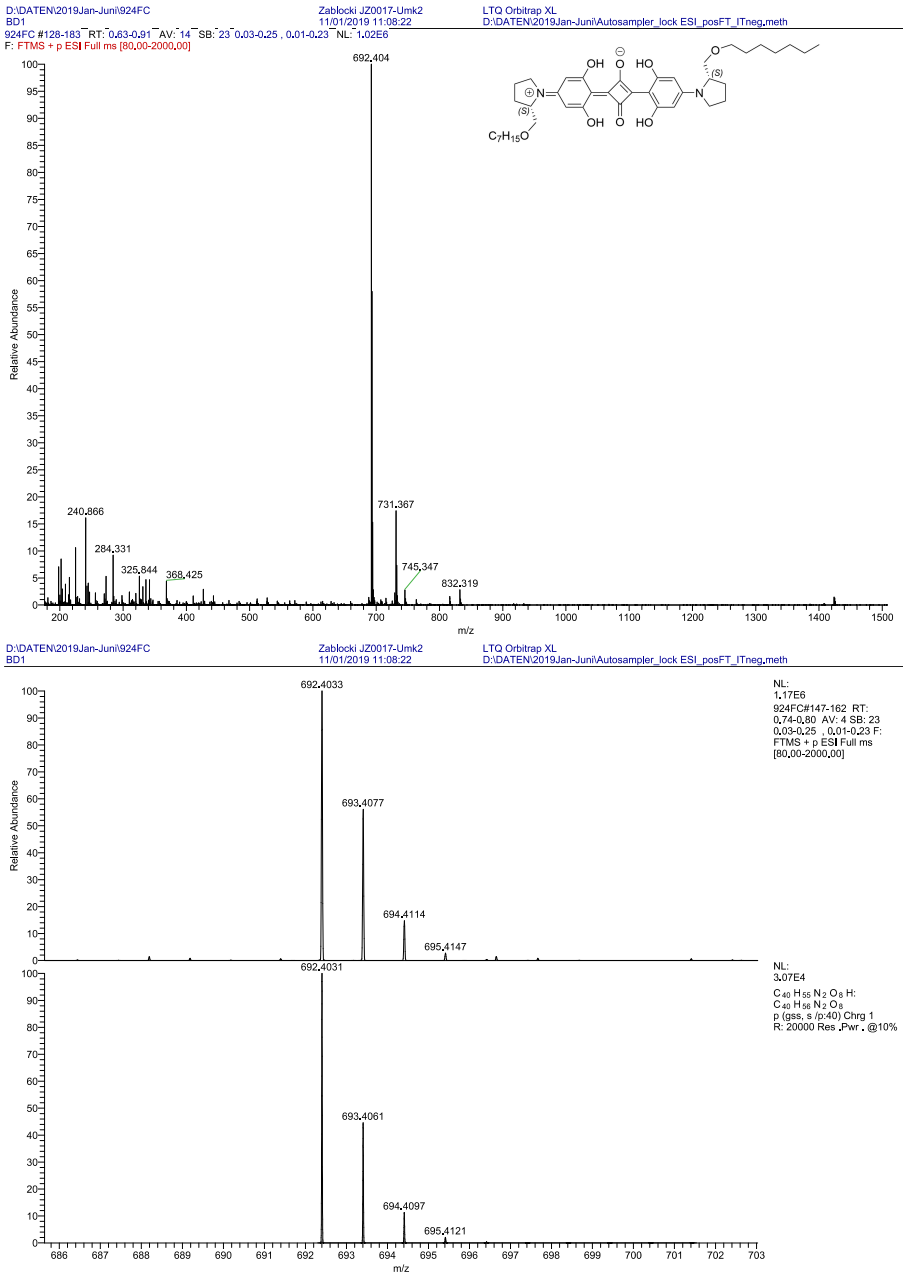

Figure S69: ESI(+) Mass spectra of (*S*,*S*)-ProSQ-C4

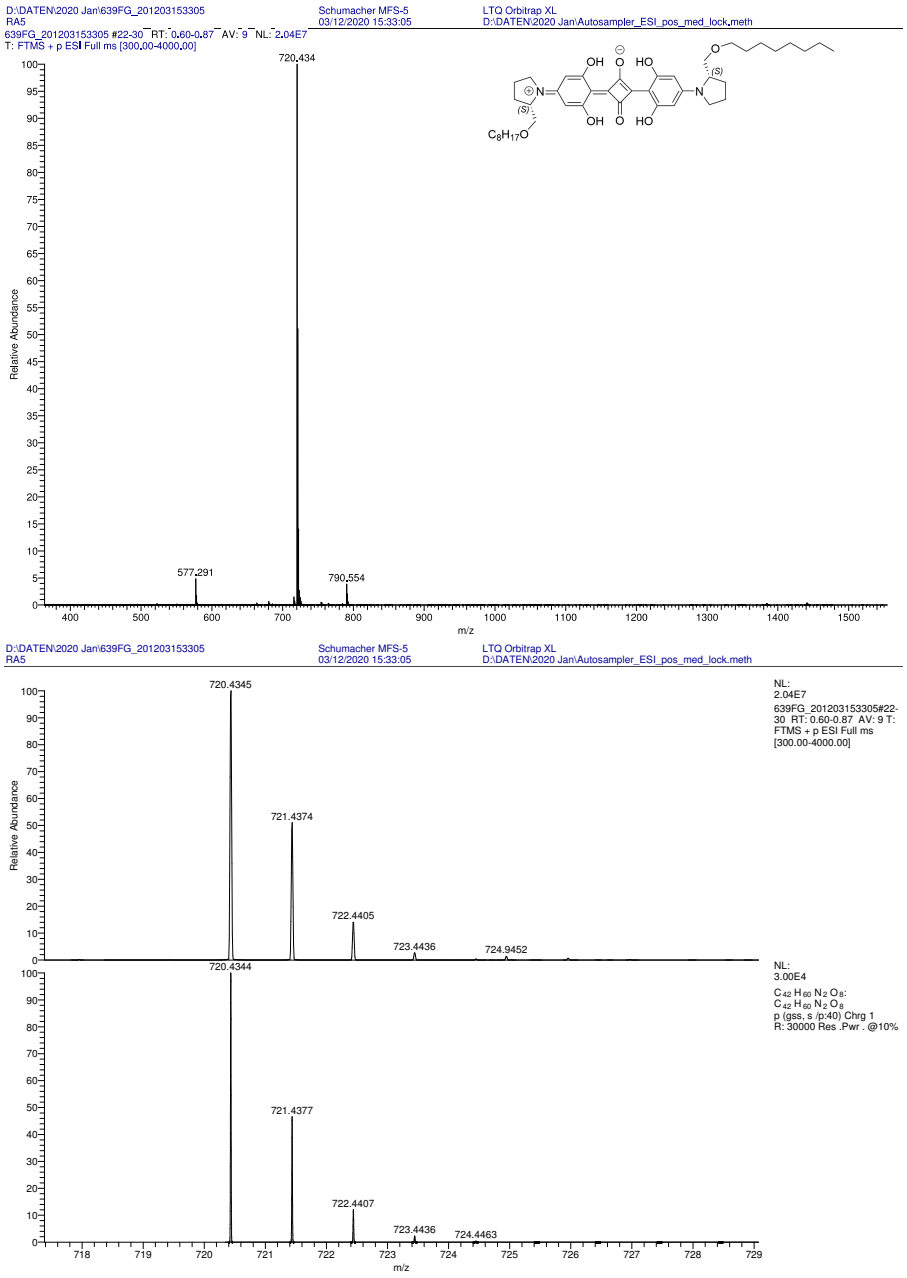

Figure S70: ESI(+) Mass spectra of (*S*,*S*)-ProSQ-C8

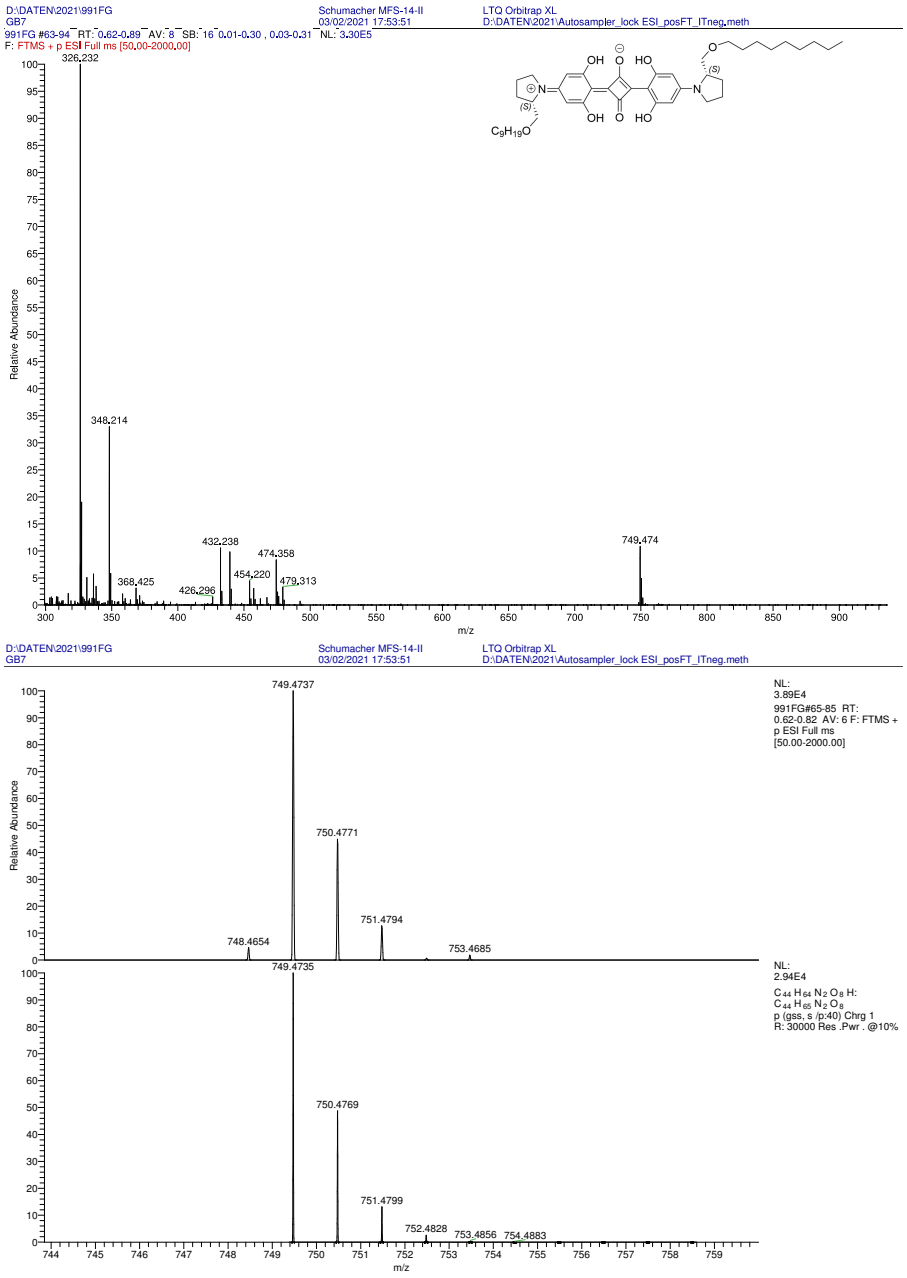

Figure S71: ESI(+) Mass spectra of (*S*,*S*)-ProSQ-C9

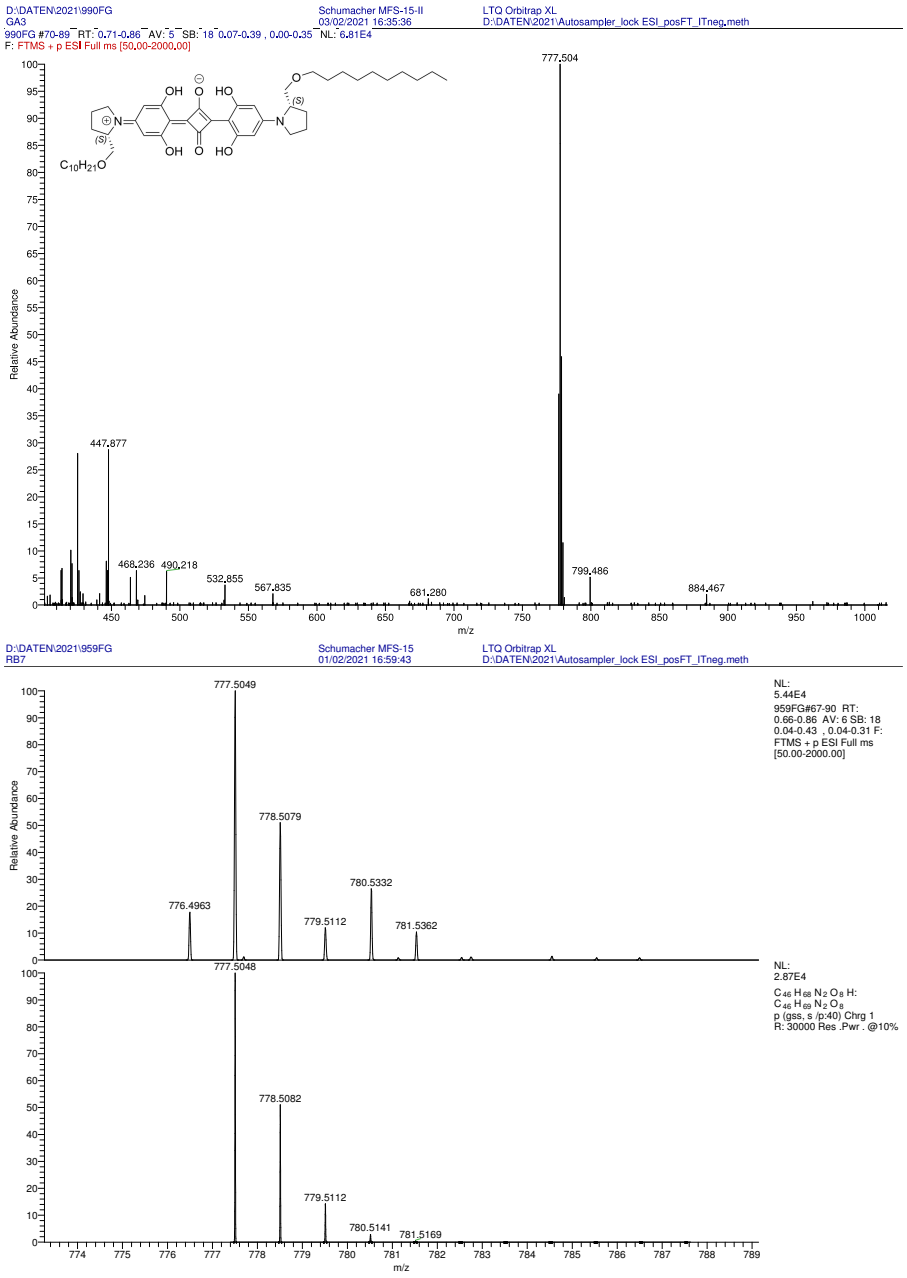

Figure S72: ESI(+) Mass spectra of (*S*,*S*)-ProSQ-C10

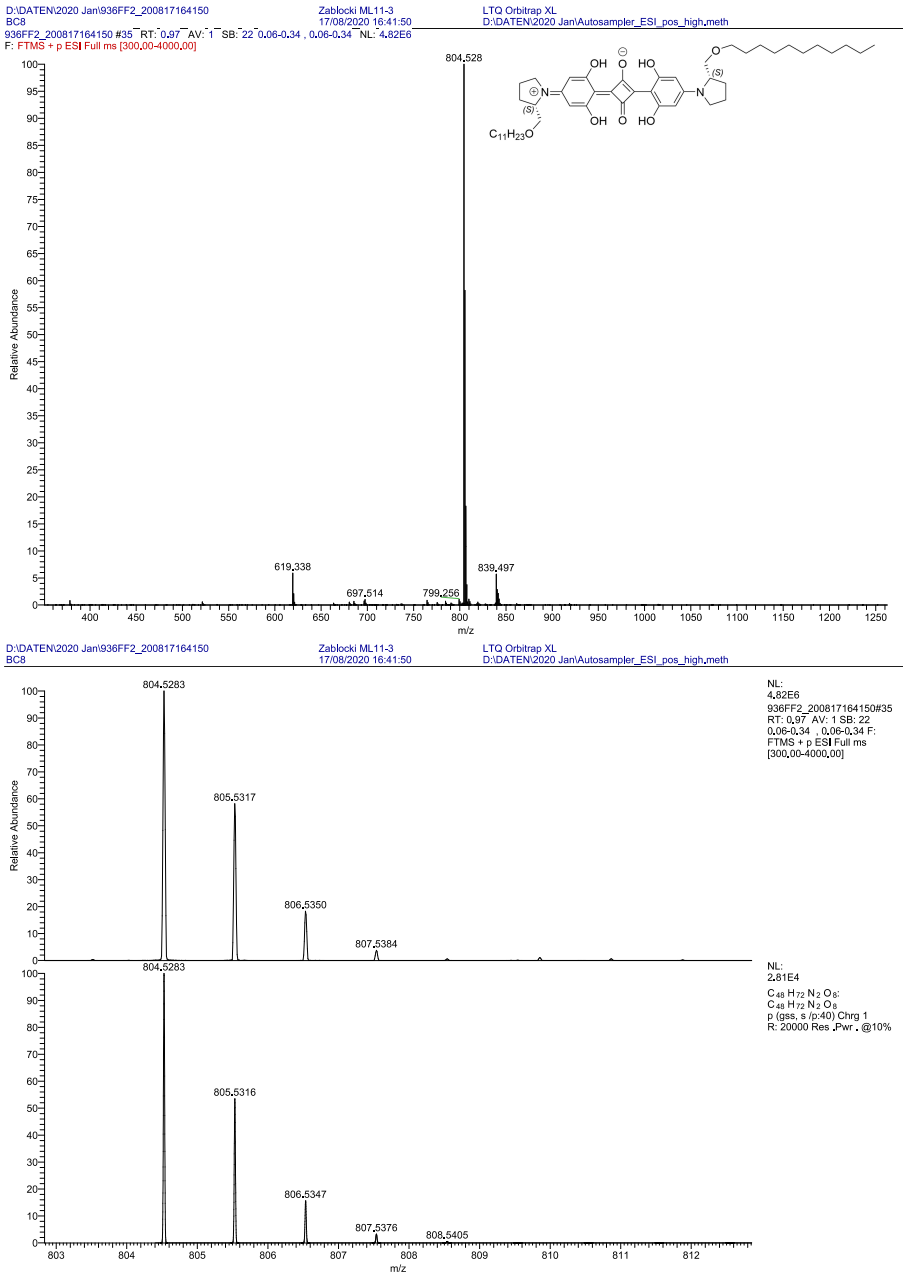

Figure S73: ESI(+) Mass spectra of (*S*,*S*)-ProSQ-C11

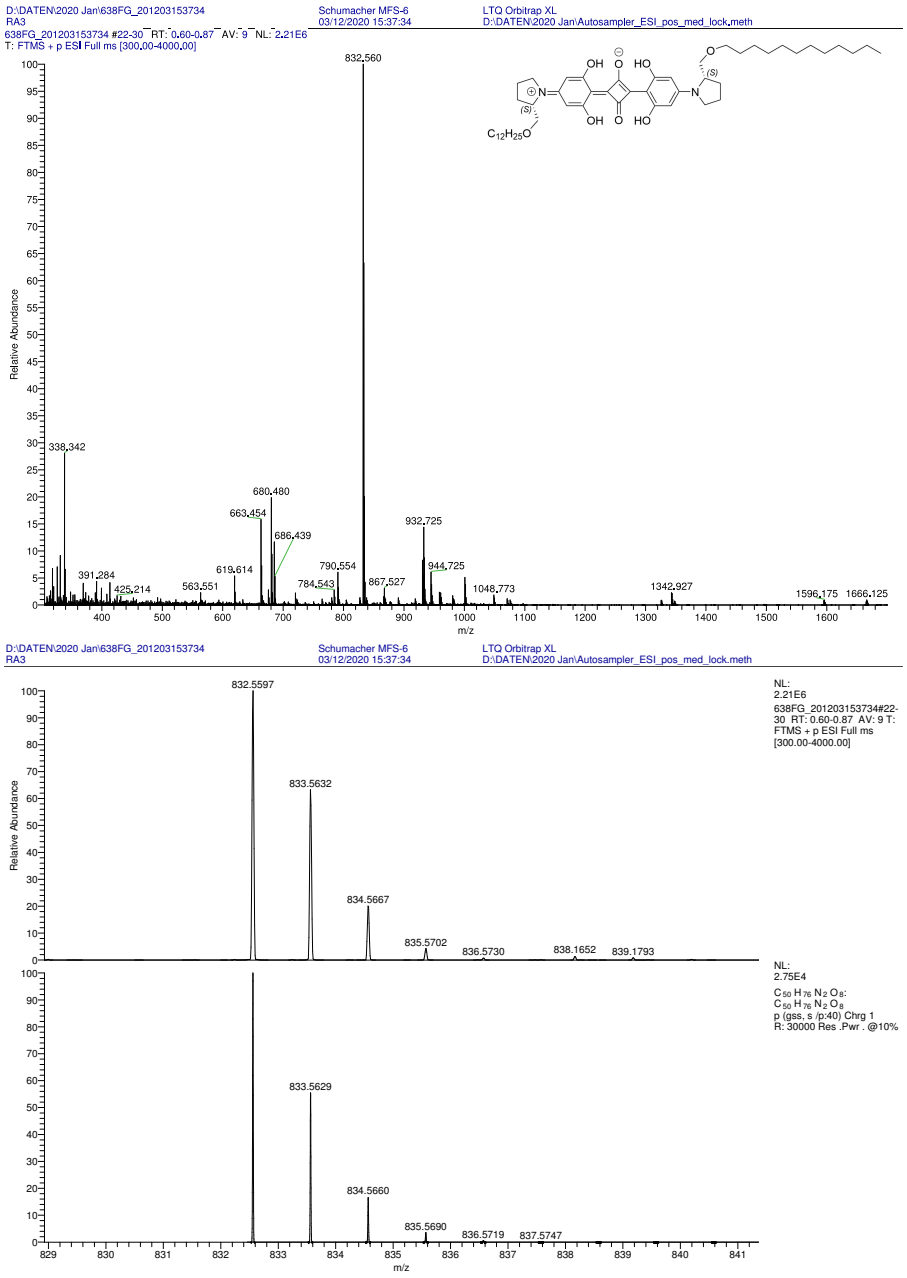

Figure S74: ESI(+) Mass spectra of (*S*,*S*)-ProSQ-C12